DISSERTATION

ADVANCED MANUFACTURING OF THERMOSET POLYMERS AND COMPOSITES

Submitted by

Morteza Ziaee

Department of Mechanical Engineering

In partial fulfillment of the requirements

For the Degree of Doctor of Philosophy

Colorado State University

Fort Collins, Colorado

Spring 2023

Doctoral Committee:

Advisor: Mostafa Yourdkhani

Donald W. Radford
Susan James
Travis Bailey

ABSTRACT

ADVANCED MANUFACTURING OF THERMOSET POLYMERS AND COMPOSITES

Thermoset polymers and composites are lightweight materials extensively used in many industries from aerospace to automotive to prosthetics due to their excellent specific mechanical properties and high chemical resistance. However, these products are conventionally manufactured by labor-intensive processes using subtractive manufactured tooling or molds followed by thermal curing inside an oven or autoclave at elevated temperatures for several hours. Hence, conventional manufacturing approaches are energy- and time-consuming and require expensive equipment. Moreover, lack of design flexibility and poor repeatability are additional challenges, which limit the structural and functional capabilities of such products.

In this dissertation, I present a novel approach to address the existing limitations in manufacturing thermosets and their composites by developing rapid curing resin systems and integrating them in additive manufacturing (AM) processes. In the first chapter, state-of-the-art manufacturing methods are reviewed and frontal polymerization (FP) as a promising curing strategy for rapid and energy-efficient manufacturing of thermosets and composites is introduced. In the second chapter, the effect of ambient conditioning and resin chemistry on thermal frontal polymerization of a high-performance resin system is explored. In the third chapter, FP is used to demonstrate, for the first time, simultaneous printing and curing of short carbon fiber-reinforced composites for high performance applications. In the following chapter, AM of a soft and stretchable elastomer with tunable thermomechanical properties manufactured via FP is discussed. In the fifth chapter, the printing process is further improved using an external localized heat source, instead of relying on the exothermic heat of polymerization of the resin, to accelerate the curing

rate and make the printing process more robust and applicable to the manufacture of large-scale components. Finally in the last chapter, bubble-free frontal polymerization of polyacrylates is introduced for the developed 3D printing process.

ACKNOWLEDGMENTS

It is my pleasure to express my sincere gratitude to many people for their continuous support and encouragement during this research. Without them, the completion of this research would not have been possible.

Foremost among those people is my research supervisor, Prof. Mostafa Yourdkhani. I would like to express my deep sense of thanks for his constructive criticism, encouragement, and enduring support. I will forever be grateful for all his valuable input for my professional and personal development.

My sincere gratitude also extends to my committee members Prof. Donald W. Radford, Prof. Travis Bailey, and Prof. Susan James for their insightful comments. Special thanks to Prof. Donald W. Radford, Prof. Kaka Ma, and their team for training and helping me to use their equipment. Also, I would like to thank all members of Multifunctional Polymers and Composites Laboratory for their assistance in this research.

Last in order but not in importance, I would like to say a heartful thank you to my parents for their love and support.

DEDICATION

To my family,

For their love and unconditional support

CONTRIBUTIONS OF THE AUTHOR

The author of this dissertation has performed all the work presented therein, with the following exceptions:

Chapter 3: Dr. James W. Johnson in the Department of Mechanical Engineering carried out flexural experiments on 3D printed and molded samples. The design of cooling device on the printhead was provided by Dr. Jia En Aw from the University of Illinois at Urbana-Champaign and assembled with the assistance of Mr. Sean Smith and Ms. Hanna Narans.

Chapter 4: Mr. Iman Naseri assisted in collecting and measuring front velocity profiles. The results of tensile properties were provided by Dr. James W. Johnson. Mr. Kevin Franklin from the Department of Chemistry performed Dynamic Mechanical Analysis (DMA) tests.

Chapter 5: Mr. Carter Dojan designed and performed 3D printing of continuous carbon fiber-reinforced composite (CFRC) parts, and assisted with polishing and measuring void content and fiber volume fraction in the 3D printed continuous carbon fiber-reinforced composite filaments.

LIST OF PUBLICATIONS, PATENTS AND PRESENTATIONS

Journal articles

1) **Ziaee M.**; Johnson J. W.; Yourdkhani M. 3D Printing of Short-Carbon-Fiber-Reinforced Thermoset Polymer Composites via Frontal Polymerization. *ACS Applied Materials & Interfaces* **2022**, 14 (14), 16694–16702.

2) Chen Z.; **Ziaee M.**; Yourdkhani M.; Zhang X. Multiphysics Modeling of Frontal Polymerization-Assisted Layer-by-Layer Additive Manufacturing of Thermoset Polymer Components. *Additive Manufacturing* **2022**, 59, 103182.

3) Naseri I.; **Ziaee M.**; Nilsson Z. N.; Lustig D. R.; Yourdkhani M. Electrothermal Performance of Heaters Based on Laser-Induced Graphene on Aramid Fabric. *ACS omega* **2022**, 7 (4), 3746–3757.

4) **Ziaee M.**; Yourdkhani M. Effect of Resin Staging on Frontal Polymerization of Dicyclopentadiene. *Journal of Polymer Science* **2021**, 59 (15), 1732–1739.

5) **Ziaee M.**; Naseri I.; Johnson J.W.; Franklin K.; Yourdkhani M. Frontal Polymerization and 3D Printing of Thermoset Polymers with Tunable Thermomechanical Properties, *ACS Applied Polymer Materials* **2022,** under review.

6) Naseri I.; **Ziaee M.**; Yourdkhani M. 3D Printing of Syntactic Foams via Frontal Polymerization, to be submitted.

7) Narans H.; **Ziaee M.**; Naseri I.; Yourdkhani M. 3D Printing of Self-Heating Molds via Frontal Polymerization, to be submitted.

8) **Ziaee M.**; Yourdkhani M. Bubble-Free Free Radical Frontal Polymerization using Redox Initiators, to be submitted.

9) **Ziaee M.**; Smith S.; Yourdkhani M., Photothermal Initiation of Frontal Polymerization in Carbon Fiber-Reinforced Polymer Composites, to be submitted.

10) Dojan, C.; **Ziaee M.**; Yourdkhani M. Rapid and Scalable Additive Manufacturing of Discontinuous and Continuous Carbon Fiber Reinforced Thermoset Composites via a Laser, to be submitted.

Patents

1) Yourdkhani M.; **Ziaee M.**; Smith S.; Naseri I. Method and Device for Printing and Curing Thermoset Resin, *US Patent No. 17,365,492*, filed July 1, **2021**.

2) Yourdkhani M.; **Ziaee M.** Frontal Polymerization of Polymers with Tunable Mechanical Properties, *US Patent Disclosure*, filed August 5, **2022**.

Refereed conference papers

1) Yourdkhani M.; **Ziaee M.**; Dojan C. Additive Manufacturing of Thermally Curable Fiber-Reinforced Thermoset Composites, *American Chemical Society*, March 26-30, **2022**, Indianapolis, Indiana.

2) Dojan C.; **Ziaee M.**; Yourdkhani M. Rapid and Scalable Additive Manufacturing of Thermoset Polymer Composites, *American Society for Composites*, September 19-22, **2022**, Tucson, Arizona.

3) Yourdkhani M.; Dojan C.; **Ziaee M.** Additive Manufacturing of Thermally Curable Thermoset Composites, *TechConnect World Innovation Conference*, June 13-15, **2022**, Washington, DC.

4) Yourdkhani M.; **Ziaee M.**; Naseri I.; Smith S. Remote Activation of Frontal Polymerization for Sustainable Manufacturing of Thermosets and Composites. *European Conference on Composite Materials*, June 26-30, **2022**, Lausanne, Switzerland.

5) Chen Z.; **Ziaee M.**; Yourdkhani M.; Zhang X. Multiphysics Modeling of Frontal Polymerization-Based Layer-by-layer 3D Printing of Thermoset Polymer Components, *Engineering Mechanics Institute Conference*, May 31-June 3, **2022**, Baltimore, Maryland.

6) **Ziaee M**.; Yourdkhani M. Additive Manufacturing of Thermosetting Polymers and Composites with Tunable Functional Properties via Frontal Polymerization, *Thermoset Resin Formulators Association*, May 2-5, **2022**, Dallas, Texas.

7) **Ziaee M.**; Yourdkhani M. Thermal Frontal Polymerization of Dicyclopentadiene in Different Staging Conditions, *American Chemical Society*, March 20-24, **2022**, San Diego, California.

8) **Ziaee M.**; Yourdkhani M. Rapid Synthesis of Thermoset Elastomers with Tunable Thermomechanical Properties, *American Chemical Society*, March 20-24, **2022**, San Diego, California.

9) **Ziaee M.**; Yourdkhani M. Simultaneous 3D Printing and Curing Thermoset Composites via Frontal Polymerization, *American Institute of Aeronautics and Astronautics*, September 29, **2021**, Boulder, Colorado.

10) **Ziaee M.**; Yourdkhani M. 3D Printing of Short Carbon Fiber Composites via Frontal Polymerization, *American Society for Composites*, September 19-21, **2021**, College Station, Texas.

11) Smith S.; **Ziaee M.**; Yourdkhani M. Manufacture of Carbon Fiber-Reinforced Polymer Composites using Photothermally Activated Frontal Polymerization, *International Materials Research Congress*, August 15-20, **2021**, Cancun, Mexico.

TABLE OF CONTENTS

LIST OF TABLES

LIST OF FIGURES

Chapter 1: Background

Thermoset polymer composites play an important role in all aspects of modern life from aerospace structures to electronic components to medical devices. When compared to metals or ceramics, thermoset polymer composites are easier to fabricate due to low processing temperatures and can easily be integrated with multiscale fillers or reinforcements to enhance their thermal, electrical, or mechanical properties.[1] However, the widespread applications of composites are still limited due to several processing challenges. One of the main challenges associated with conventional manufacturing of advanced thermoset composites is long-cure cycle of resin which makes the manufacturing process energy-inefficient and time-consuming. Present technologies for fabricating thermoset composites require the resin to be heated at elevated temperatures for several hours which leads to high energy consumption, low production rates, and producing a high amount of carbon footprint.[2,3] For example, curing a small section of Boeing 787's fuselages require heating the composite component at 180 °C for eight hours which corresponds to consumption of 350 gigajoules (GJ) of energy and production of 80 tons of carbon dioxide.[4] In addition, manufacturing scalability is costly and challenging because the internal size of the heating equipment must be scaled in size with the component.

Another major challenge with composite manufacturing is use of tooling or mold to form thermoset composites into a desired shape. Design and fabrication of tooling is an expensive, time-consuming, and labor-intensive process and often requires serval hours to a few weeks using special equipment for machining or polishing.[5] In general, complexity of manufactured parts is constrained by traditional tooling or mold design. Given that tooling represents a significant portion of composite manufacturing cost, use of alternative options with high volume production

rates seems necessary to produce composites at lower costs and shorter lead times. As a result, the use of tooling and long cure cycle resin systems are the major contributing factors impeding the widespread application of thermoset composites in various industries. In the following, most recent solutions to the above problems are discussed.

1.1. Rapid curing strategies

1.1.1. Rapid curing thermoset resin systems

The use of rapid curing resin systems substantially shortens curing time and reduces the energy required for manufacturing processes. For example, a rapid curing epoxy resin system based on 2-methylimidazole and an alcoholic type chain transfer agent was developed for manufacturing carbon fiber-reinforced composite (CFRC) parts (350 mm × 700 mm × 2 mm) within 10 mins using an isothermal resin transfer molding (RTM) process at 105 °C.[6,7] Mitsubishi Rayon Co. Ltd has developed a new epoxy resin formulations for prepreg compression molding process that realize fast curing of composite parts under 5 mins at 140 °C [8] which is within the target manufacturing time (several minutes per parts) for automotive industries. Although the use of rapid curing resins systems addresses the problems related to long cure cycles, these new resin systems have very short pot life, which makes processing of composite parts with them quite challenging.

1.1.2. Accelerated curing via irradiation techniques

Irradiation techniques have been frequently used for rapid curing of thermoset composites and can produce a highly homogenous volumetric heating compared to traditional oven curing. Several irradiation techniques have been developed based on various radio waves within the electromagnetic spectrum to accelerate the curing of thermoset composites with benefits and limitations detailed below.

E-beam (EB) curing has been successfully applied to fabricate high-performance composite parts used for airspace industries and can be considered an alternative to out-of-autoclave curing of advanced composites. In this method, the surface of uncured thermoset composite is bombarded via beams of electrons to provide sufficient energy to initiate the curing process by decomposing radiation-sensitive initiators.[9,10] However, EB curing requires high energy-electrons (5-15 MeV) to penetrate through the thickness of composites, requiring large capital investments for EB emitters. In addition, it has been reported that EB causes weak interfacial fiber-matrix bonding, hence resulting in low mechanical properties.[11]

Gamma rays or x-rays are both types of high-energy electromagnetic radiation with frequencies > 10^7 GHz, and wavelengths < 10^{-5} mm. This method has been applied to fabricate thick carbon fiber epoxy composites due to its high depth of penetration, but it has longer cure times compared to the EB curing approach due to lower dose rates, that results in dipolar polarization or ionic polarisation.[12,13] One of the major challenges that restricts its adoption in composite industries is the safety concerns related to radioactivity exposure.

UV is another form of electromagnetic radiation with frequencies of > 10^6 GHz, and wavelength of < 10^{-4} mm. UV curing offers economical, energy-efficient, and environmentally friendly curing of thermoset composites. However, its application has been limited to open mold processes with thin structures due to its low depth of penetration.[14,15]

Infrared irradiation is a medium-energy electromagnetic radiation with frequencies > 10^3 GHz, and wavelengths < 10^{-1} mm. In this method, the electromagnetic wave is absorbed by different coupled hydrocarbon groups within the polymer including CH, CH_2, CH_3 and converted to heat due to resonance vibration of these molecules. The frequency at which vibration occurs in hydrocarbon groups is within short to medium infrared region above 1.5 mm. Due to strong

resonance vibrations of these molecules at an infrared wavelength, most of electromagnetic energy is absorbed by the surface of composites limiting its penetration into the depth of the material.[16]

Microwaves are medium-energy electromagnetic waves with frequencies above 1 GHz and wavelengths below 10^3 mm. Microwave heating has excellent penetration depth compared to other irradiation techniques which provides the most efficient volume-heating process.[17] Adding dielectric nanomaterials to the polymer can improve microwave heating at molecular level.[18,19] Microwave radiation can be effectively absorbed by dielectric nanoparticles and transformed to heat due to molecular vibration via dipole moments.

1.1.3. Frontal polymerization

Frontal polymerization (FP) has a great potential for energy-efficient, low cost, and scalable manufacturing of thermosets and composites.[20] FP is a polymerization strategy where a self-sustaining reaction wave is initiated via a thermal or photo stimulus and propagates directionally through a monomer solution and converts it to a solid polymer without external energy.[21] FP can be performed in three different modes of isothermal FP, photofrontal polymerization and thermal frontal polymerization.

In isothermal FP, a piece of polymer is regionally dissolved in its monomer solution, after which the polymerization occurs via Norrish–Trommsdorff gel effect.[22,23] The dissolved polymer locally increases the viscosity of monomer and increases the rate of polymerization in highly viscous region due to reduced termination events. As a result, a propagating reaction wave is initiated in highly viscous gel regions and propagates toward low viscous monomer solution. Unlike thermal FP, which is driven by Arrhenius kinetics, isothermal FP is controlled by coupling of viscoelastic effects and diffusion rate of a polymer into its monomer. Therefore, isothermal FP is essentially a slow process, and front can only travel within a few centimeters.

Photofrontal polymerization relies on continuous input of UV light for propagation of front because the enthalpy of polymerization is low to sustain the front.[24] The presence of UV light pre-activates a photoinitiator in the monomer solution and helps to sustain the reaction wave. The front quenches once the light is removed. One application of photofrontal polymerization is remote curing of thick composite materials.[25,26] In this work, an epoxy resin system based on bisphenol-A diglycidyl ether was polymerized by cationic polymerization in the presence of onium salts as photoacid generator under UV-irradiation. Upon UV-surface activation of cationic polymerization, the heat is released which activates FP reaction by dissociating a radical thermal initiator in deeper layers. This elegant method enables fabrication of high-quality thick composites with same mechanical properties to thermally cured composites. Another application of photofrontal polymerization is producing hydrogels which allows FP propagation to take place in water-based systems.[27]The advantage of photofrontal polymerization is that the front can propagate below boing temperature that enables rapid fabrication of bubble-free hydrogels with desired optical and mechanical properties.

Thermal frontal polymerization is the most common form of FP, which I will refer to as FP in the remaining part of dissertation. FP is driven by the heat released during an exothermic polymerization. A local thermal stimulus activates a thermal latent initiator in an uncreated monomer solution. The activated initiator reacts with adjacent monomers which releases heat upon reaction, thus, in turn, activates more initiators. The process of activation and heat generation is continued, resulting in a reaction wave propagating through monomers and transforming them to a solid polymer (Figure 1.1).[21] Once all monomers are consumed by the reacting front, the rate of heat generations decreases, inhibiting further activation. The propagating reaction wave or front can travel at high speeds of up to 10 cm/min and its temperature can reach above 300 °C.[28,29]

Among various FP resin systems, dicyclopentadiene (DCPD), which is a cyclic olefin resin, is of great interest for various industrial applications due to the high fracture toughness, impact resistance, stiffness, and chemical and thermal stability of the resulting polydicyclopentadiene

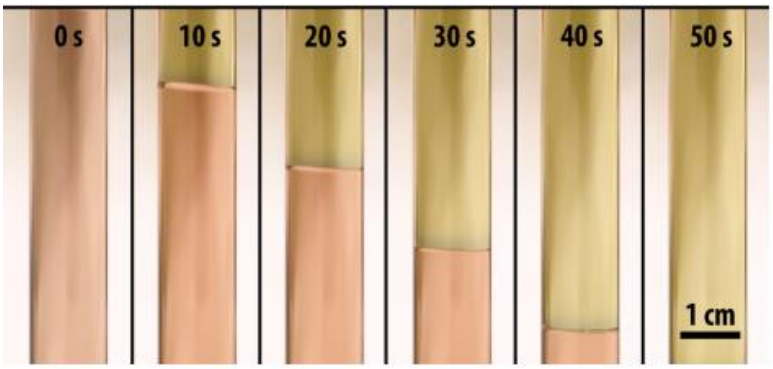

Figure 1.1. Sequential snapshots captured from initiation and propagation of FP reaction. FP reactions is initiated by local heating of a thermoset resin using a hot soldering iron and propagates through a self-activating process without any energy input.[40]

polymer.[30,31] Polydicyclopentadiene (PDCPD) can be prepared by frontal ring opening metathesis polymerization (FROMP) of DCPD using a ruthenium catalyst. FROMP of DCPD was first carried out using first generation Grubb's catalyst in the presence of triphenylphosphine inhibitor.[32] The inhibitor was not effective in preventing the solution from spontaneous polymerization. Therefore, the solution had to be frozen before use. In another study, 4-dimethylaminopyridine was introduced as an inhibitor for second generation Grubbs' catalyst (GC2), increasing the pot life up to 30 min.[33] Robertson et al. revisited FROMP of DCPD in 2017 and demonstrated that phosphite inhibitors have a great potential to extend the pot life of the resin up to 30 h, while still allowing FP at room temperature without compromising the mechanical properties of the end polymer.[34] Also, it was found that phosphite inhibitors can control the reaction rate of the DCPD resin at room temperature, allowing to gradually increase the viscosity of the resin to transform it from a low-viscosity liquid to a soft gel to a stiff gel. Resins with different initial viscosities were used to develop new advanced manufacturing techniques including rapid fabrication of carbon fiber-

reinforced composites, moldless manufacturing of thermoset polymers, 3D printing of thermosets, creation of anisotropic foams, and rapid fabrication of vascularized thermosets (Figure 1.2).[35–37]

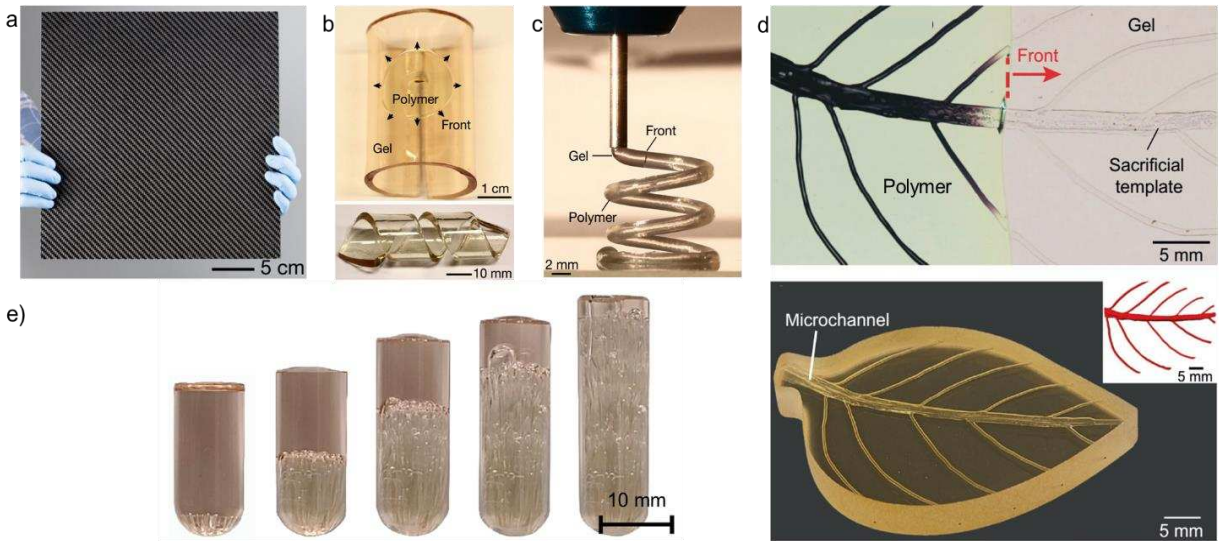

Figure 1.2. Examples of advanced manufacturing via FP. a) A 30 cm × 30 cm composite panel fabricated in 5 mins.[36] b) Moldless manufacturing of thermoset polymers.[36] c) *In-situ* 3D printing and curing of a frontal curable gel.[36] d) Synchronized depolymerization and polymerization to create of vascular networks.[35] e) FP reaction in the presence of a blowing agent to create foams.[37]

1.2. Additive manufacturing

Additive manufacturing (AM) eliminates the use of tooling and addresses the energy inefficiencies and long manufacturing times of thermoset composites to some extent.[38] In addition, AM provides more flexibility in designing and fabricating complex part geometries that are hard to achieve using conventional manufacturing techniques. In the following, AM techniques for creating thermosetting polymer and composite parts are reviewed.

1.2.1. Stereolithography (SLA)

Stereolithography (SLA) is the earliest type of AM techniques that uses photocurable resin systems to manufacture three-dimensional (3D) objects by iteratively photocuring thin layers of resin.[39] The resolution of SLA varies between 50-200 mm for most commercial SLAs and the size

of SLA parts is limited to the size of the resin bath. Typical SLA machines are not very fast in printing; however, newer methods including digital projection lithography (DLP) and continuous liquid interface production (CLIP) have been developed to increase the speed of printing. Unlike SLA, which relies on curing one volume element (i.e., a voxel) at a time, these new technologies enable creation of entire layer at once by projecting a mask pattern on the liquid-resin reservoir using micro-mirror array devices or dynamic liquid-crystal masks.[40,41]

While SLA is often favored to manufacture neat thermoset polymers, there are a few reports on incorporating reinforcing fibers to SLA to enhance mechanical properties of the parts. For example, in a recent study 20 vol% of 1.6 mm short glass fibers was added to a photocurable resin system and the composite mixture was deposited layer-by-layer into a printing vat and selectively cured by a laser. As a result, semi-isotropic parts with enhanced elastic modulus and strength as well as reduced thermal shrinkage compared to unreinforced parts were produced .[42] In addition to short fibers, non-woven glass fiber mats were also used to make composites using SLA. The addition of glass fiber mats to the composite improved the strength and modulus of the epoxy-based composite by 48.8% and 50%, respectively.[43] In contrast to glass fibers, applying carbon fibers in SLA is rather difficult due to its opaque nature that causes incomplete curing of resin. A recent study tried to avoid this drawback by utilizing two-stage polymerization paradigm including UV-irradiation and thermal treatment for the complete curing of carbon-filled composites.[44]

1.2.2. 2-photon-polymerization (2PP)

2PP is a type of SLA technique where a 2-photon infrared femtosecond laser is used to polymerize the resin in a sphere-like shape unit cells called voxels. This technique allows to fabricate well-defined micro and nanostructures with sub 100 nm resolution.[45] One area of focus on printing via 2PP is developing new photoresist materials based on polymer nanocomposites to

achieve desired mechanical, electrical, or optical properties. However, one of the main limitations of this approach is very slow printing speeds, as it would take 104 days to print 1 mm^3 of material.[46] In addition, light screening effects of fillers restrict the use of high concentrations of fillers in resin.

1.2.3. Laminated object manufacturing (LOM)

Laminated object manufacturing (LOM) is a rapid AM technique for creating continuous fiber-reinforced composites using sheet lamination process. The process involves sequential stacking and cutting composite prepregs into a desired geometrical shape followed by bagging and oven curing to bond the layers together.[47] The precision of produced parts mostly depends on the precision of the cutting mechanism and the thickness of composite prepregs. The main drawback of this method is the high void contents (> 5%) and poor interfacial bonding that exists between layers. Hence, a post-consolidation cycle is often required to reduce the void content and improve the interfacial bonding strength.[48]

1.2.4. Material extrusion

Material extrusion is widely used method for AM of thermoset polymers and composites. Compared to other AM techniques, manufacturing thermoset composites via material extrusion is faster and more compatible with various fillers and reinforcements including discontinuous or continuous fibers for imparting multifunctional properties to the host polymer. This process was originally developed for fused deposition modeling (FDM) of thermoplastic materials, where a thermoplastic filament is fed through a heated nozzle and deposited on a building platform layer-by-layer to construct a 3D structure. However, thermoplastic composites fabricated via material extrusion suffer from poor interfacial adhesion between printed lines, high level of porosity produced during manufacturing process, and low thermomechanical performance of thermoplastic matrices.[49–51] AM of thermoset composites via material extrusion, also known as direct ink writing

(DIW), addresses these shortcoming and is becoming increasingly popular both in academia and industry.

The fabrication procedure via DIW technique involves robotic deposition of a shear-thinning ink on an *x*-*y* platform to create a 2D pattern. After generating the first layer, the deposition nozzle, mounted on a *z*-stage, is raised a finite height and then prints the second layer. This process is continued until the structure is created. As a result, this process is mostly useful for layer-by-layer printing of simple shapes.[52–54] The ink used in this direct assembly technique should exhibit a shear-thinning behavior to allow the ink extrusion through the deposition nozzle and develop a stable structure prior to network formation. One of the frequently used methods for imparting shear-thinning properties is mixing thermoset resins with rigid fillers or particles including shorts fiber, carbon nanotube, graphene, boron nitride, alumina, cellulose nanocrystal, and fumed silica.[55–59] Adding rigid fillers is also advantageous for tuning the mechanical, electrical, and thermal properties of the matrix polymer. A less common approach to modify the rheological properties is the use of high molecular weight polymers that swell in the resin and increase its viscosity.[60,61] However, the mechanism at which high molecular weight polymers functions strongly depends on their solubility in the resin, hence restricting their application.

In DIW method, various thermoset composite parts with a high resolution and fast printing speed can be produced, but curing of composite inks remains a main challenge. In DIW of thermoset composites, the ink is often cured at elevated temperatures for several hours after the printing is completed, which results in the loss of the print fidelity due to thermal yielding of the ink and limits prints to simple 2D geometries with a few layers of materials.[62] An alternative approach for avoiding long-cycle, oven-curing of printed materials is reactive extrusion of thermoset inks, where the components of a fast-curable resin are mixed at the printing nozzle and

spontaneously polymerized a few seconds or minutes after deposition on a substrate.[63] This approach allows for rapid and energy-efficient curing of thermoset resins with a relatively good control over geometrical accuracy; however, the process cannot be applied to freeform printing of 3D structures, often requires post-curing steps, and results in non-uniform material properties throughout the structure.[63,64,64] In addition to thermal curing approaches, photocuring strategy has been widely used for AM of thermoset resins, where a UV-curable ink is printed and immediately cured by exposure to UV light to capture the print geometry as the material is extruded from the printing nozzle.[65] Use of photocurable resins in DIW technique typically limits the use of functional additives and reinforcements in the resin due to the low cure conversion of photocurable resins, requires post-curing steps, and results in polymers with inferior mechanical performance and thermal stability compared with thermally curable systems.[54,66,67]

Recently, FP has shown a great potential for rapid printing of high-performance thermoset polymers.[36] In this method, a frontally curable ink is deposited on a heated substrate with an average temperature of 70 °C. A few seconds after deposition, a reaction front becomes activated and propagates along the filament, transforming the ink to a solid part. Therefore, a high-fidelity object could be created in one step without requiring any post-processing. As opposed to conventional layer-by-layer printing, this method enables fabrication of freeform structures only by matching the print speed with the front velocity. DIW via FP has been demonstrated for DCPD and epoxy resins which have high reactivity and workable pot lives.[36,68] It has been estimated that using FP for printing a large part (2000 cm^3) of epoxy composite can reduce the manufacturing energy by six orders of magnitude compared to the conventional oven curing process.[69] However, the highest print speed reported by FP is 2.3 mm/s which is still not fast enough for manufacturing large composite structures.[70]

As described earlier, AM via material extrusion holds a great promise to manufacture continuous fiber composites. While continuous fiber reinforcements offer higher mechanical performance compared with discontinuous fiber reinforcements, most AM reports are based on using short fibers because of the challenges exists in printing continuous fibers. One limiting factor that prevents achieving higher mechanical properties for additively manufactured short fiber composites is ineffective load transfer between adjacent fibers. For example, the critical fiber length required for an effective load transfer in a carbon fiber epoxy composite is estimated as 590 mm, whereas most fibers used in AM are below 150 mm in length.[71,72] The first demonstration of AM of continuous fiber thermoset composites was performed by impregnating a continuous 3K carbon fiber tow (3000 fibers in a bundle) in a high viscosity epoxy resin and printing parts on a build platform followed by curing at a high-temperature chamber. The parts printed with this technique had tensile strength of 792 MPa and tensile modulus of 161 GPa which are far beyond the maximum mechanical properties that can be achieved by 3D printing of short fiber composites. Following this study, more research has been conducted to use UV irradiation to simultaneously print and cure composite filaments. However, the presence of continuous fibers causes significant attenuation of UV energy, resulting in partial curing of the composite part.[73–75] In a recent study, a new technique for simultaneous printing and curing of continuous carbon fiber composite was developed which enabled fabrication of composite parts with a high degree of cure (95%) and a high fiber volume fraction (58.6%) in one step.[76] In this technique, named as dynamic-capillary driven AM, a thermoset resin was jetted onto continuous fiber tows for wetting and impregnation and subsequently cured via a localized external heat source (Figure 1.3).

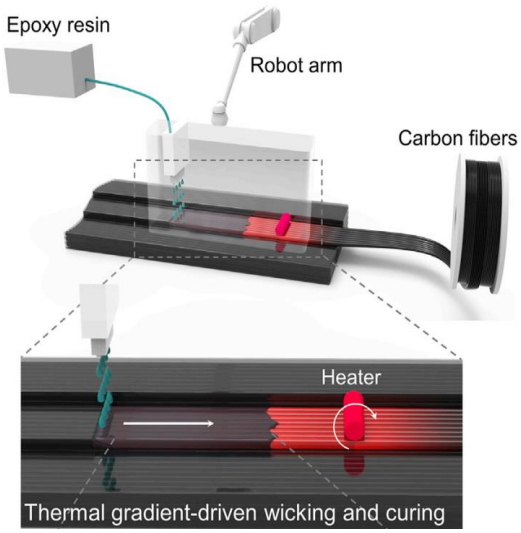

Figure 1.3. Schematic illustration of dynamic-capillary driven 3D printing of continuous carbon fiber thermoset composites. A heater touches a dry fiber and produces a temporary temperature gradient that makes the dispensed liquid resin to infuse the carbon fiber and cures instantaneously.[76]

1.3. Motivation and outline of dissertation

Despite widespread application of thermoset polymer composites across a broad range of industrial sectors, their adoption in AM has been limited by their challenging curing process. The overarching goal of this dissertation is to develop new AM techniques for rapid and energy-efficient manufacturing of thermally curable thermosetting composites. This goal is achieved by using cure-on-demand thermoresponsive resin systems, as the matrix resin of thermoset composites, in the AM processes and immediately curing and rigidizing the matrix resin following deposition by a robotic platform. Thermoset composites with tunable properties are fabricated using various types of carbon reinforcements, including continuous fibers, short fibers, and nanoparticles, demonstrating the versatility of the developed techniques. The thermoset resin systems used in the AM processes are based on frontally curable DCPD resin; however, the developed AM processes are amenable to other cure-on-demand and/or FP-curable thermoset

resins including epoxies and urethanes as well as *in-situ* curable thermoplastic resins such as acrylates. The research work presented in this dissertation is divided into five chapters as follows:

DCPD resin is a Newtonian fluid with a low viscosity; therefore, it is necessary to tune its rheological profile to make it extrudable with a shear thinning behavior. Increasing the viscosity of liquid resin can be obtained by partially curing the resin via staging at room temperature. The process to change the viscosity of resin depends on staging conditions or ambient conditioning, which is a time- and temperature-dependent phenomenon. However, resin staging can adversely affect the pot life and reactivity of the resin, which are crucial for successful 3D printing of thermoset composite structures. In Chapter 2, the effect of staging conditions on the pot life, rheological profile, and FP behavior of the FP-DCPD resin is studied to better understand the kinetics of the reaction and design proper conditions for 3D printing with the resin.

In Chapter 3, rapid and energy-efficient AM of short carbon fiber-reinforced thermoset composites via FP is presented. Two different printing strategies are developed: synchronous (self-equilibrating) freeform printing, and asynchronous supported (layer-by-layer) printing for AM of composites. In synchronous deposition and curing strategy, in-the-air printing of thermoset composite structures without any support materials is demonstrated. In asynchronous deposition and curing strategy, the superior thermal conductivity and rheological properties of carbon-fiber-modified inks are exploited to enable fast and layer-by-layer printing of composites.

The ability to rapidly print and cure a thermoset polymer via FP can have a variety of applications. However, the previous demonstration of printing with FP produced highly cross-linked PDCPD polymer with fixed mechanical properties. In Chapter 4, a new approach for tunning the thermomechanical properties of the resulting polymer is developed by copolymerization of DCPD and DCPD-modified linseed oil (DML). DML is a commercially

available resin based on vegetable oil that can modify the mechanical properties of PDCPD polymer by reducing its cross-linking density. Various copolymers with a wide range of mechanical properties from rigid to soft, stretchable elastomers are produced via FP at ambient condition. Using DLM as a comonomer, simultaneous printing and curing of an elastomeric object is demonstrated for the first time, expanding the library of materials (with unique properties) that can be printed using this novel AM technique.

While the FP-assisted curing technique enables unprecedented manufacture of thermoset composites, its scalability is limited by relatively low printing speeds, high sensitivity to ambient and boundary conditions, and inability to incorporate high concentrations of fillers or reinforcements due to potential quenching of the FP reaction. These limitations are addressed in Chapter 5 by developing a new AM technique where a localized external energy source is used to instantaneously heat and cure the extruded composite materials at high printing speeds (up to 1.5 m/min), irrespective of the boundary conditions and reinforcement content.

In 3D printing via an external energy source, DCPD resin is utilized to manufacture high-performance composite parts via on-demand curing technique. While the printing process produces high quality parts with excellent mechanical properties and thermal stability compared to existing techniques, difficulty in recycling of these materials may bring environmental concerns toward the use of developed printing materials. Thus, motivated by manufacture of recycled polymer composites, in the last chapter FP of polyacrylates is explored to demonstrate applicability of this novel printing technique to other on-demand curable resin systems with potential modification of resin formulation to develop recyclable thermoplastic polymers.

Chapter 2: Effect of Resin Staging on Frontal Polymerization of Dicyclopentadiene

2.1. Introduction

Thermoset polymers and their composites are commonly used in a wide variety of structural applications in aerospace, automotive, marine, and energy sectors due to their combination of excellent specific strength and modulus, thermal stability, and chemical resistance.[77,78] Conventional curing of high-performance thermoset polymers and composites relies on heating the material in autoclaves or ovens at elevated temperatures for several hours, leading to high energy consumption and carbon footprint, low production rates, and high cost of manufacturing. [4,2,79] In addition, the size of components that can be produced is restricted by the internal volume of the heating equipment, making the scalability of the manufacturing process difficult and costly.

An alternative and promising curing strategy that can eliminate the need for external, bulk heating of thermosetting resins is frontal polymerization (FP), in which the exothermic heat of polymerization of the resin is directly employed for material synthesis.[80] In FP, local heating of the monomer solution initiates the polymerization reaction, which produces enough heat to further drive the reaction in an autoactivating process. The result is a propagating reaction wave that rapidly transforms the monomer into polymer. FP has been previously demonstrated for various resin chemistries, including hydrogels,[81–83] acrylates,[84–86] polyurethanes,[87] epoxies,[88,89] thiolenes,[90] and cyclic olefins.[91,92] Development of FP resin chemistries requires the material to have a high energy density and very high rate of reaction at the front temperature but be stable and exhibit low rate of reaction at initial resin temperature.[80] However, the high resin reactivity required for self-sustaining propagation of the chemical reaction at front temperature often limits

the stability of the resin at low temperatures, resulting in short pot lives and limited applications of FP chemistries.

Recently, an FP resin system with controllable and extendable pot lives has been developed based on frontal ring opening metathesis polymerization (FROMP) of dicyclopentadiene (DCPD).[36] Using a latent catalyst system comprised of second-generation Grubbs catalyst inhibited by alkyl phosphites allows for controlling the pot life of DCPD resin up to 30 hours.[34] The resulting polymer is polydicyclopentadiene (PDCPD), which is a high-performance thermoset with mechanical properties comparable to those of aerospace-grade epoxies.[93–95] It has also been found that the low reaction rates of the FP-DCPD resin at room temperature causes the resin to gradually transform from a low viscosity liquid to a frontally polymerizable viscoelastic gel. This rheological transformation of resin, while being frontally polymerizable, enables new applications from composite and nanocomposite manufacturing to freeform 3D printing to moldless fabrication of thermosetting objects.[36,96,97]

Use of FP resins in various manufacturing techniques requires controlling the pot life and reactivity of resin and maintaining the stability of the rheological profile throughout the manufacturing process. For example, in 3D printing with FP resin, it is necessary to tune the initial viscosity of resin to be extrudable with a shear thinning behavior while having a long enough pot life and stable rheological profile during printing. The time-dependent, background polymerization of DCPD resin, which has been exploited to deliberately control its rheological transformations, shortens its pot life, reduces the frontal reactivity, and can change its rheological profile during manufacturing processes. In addition, changes in resin reactivity and viscosity can affect the activation time of the FP reaction. The rate of background polymerization and changes in resin properties is also a temperature-dependent phenomenon and follows Arrhenius relationship.[86] As

a result, it is crucial to understand how the frontal properties of FP resins change as a function of time and temperature for better control over resin properties and developing new applications using FP.

Here, we present the results of a systematic study on time- and temperature-dependent FP of DCPD. While the effect of initiator,[98] inhibitor,[33,34] copolymerization,[99] and isomerization[100] on the formation and travelling behavior of FROMP of DCPD has been previously reported, no studies have focused on characterizing and understanding the effect of staging of resin on its frontal properties. Varying the staging (i.e., incubation) time and temperature as well as inhibitor concentration allows us to tune the initial properties of resin and elucidate their effect on various front properties, including activation time, front velocity, and front temperature. An experimental setup is designed to properly stage resin formulations with a fixed catalyst concentration but with variable inhibitor concentrations at various incubation times and temperatures. A local thermal stimulus is used to initiate the FP reaction, after which front properties are measured using contact and non-contact measurement techniques. In addition, rheological and thermal characterizations are performed to gain a better insight into resin curing and processability. The results of this study therefore reveal the effect of staging conditions on various aspects of FP resins and can be used to develop new applications using this promising polymerization technique.

2.2. Experimental section

2.2.1. Materials

Dicyclopentadiene (DCPD), 5-ethylidene-2-norbornene (ENB), and second-generation Grubbs catalyst (GC2) were obtained from Sigma-Aldrich and used as received without further purification. Tributyl phosphite (TBP) and phenylcyclohexane (PCH) were purchased from TCI America. GC2 and TBP are sensitive to temperature and air, and they were stored in a proper

condition prior to use as described in Appendix A. A 26-gage Kanthal resistive wire (diameter 0.40 mm; resistivity 0.98 Ω.m at room temperature) was used to thermally trigger FROMP upon passing electric current and based on resistive heating effect.

2.2.2. Frontal polymerization

Given that DCPD is solid at room temperature, 5 wt% ENB was added to DCPD to depress its melting point (see Appendix A for preparation of DCPD/ENB solution). All future references to DCPD herein refer to this mixture. The prepared mixture was then degassed at 20 kPa for 4 hours. For all experiments, 3.21 mg of GC2 was weighed out into an Eppendorf tube and dissolved in 400 μL phenylcyclohexane. Various concentrations of TBP inhibitor (i.e., 1, 2, and 4 molar equivalents with respect to GC2) were added to the solution using a volumetric syringe. The catalyst/inhibitor solution was then added to 5g DCPD to obtain a 100-ppm concentration of GC2 in DCPD resin solution. The solution was then transferred to a test tube inside a preheated incubator oven and incubated at various temperatures (i.e., 25, 35, and 45 °C) for different time intervals. FP reaction was triggered using a resistive wire immersed at about 5 mm below the free surface of the liquid solution by applying a constant current of 2.5 A for 2 minutes. After applying electric current, the temperature of test tube was recorded using a FLIR T540 thermal infrared camera placed inside the incubator oven to track front initiation and propagation. Front velocity was calculated based on the slope of a best-fit straight line for front position versus time. Front position was identified as a sharp thermal gradient in infrared images. Front temperature was obtained using a T-type thermocouple immersed in the resin and placed about 3 cm below the position of resistive wire. Temperature profile was collected using a thermocouple reader (Phidgets Inc., model 1048) and a custom LabVIEW code (National Instrument) at 3 Hz. All experiments

were performed in duplicate. A schematic of the experimental setup is shown in Figure 2.1a (see Appendix A for more details).

2.2.3. Rheological measurements

Isothermal rheological properties were measured using a Discovery Hybrid Rheometer (DHR-2, TA instrument) equipped with 25 mm and 40 mm diameter parallel aluminum plates. Resin solutions were prepared by mixing GC2 and an appropriate amount of phosphite inhibitor (1, 2 and 4 equivalents with respect to GC2) in PCH solvent and mixing the resulting solution in DCPD resin. Around 1,200 μL of resin solution was then placed between two rheometer plates and the gap between the plates was adjusted to be ~1,000 μm. Time-sweep measurements were performed in the linear viscoelastic regime at a constant strain of 0.1% and frequency of 1 Hz at desired incubation temperatures. The gel time was determined from the crossover of the storage modulus, G', and loss modulus, G''. All rheological measurements were carried out in duplicate.

2.2.4. Differential scanning calorimetry measurements

Differential scanning calorimetry (DSC) was carried out using a TA instrument modulated DSC 2500 to determine the heat of reaction of various resin samples. DCPD resin specimens (2-3 mg) were transferred to aluminum hermetic pans and sealed. Specimens were subjected to dynamic ramp scans from -50 °C to 120 °C at 5 °C/min. The enthalpy of curing was calculated by integrating heat flow over the residual exotherm peak after baseline correction.

2.3. Results and discussion

A systematic study was performed to determine the effect of inhibitor concentration and staging conditions on the pot life and frontal reactivity of DCPD resin. In this regard, different solutions with variable inhibitor concentration were prepared in glass test tubes and stored in an

incubator oven for different incubation time intervals. Apart from room temperature (25 °C) staging, two other incubation temperatures (i.e., 35 °C and 45 °C) were considered to thermally accelerate the gelation process. After preparing the solutions, FROMP was triggered by powering a resistive heating wire placed inside the test tube (Figures 2.1a and Figure A1 in Appendix A). A thermal video camera was used to capture front position during FP (Figure 2.1b). For all studied conditions, a plot of front position against time produced a straight line, the slop of which was calculated as front velocity (Figure 2.1c). Front temperature was determined as the maximum temperature in the temperature profile collected by a T-type thermocouple (Figure 2.1d).

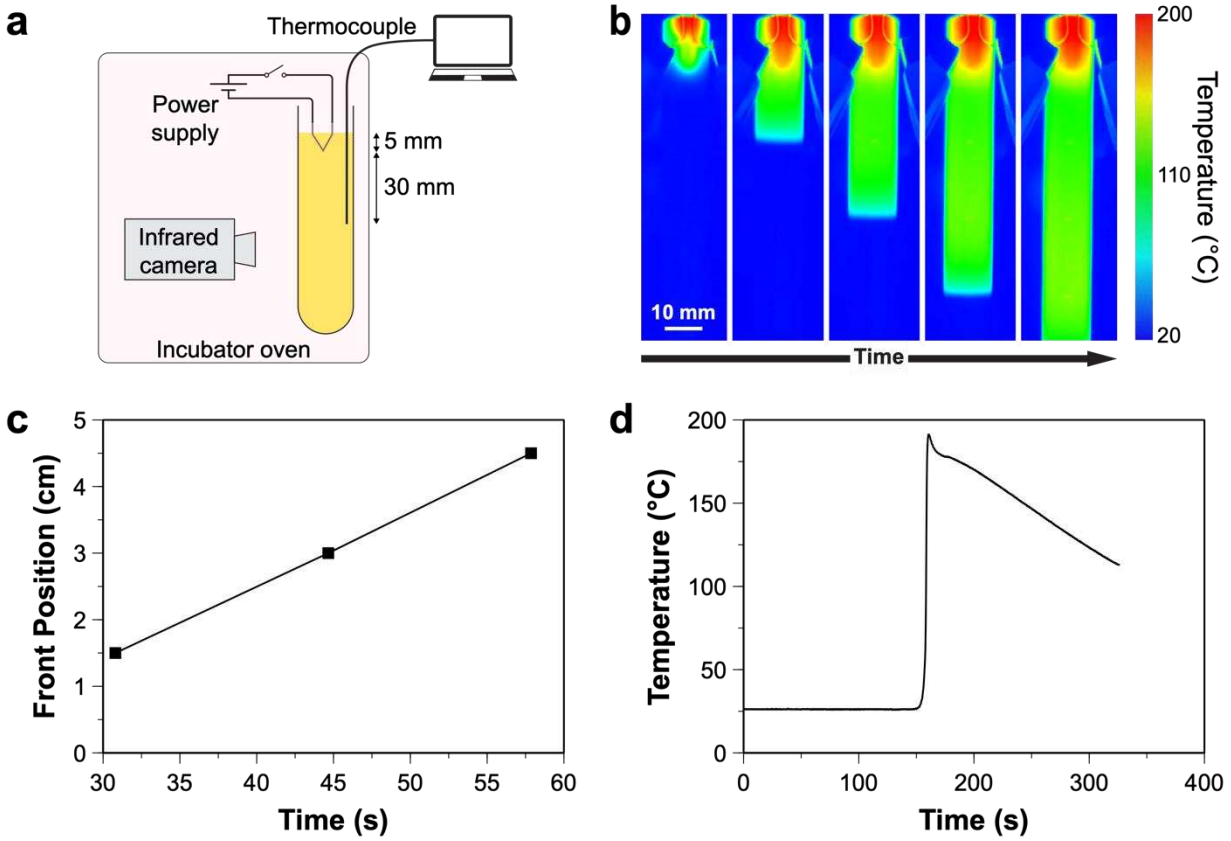

Figure 2.1. Design of experiment for measurement of front properties in staged conditions. a) Schematic representation of the experimental setup. b) Still thermal images of front position captured at various time intervals using a thermal infrared camera. c) Position of reaction front measured as a function of time. d) Temperature profile collected by a thermocouple embedded in the test tube. Figures b-d were obtained using a sample containing 1 molar equiv. of TBP inhibitor with respect to GC2 catalyst staged for 10 minutes at 25 °C.

2.3.1. Effect of inhibitor concentration

Use of alkyl phosphite inhibitors (e.g., TBP) allows for controlling the reactivity and pot life of the FP resin. The inhibitor forms a complex with the catalyst during mixing and dissociates from the catalyst upon thermal activation at front temperatures.[34] During incubation, available free catalyst molecules react with resin, leading to background polymerization and changes in the rheological profile and reactivity of resin. We first studied the effect of room-temperature staging of resin solutions containing various inhibitor concentrations (i.e., 1, 2, and 4 molar equivalents of TBP with respect to GC2) on the front properties of DCPD resin. After incubating the resin solutions in a temperature-controlled environment at predetermined time intervals, the FP reaction was initiated via resistive heating of a nichrome wire embedded in the resin solution. Front velocity, activation time, and front temperature were then measured using various experimental techniques.

As expected, for a given incubation time, an increase in inhibitor concertation resulted in reduced front velocity due to lower resin reactivity (Figure 2.2a). It has been hypothesized that phosphite inhibitors enthalpically favor to coordinate to the metal center of the ruthenium alkylidene and form a latent precatalyst complex that inhibits the spontaneous polymerization of DCPD resin.[34,101] At front temperatures, this complex dissociates due to entropic effects, releasing the catalyst and enabling the FP reaction. Higher concentrations of inhibitor can therefore inhibit more catalyst molecules and reduce resin reactivity at room temperature and also decrease the rate of polymerization at front temperatures.

Opposing trends were observed for the effect of incubation time on front velocity (Figure 2.2a). For resin formulations with 2 and 4 molar equivalents of TBP, increased incubation time resulted in lower front velocities, while for the resin formulation with 1 molar equivalent of TBP,

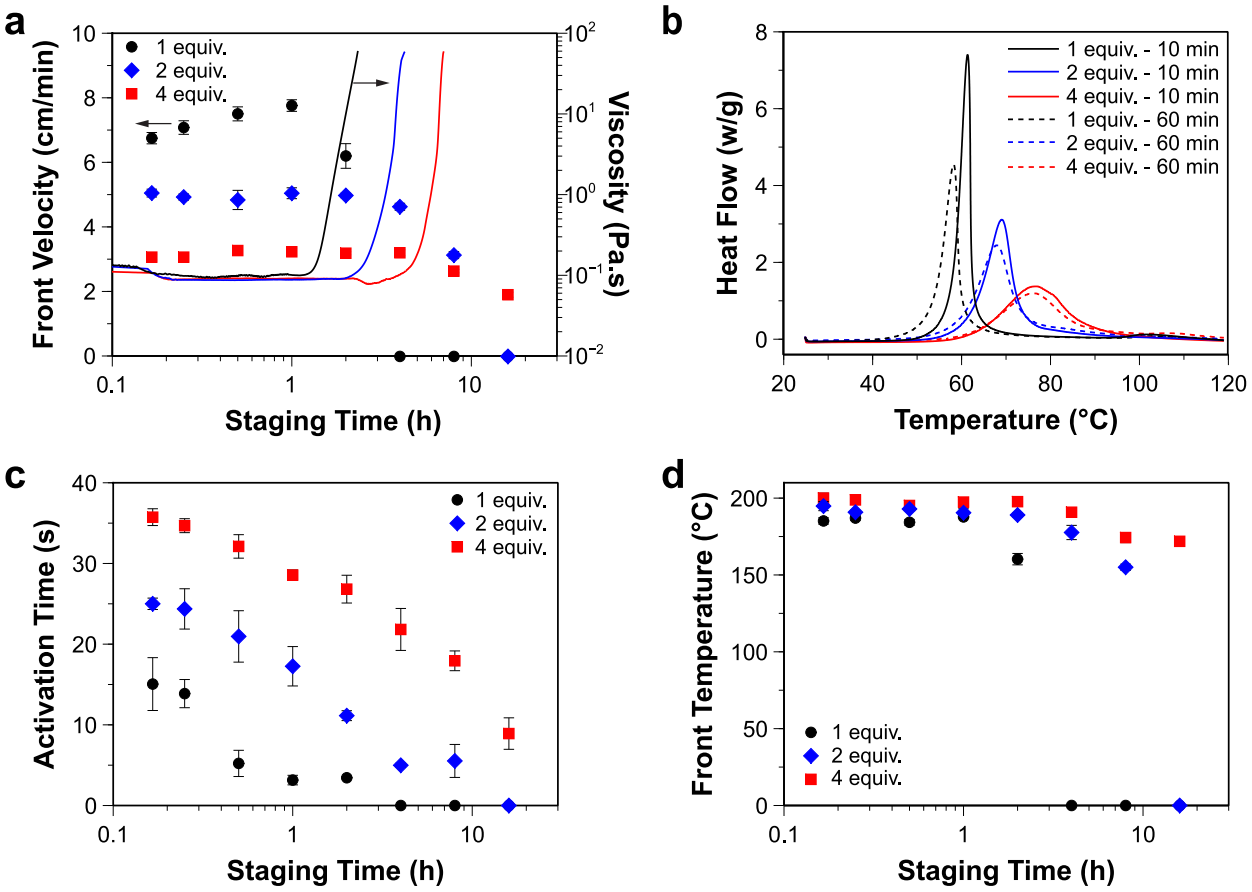

Figure 2.2. Effect of inhibitor concentration (1, 2, and 4 molar equiv. with respect to GC2) on front properties of samples staged at 25 °C for various time intervals. a) Front velocity and rheological profiles measured as a function of staging time. b) Heat of reaction, measured by DSC experiments, for samples staged at 25 °C for 10 and 60 minutes. c) Activation time of FP measured as a function of staging time. d) Front temperature measured as a function of staging time. A value of zero in a, c, and d represent cases where either the FP reaction did not propagate upon thermal activation or the resin sample spontaneously polymerized.

front velocity initially increased and then decreased at higher incubation times. This observation is caused by two independent and competing phenomena. During resin staging, the background polymerization consumes a fraction of available monomer and reduces the energy density of the FP resin. As a result, a decrease in frontal reactivity and velocity is typically expected for longer incubation times as observed for formulations with high inhibitor concentrations.[34,36] However, the reactivity of resin is also affected by the stability of ligand-metal association in the catalyst-inhibitor complex. For resin formulation containing 1 molar equivalent of TBP, the ligand-metal association is less stable compared to the two other formulations. We hypothesize that the ligand-

metal association loosens with time, leading to the release of free catalyst and an increase in the overall rate of polymerization. At higher inhibitor concentrations (i.e., 2 and 4 molar equivalents of TBP), however, the released catalyst molecules are quickly capped and form new ligand-metal association due to the availability of free inhibitor molecules.[34] Results of differential scanning calorimetry (DSC) experiments on samples containing 1, 2, and 4 molar equivalents of TBP incubated for 10 and 60 minutes support this hypothesis (Figure 2.2b). An increase in the incubation time from 10 minutes to 60 minutes slightly broadens the exothermic peak of the formulation containing 1 molar equivalent of TBP, but does not change the peak broadness in two other formulations. In addition, increased staging time results in reduced enthalpy of reaction and slightly shifts the exothermic peak to lower temperatures as curing proceeds (Table 2.1). The shift in the temperature of the exothermic peak becomes more pronounced for lower inhibitor concentrations, indicating higher sensitivity and instability of the FP resin system. As a result, for resin formulations containing 2 and 4 molar equivalents of TBP, front velocity is mainly influenced by the monomer consumption during resin staging; however, the front velocity of the formulation containing 1 molar equivalent of TBP initially increases due to the higher instability of catalyst-inhibitor complex and then decreases due to monomer consumption and reduced energy density of resin. Isothermal rheological profiles of the three resin formulations are also shown in Figure

Table 2.1. Summary of DSC measurements indicating the heat of reaction (ΔH) and peak temperature (T_{peak}) of the polymerization reaction.

Staging temperature (°C)	**TBP concentration (molar equiv.)**	**Staging time (min)**	**ΔH (J/g)**	**T_{peak} (°C)**
25	1	10	243.0	61.5
	2	10	247.0	69.1
	4	10	321.5	76.9
	1	60	199.5	58.4
	2	60	214.4	68.0
	4	60	266.3	76.6
35	1	10	240.4	58.4

2.2a, which indicate substantial drop in front velocity as resin gels, further verifying the effect of monomer consumption at prolonged staging times.

Activation time ($t_{act.}$) of FP reaction is defined as the time required from the application of thermal trigger to the formation of self-propagating reaction front and is calculated as,[33,97]

$$t_{act.} = t_m - \frac{d}{V_f} \quad (1)$$

where t_m is the time between the onset of applying electric current and the observed increase in the temperature of thermocouple (Figure 2.1d), V_f is front velocity, and d is the distance between resistive wire and thermocouple junction (d = 3 cm for all experiments). The results of activation time measurements for various staging times and inhibitor concentrations are shown in Figure 2.2c. Interestingly, the activation time for all inhibitor concentrations reduces as staging time is increased, further verifying the sensitivity of resin formulations at longer incubations. In addition, increased resin viscosity due to background polymerization with time restricts resin mobility and convective heat transfer, allowing for effective, localized heating of resin volumes surrounding the resistive wire. An increase in activation time is observed by increasing the inhibitor concentration, which is again caused by reduced resin reactivity. A similar trend on the effect of inhibitor concentration on activation time has also been reported on FROMP of DCPD in presence of GC2 and limonene inhibitor.[33]

Front temperature as a function of staging time for various inhibitor concentrations is shown in Figure 2.2d. For a fixed incubation time, higher front temperatures were obtained using higher concentrations of inhibitor, mainly due to lower background polymerization and higher energy density of resin available for polymerization. However, front temperature starts to drop as resin gels and its energy density is reduced by background polymerization and monomer consumption. This finding is consistent with the results of heat flow measurements obtained by DSC

experiments. According to Table 2.1, the heat of reaction increases with an increase in inhibitor concentration for both 10- and 60-minutes incubations, while it decreases by increasing the incubation time from 10 minutes to 60 minutes. This observation, however, is in contrast to the results of a previous study on FP of polyurethanes, where an increase in the amount of inhibitor resulted in a decrease in front temperature due to higher rates of heat loss by a slower moving front.[87,102,103]

2.3.2. Effect of incubation temperature

FP reactions and their front properties are highly dependent on the initial resin temperature. We studied the effect of incubation temperature on front velocity, activation time, and front temperature to quantitatively determine and evaluate this temperature dependance. Three incubation temperatures, i.e., 25, 35, and 45 °C, were initially considered for the experiments. However, we noticed that the resin pot life becomes severely limited at 45 °C and resin samples either spontaneously polymerize after a few minutes of incubation when using 1 or 2 molar equivalents of TBP or become unreactive to FP after 60 minutes of incubation when using 4 molar equivalents of TBP (Figure 2.3). As a result, for the remainder of this study, only incubation temperatures of 25 and 35 °C were examined and the inhibitor concentration was fixed to 1 molar equivalent with respect to GC2.

Results of front velocity measurements (Figure 2.4a) indicate a slight increase in front velocity as the incubation temperature was increased from 25 °C to 35 °C. DSC experiments were used to assess and compare the resin reactivity at two incubation temperatures after 10 minutes of staging (Figure 2.4b). When the incubation temperature was increased to 35 °C, the exothermic peak broadened and shifted to lower temperatures, indicating the sensitivity of resin and higher rate of

polymerization. However, the pot life of resin was reduced at 35 °C because of the same reason, where spontaneous polymerization was observed in resin samples after 1 hour of staging.

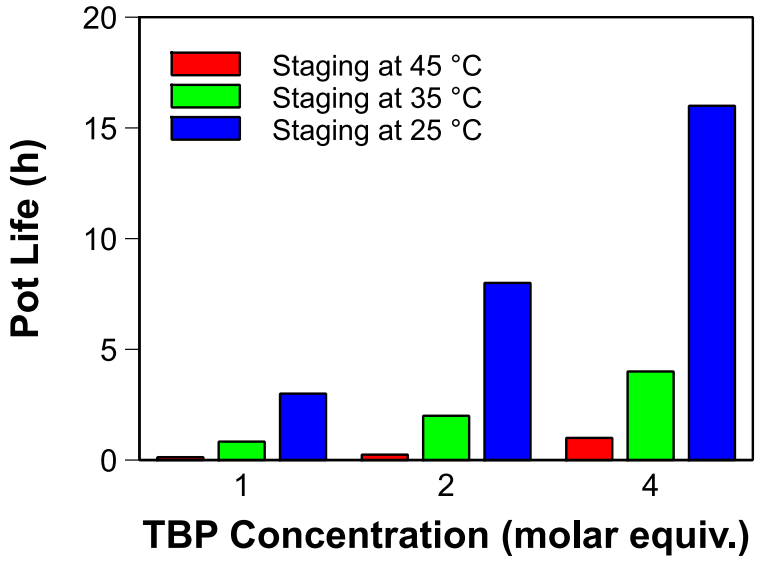

Figure 2.3. Effect of staging temperature on the pot life of resin samples containing various concentrations of TBP inhibitor. Pot life is defined as a point at which there is no longer enough chemical energy in the reactive formulation for the self-sustaining FP reaction to occur.

The activation time of FP reaction substantially decreased as the incubation temperature was increased (Figure 2.4c). This change in activation time is attributed to the higher resin sensitivity that can reduce the activation temperature and also to the less amount of time it takes to reach to activation temperature from initially raised resin temperature. Similar to room-temperature measurements as discussed previously, faster activation times were observed for higher staging times at 35°C, due to increased resin sensitivity and viscosity (Figure 2.4a,b). Similarly, an increase in front temperature was observed for samples incubated at 35°C (Figure 2.4d). The difference in front temperatures of samples tested at two staging temperatures was ~10 °C, which corresponds to the difference in initial temperature of resin in these two staging conditions prior to FP.

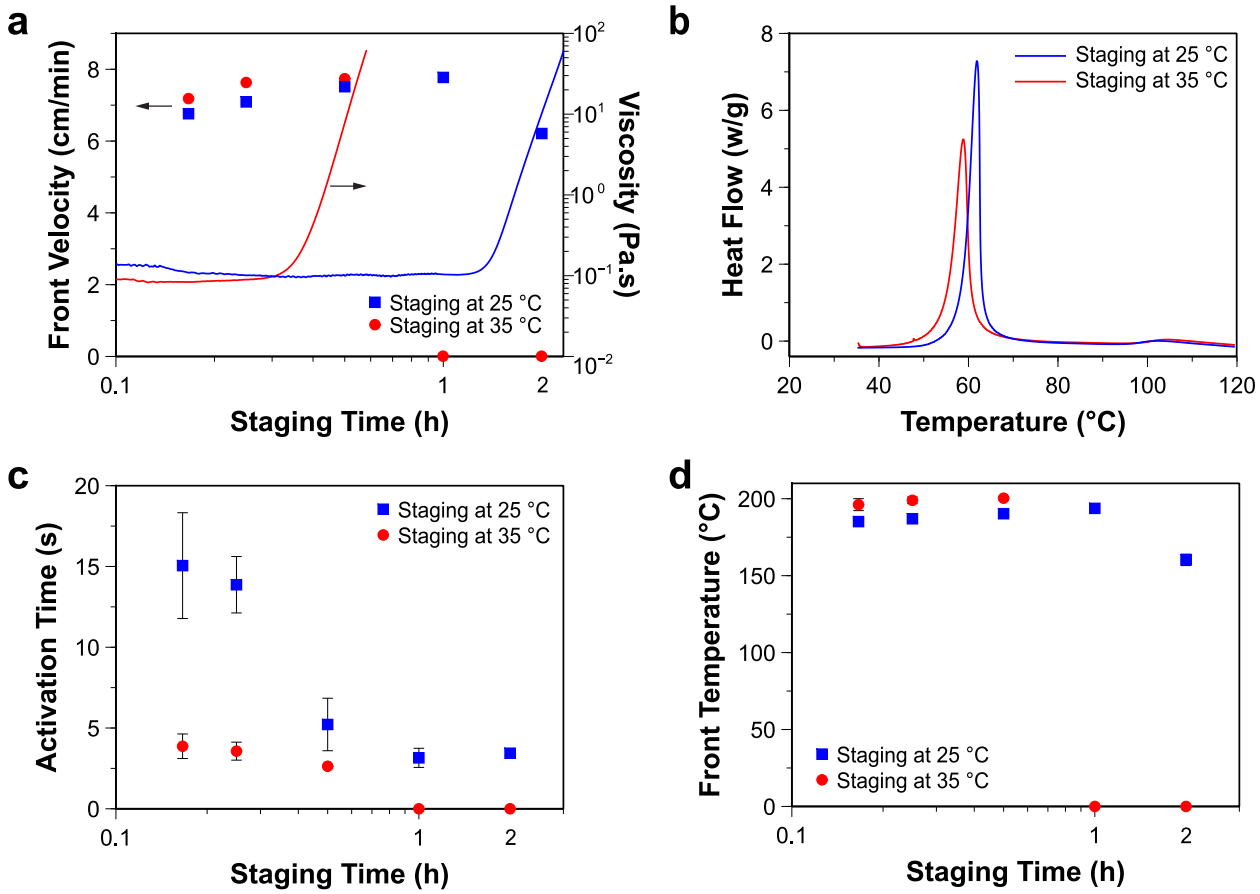

Figure 2.4. Effect of staging temperature on front properties of samples containing 1 molar equiv. of TBP relative to GC2 and staged for various time intervals. a) Front velocity and rheological profiles measured as a function of staging time. b) Heat of reaction, measured by DSC experiments, for samples staged at 25 °C and 35 °C for 10 minutes. c) Activation time of FP measured as a function of staging time. d) Front temperature measured as a function of staging time. A value of zero in a, c, and d represent cases where either the FP reaction did not propagate upon thermal activation or the resin sample spontaneously polymerized.

A key advantage of staging FP resins at elevated temperatures is the acceleration of the background polymerization and gelation process. However, the resin will have a shorter pot life and it would be difficult to perform large-scale manufacturing at elevated temperatures compared to room temperature processing. We carried out an experiment to demonstrate the feasibility of high-temperature staging of DCPD resin followed by room-temperature frontal polymerization where a higher resin pot life is expected. Resin samples were first incubated at 35 °C for various time intervals to change their viscosity. The resin temperature was then quickly reduced to 25 °C and FP was initiated to determine the room-temperature front properties of high-temperature-

staged resin samples. The results of this experiment are shown in Figure 2.5. For comparison, front properties for isothermal staging and frontal polymerization at 25 °C and 35 °C are also presented. Samples staged at 35 °C and frontally polymerized at 25 °C had lower front velocities than isothermally staged and frontally polymerized samples due to lower energy levels of resin after this conditioning process (Figure 2.5a). Similar activation times were observed for samples staged at 35 °C but frontally polymerized at 25 °C and 35 °C (Figure 2.5b). The activation times of both types of samples staged at 35 °C were lower than those of isothermally staged and frontally polymerized samples at 25 °C. These results further verify the role of resin viscosity and temperature sensitivity on controlling the activation times of FP resins. The insights gained from this experiment can be used to design new processes for fast preparation of 3D printing inks, develop FP composite prepregs, and develop new products and applications where tuning of viscosity and pot life is required.

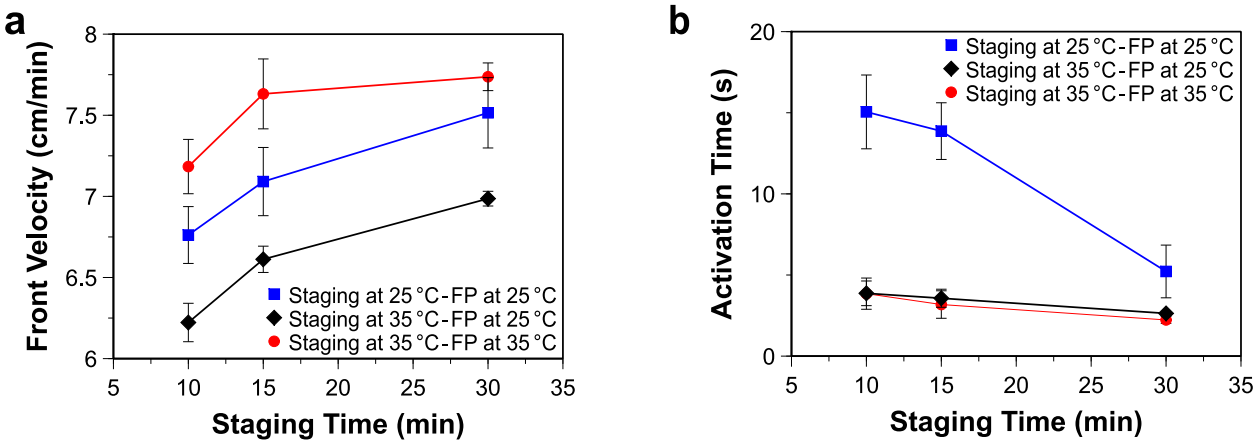

Figure 2.5. Front properties of samples staged 35 °C and frontally polymerized at room-temperature (25 °C). Front properties for isothermal staging and frontal polymerization at 25 °C and 35 °C are also presented. a, b) Front velocity and activation time measured as a function of staging time, respectively.

2.4. Conclusions

In thermal frontal polymerization, resin behavior and front properties are highly affected by ambient temperature and staging conditions, which should be considered in the design of new manufacturing processes and applications using this promising polymerization technique. In this study, we experimentally characterized the effect of staging time and temperature on FROMP of DCPD by measuring the front velocity, activation time, and front temperature. Varying the inhibitor concentration allowed for controlling the resin pot life, gelation time, and reactivity. Front velocity was found to be influenced by two opposing mechanisms, namely by reduced energy density of resin due to background polymerization and instability of catalyst-inhibitor complex, whereas activation time was affected by resin viscosity and resin reactivity. Front temperature decreased as resin staged, specifically where substantial changes in resin viscosity occurred. An increase in staging temperature resulted in faster front propagation, lower activation times, and hotter fronts, while reducing the pot life of resin. The insights gained from this study can be extended to other resin systems with similar polymerization schemes and can be used for development of 3D printing inks, composite prepregs, and new applications where exquisite control over resin viscosity and front properties are required. In addition, the results of this study can provide useful information for developing detailed analytical or computational models to accurately predict front properties.

Chapter 3: 3D Printing of Short Carbon Fiber-Reinforced Thermoset Polymer Composites via Frontal Polymerization

3.1. Introduction

Fiber-reinforced polymer composites (FRPCs) are widely used in many structural applications owing to their excellent specific mechanical properties, chemical resistance, and thermal stability.[104] Conventional manufacture of FRPCs relies on manual handling and placement of raw materials on subtractively manufactured tooling followed by a long cure process in an oven or autoclave, leading to a high cost of manufacturing, low production rates, labor-intensive processes, and uncertainties in product quality.[76] In addition, manufacturing of parts with complex geometries is quite challenging or even impossible using the traditional tooling and mold design. Additive manufacturing (AM), also known as 3D printing, has recently revolutionized the manufacture of three-dimensional (3D) objects and is promising for cost-effective, rapid, and reliable manufacturing of composite materials and structures.[72]

Recent efforts in AM of discontinuous- and continuous-FRPCs have mainly focused on thermoplastic-matrix composites processed via fused deposition modeling (FDM).[105–108] While FDM allows for easy production of composite prototypes, the resulting products are typically not suitable for use in structural applications due to the low service temperature and inferior mechanical performance of the matrix polymers, high processing temperatures, and large void contents and low fiber volume fractions of produced composites.[75,109] Thermosetting resins offer the superior thermo-mechanical properties and low viscosities required for AM of high-quality FRPCs; however, a major processing issue in AM of thermoset-based polymers and composites is

the underlying curing process for transforming the resin to a solid polymer during the rapid printing processes.[110–112]

Several approaches for AM of thermoset composites have been previously developed based on the direct ink writing (DIW) technique, where a shear-thinning ink containing fiber reinforcements is deposited via extrusion through the printing nozzle at room temperature and cured simultaneously or post-printing via light irradiation, thermal curing, or a hybrid thereof.[67,113–116] In photocuring approach, use of ultraviolet (UV) or visible light allows for *in-situ* curing of the ink following extrusion from the printing nozzle; however, most photocurable resins do not have the sufficient curing rate to preserve the dimensional accuracy of the original print model, cannot be used with opaque or highly filled inks, often require additional post-processing steps, and result in polymers with poor mechanical properties.[74,75,117–119] Alternatively, thermal curing of 3D-printed thermoset composites has been demonstrated by post-curing the deposited material in an oven or via reactive extrusion technique, where two separate streams of resin and hardener are passively mixed and deposited on a heated substrate in a layered structure and cured rapidly at ambient conditions.[63,120–123] These approaches have a limited processing window, are limited to simple 2D geometries with a few layers of material, and cannot be used for AM of freeform structures.

Frontal polymerization (FP) is an alternative and promising thermal curing strategy for rapid and energy-efficient curing of thermoset composites during AM processes. In FP, polymerization of a thermoset resin is initiated locally via a thermal stimulus, which then rapidly proceeds in an autoactivating and self-sustaining fashion by exploiting the exothermic heat of reaction released at the reaction front.[124,125,33,32] Integration of thermal FP in the DIW technique allows for simultaneous printing and curing of thermosetting materials with a high print fidelity and ability

to print freeform structures.[36] Recently, frontal ring-opening metathesis polymerization (FROMP) of dicyclopentadiene has been used to print neat thermoset polymer structures by matching the printing (deposition) speed of the ink with the velocity of the FP reaction.[36] The resulting polymer is polydicyclopentadiene (PDCPD), which is a high-performance thermoset polymer with a good combination of stiffness, strength, fracture toughness, thermal stability, and chemical resistance.[30,31,126]

Here, we present a novel approach for 3D printing of fiber-reinforced thermoset polymer composites via *in-situ* curing of the matrix resin during the printing process. Using a combination of the DIW technique and frontally curable DCPD-based composite inks containing discontinuous carbon fiber (CF) reinforcements allows for unprecedented 3D printing of high-quality composite structures. Incorporation of CFs into the ink is crucial for enhancing the rheological properties and printability of the inks as well as the mechanical properties of the final composite material. We demonstrate that by tuning the processing conditions we can print freeform or supported composite structures at different printing speeds. Our approach results in high-fidelity printing of high-quality composite structures without any post-curing or post-processing steps

3.2. Experimental section

3.2.1. Materials

Dicyclopentadiene (DCPD), 5-ethylidene-2-norbornene (ENB), and second-generation Grubbs' catalyst (GC2) were purchased from Sigma-Aldrich and used as received without further purification. Tributyl phosphite inhibitor (TBP, 93%) was obtained from TCI Chemicals. Cyclohexylbenzene (Acros Organics, 98%) was used to dissolve GC2. Short carbon fibers ($L_{avg.}$ = 72 μm, $D_{avg.}$ = 7.2 μm) used in all experiments were kindly donated by Zoltek Corporation.

3.2.2. Preparation of 3D printing inks

We use a frontally curable DCPD-based resin (Figure 3.1a) for developing composite inks.[36,127] Given that DCPD is solid at room temperature, first DCPD is melted in an oven at 60 °C and mixed with 5 wt% ENB to suppress the melting point of DCPD. The solution is stirred for one hour to obtain a homogenous mixture and degassed at 20 kPa overnight. All subsequent references to DCPD resin herein refer to the 95:5 DCPD/ENB solution. For all specimens, 6.42 mg GC2 (100 ppm with respect to DCPD) and 2.38 μL TBP (1 molar equivalent with respect to GC2) are completely dissolved in 500 μL cyclohexylbenzene by sonication for 10 minutes, followed by mixing the solution with 12 g of DCPD. The freshly prepared DCPD solution is transferred to an oven to partially cure the resin at 30 °C for one hour to increase the resin viscosity for effective mixing of CFs and preventing precipitation of dispersed fibers. Various concentrations of CFs (0, 5, 10, and 15 vol%) are added to the resin solution and mixed for 5 minutes using a planetary centrifugal mixer (AR-100, Thinky USA) to obtain a uniform suspension. The resulting ink is then placed in an oven at 30 °C for another 20 minutes to allow further cross-linking and pre-curing of

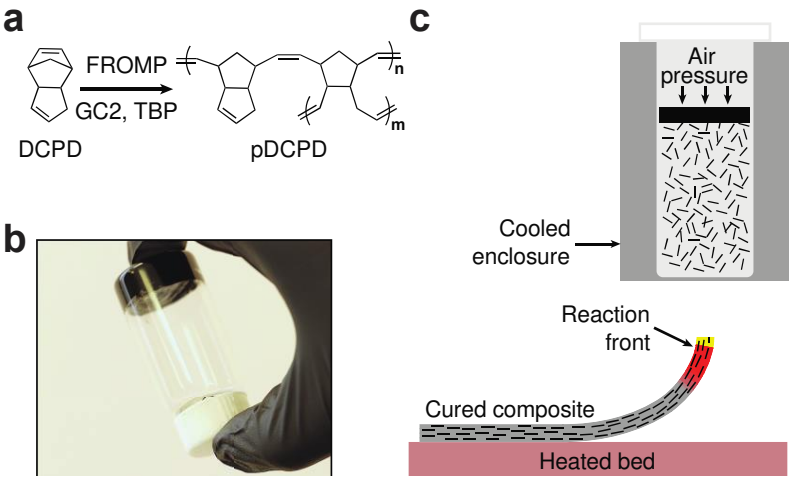

Figure 3.1. Overview of the 3D printing technique. (a) Scheme of the FROMP of DCPD resin in the presence of second-generation Grubbs catalyst (GC2) and tributyl phosphite (TBP) inhibitor. (b) Prepared composite inks are highly viscous and suitable for use in DIW technique. (c) Schematic representation of the 3D printing setup. Upon printing the ink on a hot substrate, frontal polymerization initiates and propagates along the length of the filament.

DCPD resin to form a highly viscous ink amenable to 3D printing (Figure 3.1b). The prepared ink is transferred to a 10-mL syringe barrel and centrifuged at 2,000 rpm for 5 minutes to remove any bubbles (see Appendix B for more details).

3.2.3. Rheological characterization of 3D printing inks

The rheological properties of the prepared inks are determined using a Discovery HR-2 Rheometer (TA Instruments) with a 40-mm flat geometry and a gap size of 1,000 μm at a reference temperature of -5 °C. Dynamic oscillatory measurements are performed over a range of shear stress from 1 to 10,000 Pa at a frequency of 1 Hz to determine storage and loss moduli (G' and G'') as a function of shear stress. Steady-state flow experiments are conducted at controlled shear rates ranging from 0.01 to 100 1/s to measure the rheological response of inks containing various concentrations of carbon fibers.

3.2.4. 3D printing via FP

The syringe barrel filled with the ink is placed in an aluminum syringe holder mounted on a three-axis gantry robot (F5200N, Fisnar). The ink is pneumatically driven through a micronozzle with an inner diameter (ID) of 1.60 mm, unless otherwise specified, using a digital high precision dispenser (DC100, Fisnar). The ink temperature is decreased to -5 °C using two thermoelectric Peltier coolers embedded inside the aluminum syringe holder to prevent further crosslinking of the composite ink and maintain a constant ink viscosity during printing and also to extend the pot life of the ink to more than 10 hours. The ink is printed on a 3D printing heated bed with an average temperature of 80 °C. A few seconds after depositing the ink on the heated substrate, the front thermally initiates and propagates along the filament, transforming the ink to a solid part (Figure

3.1c). 3D structures are printed using air pressures of 40 - 400 kPa depending on the ink viscosity and manually written g-codes (See Appendix B).

3.2.5. Flexural tests

We perform three-point flexural tests on bar specimens using a servo-hydraulic material testing system (858 MiniBionix; MTS 16 Systems) equipped with a 5-kN force capacity transducer. The flexural strength and modulus of printed and control samples are determined according to the ASTM D790 standard at ambient temperature, crosshead speed of 1.5 mm/min, and span length of 52 mm. Bar specimens with dimensions of 65 mm × 12 mm × 3 mm are printed using each ink formulation and at least three specimens are tested for each sample. The flexural strain, ε, on the outer surface of test specimens at midspan is calculated as,

$$\varepsilon = \frac{6Dd}{L^2} \tag{1}$$

where D is the crosshead displacement, d is the thickness of the beam, and L is the support span length. Flexural stress, σ, is calculated as,

$$\sigma = \frac{3PL}{2bd^2} \tag{2}$$

where P is the applied load at the center of the beam and b is the width of the beam. It is assumed that the beam fails at the midspan of the beam. Flexural modulus and strength are estimated as the slope of the flexural stress-strain curve and the maximum stress sustained by the test specimens according to the ASTM D790 standard, respectively.

As a control, frontally polymerized samples with the same resin formulation and fiber contents as the 3D-printed samples are prepared using the traditional casting (molding) method. Control specimens are manufactured by pouring the neat or composite resins in a silicone mold with a 65

mm × 12 mm × 3 mm cavity sandwiched between two glass plates, followed by curing the resin at room temperature by applying a hot soldering iron on top of the mold to initiate FP.

3.2.6. Differential scanning calorimetry

Differential scanning calorimetry (DSC) measurements are carried out using a modulated DSC (DSC 2500, TA Instrument) to measure the degree-of-cure and glass transition temperature (T_g) of the cured samples. Uncured resin specimens (2-3 mg) and cured specimens (5-10 mg) are placed in aluminum hermetic pans, sealed, and heated from 25 to 250 °C at a heating rate of 5 °C/min to measure the total heat of reaction (H_t) and residual heat of reaction (H_r), respectively. The degree-of-cure (a) is calculated as,

$$\alpha = 1 - \frac{H_r}{H_t} \tag{3}$$

Glass transition temperature, T_g, is determined as the inflection point of the heat flow curve.

3.2.7. Optical microscopy

We use optical microscopy to visually assess the quality of printed parts as well as the orientation of fibers in printed filaments. Microscopy specimens are cast in a mounting epoxy resin and polished using a polisher machine (PACE Technologies). Polished specimens are then imaged using a digital microscope (VHX-6000, Keyence). More information for preparation of microscopy specimens is available in Appendix B.

3.3. Results and discussion

3.3.1. Rheological behavior of composite inks

Inks used in DIW techniques should exhibit a shear-thinning behavior to allow easy extrusion and flow of the ink through fine deposition nozzles in response to an applied external pressure but to maintain the printed filamentary shape following deposition from the nozzle.[128–130] Figure 3.2a

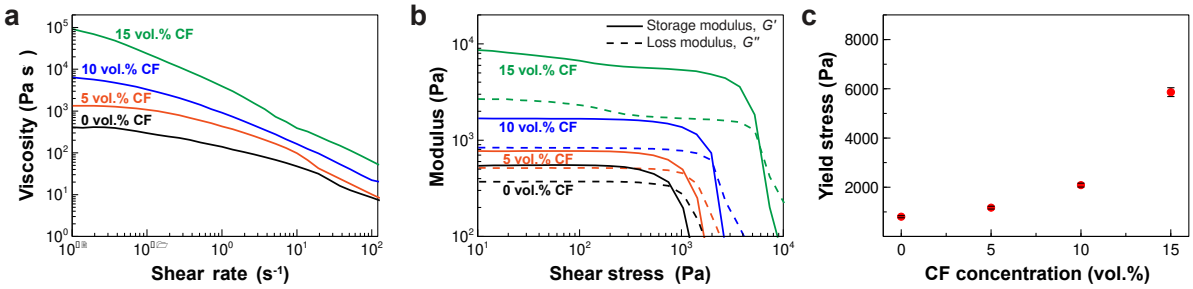

Figure 3.2. Rheological profiles of printing inks. (a) Results of steady-state shear experiments indicating the effect of shear rate on the viscosity of inks. (b) Viscoelastic response of inks determined by oscillatory rheology measurements. (c) Yield stress of inks as a function of carbon fiber (CF) content determined from the crossover of storage modulus (G') and loss modulus (G") curves shown in (b).

depicts the rheological behavior of the neat DCPD gel and composite inks containing various concentrations of carbon fibers under steady-state shear experiments. The neat DCPD gel (i.e., 0 vol% CF) has a shear-thinning behavior, where its viscosity drops by around one order of magnitude from ~400 Pa s to ~10 Pa s as the shear rate is increased from 10^{-2} 1/s to 50 1/s, a typical shear rate experienced during 3D printing.[57,131] When carbon fibers are added, the ink viscosity increases substantially and stronger shear-thinning responses are observed. For example, the composite ink containing 15 vol% CF possesses a viscosity close to 10^5 Pa s at low shear rates (~10^{-2} 1/s), which is three orders of magnitude higher than its viscosity (~10^2 Pa s) at the printing shear rates (~50 1/s). The stronger shear-thinning behavior of the composite inks is attributed to the formation of a transient, interconnected 3D network of fibers in the absence of external shear stresses.[132,133] Upon applying an external shear stress, the 3D network breaks down, leading to a substantial drop in viscosity and easy flow of the ink through a fine deposition nozzle; however, as soon as the shear stress is removed, the 3D network is rebuilt immediately, causing the material to become solid-like again.

Oscillatory rheology measurements demonstrate the viscoelastic properties of the composite inks (Figure 3.2b). The results of these measurements reveal that all prepared inks possess predominantly elastic behavior at low shear stresses ($G' > G''$). When the applied shear stress

exceeds the yield stress of the ink, t_y, the shear loss modulus (G'') transcends the shear storage modulus (G'), indicating the ink is transforming from the solid state to a liquid state suitable for 3D printing.[134] Addition of carbon fibers to the base DCPD ink results in an increase in the shear storage modulus as well as the yield stress of the inks (Figure 3.2b, c). A high yield stress is ideal for DIW, especially for printing freestanding or unsupported structures, as it allows the ink to maintain its filamentary shape under relatively low stresses induced by gravity.[135] When coupled by *in-situ* FP curing, such high yield stresses will enable in-the-air printing and curing of composite structures with a high print fidelity. Carbon fibers can therefore enhance the rheological properties and printability of the DCPD ink by both increasing the yield stress and improving the shear-thinning behavior of the base ink. While we were able to prepare printable inks with up to 25 vol% CF, which is higher than the concentrations reported in other works on the DIW of thermoset composites,[45,52,57,136,137] we could not use the inks with ³ 20 vol% CF for 3D printing because the yield stress of the inks were higher than the maximum operating pressure of our dispenser. Inks filled with ≤ 15 vol% CF have a yield stress within the pressure range of the pneumatic dispenser used in this study; therefore, for the remainder of this study, only inks with carbon fiber concentrations of ≤ 15 vol% were considered.

3.3.2. In-situ printing and curing of composites

Use of frontally polymerizable inks with a shear-thinning behavior allows for *in-situ* printing and curing of composite structures using the DIW technique (Figure 3.1c). For 3D printing, prepared inks are transferred into a syringe barrel, which is then placed in a temperature-controlled aluminum holder mounted on a dispensing robot. The temperature of the ink is maintained at -5 °C to minimize the background polymerization and changes in the rheological behavior of the ink during the printing process. Inks are deposited on a heated substrate with an average temperature

of 80 °C using a nozzle with an inner diameter of 1.6 mm under a constant flow rate. A few seconds after depositing the ink on the heated substrate, polymerization front initiates and propagates along the printed filament, curing and transforming the viscoelastic gel into a solid polymer. Matching the printhead velocity with the front velocity allows for printing freeform structures by simultaneously printing and curing the ink as it exits the nozzle (Figure 3.3a). The subzero temperature of the ink prevents the front from entering into the nozzle, causing the front to follow the nozzle as the printhead moves along the printing path.

We perform controlled experiments to understand the effect of carbon fiber content and boundary conditions on the printing process. Two printing strategies are developed: synchronous (self-equilibrating), freeform printing and asynchronous, supported (layer-by-layer) printing. In the self-equilibrating printing, the print speed should be matched with the front velocity to ensure simultaneous curing of the thermoset ink and capturing the print geometry and circular filamentary shape as the ink exits the nozzle (Figure 3.3b). When the print velocity is lower than the front velocity, the frontal reaction self-equilibrates to follow the nozzle due to the reduced reactivity of the cold ink prior to deposition in the air. As a result, trial and error is used to find the maximum print speed for each ink composition while minimizing the spanning length of uncured resin between the nozzle tip and reaction front for capturing the exact print geometry. Addition of carbon fibers to the DCPD ink leads to a linear increase in front velocity, and consequently, in the printing speed from 1.2 to 2.6 mm/s as a function of the carbon fiber content (Figure 3.3c). Although incorporation of carbon fibers into the resin decreases the resin volume fraction and energy density available for FP, the resulting enhanced thermal conductivity of the ink facilitates heat transfer to the monomer ahead of the front, pre-heating the resin, and increasing its reactivity and front

velocity.[36,97,138] Examples of 3D-printed structures created by the self-equilibrating printing approach are shown in Figure 3.3d, e.

In contrast to the self-equilibrating printing strategy, printing on solid substrates (layer-by-layer) does not require exact matching of the print velocity with front velocity, as the shear-thinning ink can maintain its shape following deposition on the substrate. We carry out simple experiments by depositing straight filaments of various lengths (40, 80, and 120 mm) on the heated substrate at a fixed print speed of 10 mm/s, which is higher than typical front velocities, to measure the overall cure time of the deposited material. Average front velocity is then calculated by dividing the deposited length by the overall cure time (i.e., the time from the beginning of deposition to complete curing of the filament). The neat resin and 15-vol% composite inks, which respectively have the lowest and highest thermal conductivities among various inks, are used for these experiments. Similar to the self-equilibrating printing, the average front velocity of the composite ink is higher than the neat resin ink due to its higher thermal conductivity (Figure 3.4a). The measured front velocities are higher than those of freeform printing, resulted from through-

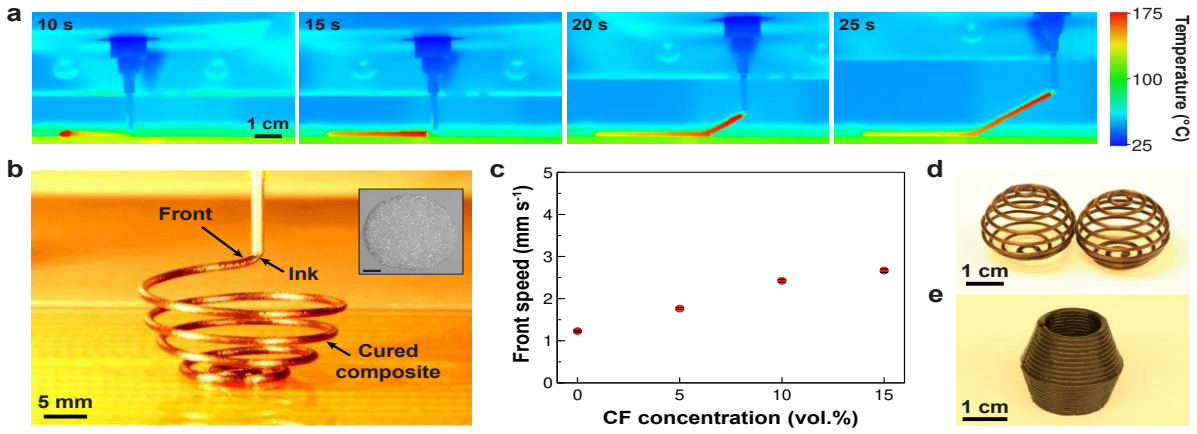

Figure 3.3. Self-equilibrating printing strategy. (a) Upon deposition of the ink on a heated substrate, front initiates and propagates along the filament length. Matching the print speed with front velocity allows for in-the-air printing of thermoset polymers and composites. (b) Freeform printing of a composite helix containing 15 vol% CF. The inset depicts the circular geometry of the printed filament. Scale bar represents 200 μm. (c) Increasing the concentration of carbon fibers results in enhanced front velocity and print speed. (d, e) Examples of composite structures created using this printing strategy. The composite material in these structures contains 15 vol% CF.

thickness heat transfer from the heated substrate and increased reactivity of the deposited material. Additionally, as the length of the printed filament increases, higher average front velocities are measured for both ink formulations. This observation can be explained by the kinetics of frontal propagation. Once the material is deposited, irrespective of the deposited length, a fixed activation time is required to initiate frontal polymerization. However, as the length of the deposited filament increases, the temperature and reactivity of the ink in regions far from the initiation point keeps increasing before the front reaches those regions, caused by the conductive heat transfer from the underlying substrate. The increased reactivity of the resin along the filament length results in faster frontal propagation and increased average front velocity as the length of the printed filament increases. In another experiment, we explore the effect of printing (deposition) speed on the overall cure time and average front velocity by printing the composite ink along a 200-mm long filament (Figure 3.4b and Figure B2 in Appendix B). The overall cure time in this experiment is affected by the combination of the time required to completely deposit the ink along the path, the activation time of the FP reaction, and the time required for the front to propagate and cure the entire ink along the printed path. At low print speeds, the overall cure time is mainly affected by the long deposition times, during which the front forms and propagates along the print path. As the printing speed increases from 5 mm/s to 80 mm/s, the deposition time becomes shorter and the overall cure time decreases from 45 s to 18 s (Figure B2 in Appendix B). At high print speeds, the entire 200-mm path is printed within a few seconds, reducing the effect of deposition time on the overall cure time and decreasing the temperature gradient along the print path as the ink heats up following deposition on the heated substrate. As a result, once the front initiates, it propagates quickly along the print path due to the high temperature and reactivity of the ink throughout the filament, leading to front velocities as high as 11 mm/s (Figure 3.4b).

The ability to print the ink at a desired rate followed by FP curing allows for additive manufacture of composite structures that are not easy to make using other techniques. For example, in traditional DIW technique, where the material is first printed and then cured in a separate step, a limited number of layers can typically be printed as the added weight of additional layers will deform the underlying layers and adversely affect the quality of the printed layers.[55,139,140] We demonstrate that we can print and cure 30 layers of a composite structure by depositing the material at 3 mm/s while ensuring that the new, uncured ink is always deposited on a cured substrate layer to prevent any gravity-induced deformations in the underlying layers (Figure 3.4c). Monitoring the thermal video of the printing process reveals that the front propagates steadily with a relatively constant lag with respect to the printing nozzle, caused by the initial activation time of the FP

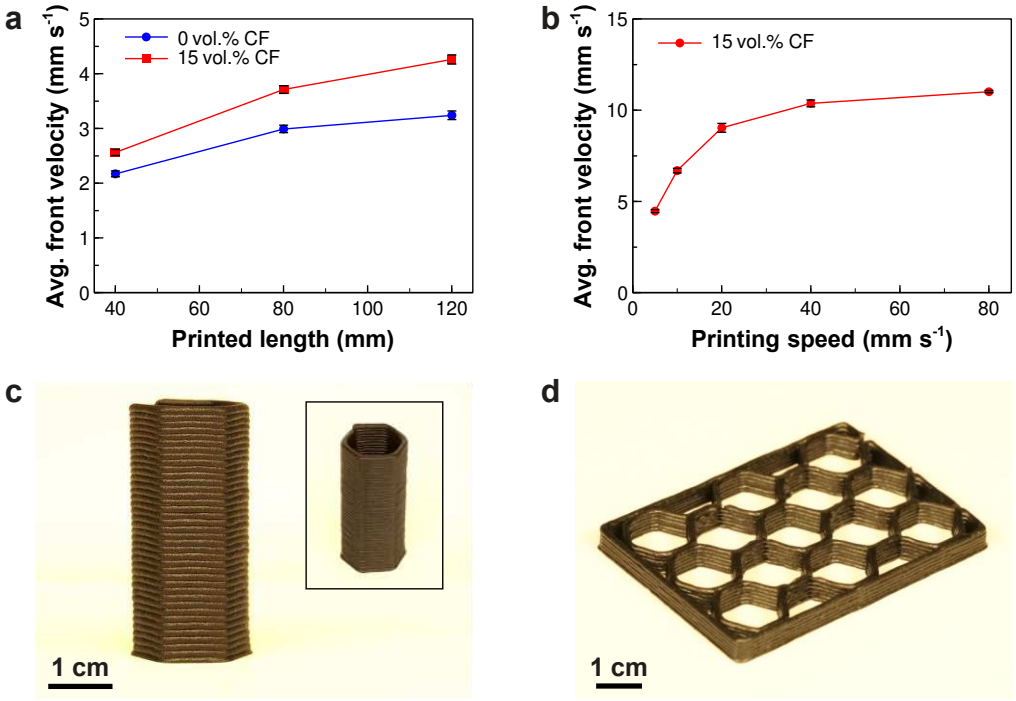

Figure 3.4. Supported (layer-by-layer) printing strategy. (a) Average front velocity measured for printing straight filaments with various lengths at a print (deposition) speed of 10 mm/s. (b) Average front velocity measured for printing a 200-mm long filament at various print (deposition) speeds. (c) A hexagonal composite (15 vol% CF) structure printed using 30 layers of material at a print speed of 3 mm/s. (d) A composite (15 vol% CF) lattice structure printed at a high print speed of 28 mm/s.

reaction (Figure B3a-c in Appendix B). The steady temperature and propagation of the front (Figure B3d in Appendix B) as the printing height increases is resulted from printing the uncured ink on a hot, cured layer that acts similarly as the heated print bed. Use of the thermally conductive composite material is crucial for maintaining a similar substrate temperature for each new printed layer in the layer-by-layer printing strategy, as the material can effectively transfer the heat from the heated print bed and the released exothermic heat from the underlying layers. Our attempts to print the same hexagonal structure using the neat resin ink and under the same printing condition are unsuccessful. The low front velocity and thermal conductivity of the neat resin ink limits the number of layers that can be printed by the layer-by-layer printing strategy, as the temperature of the front and its underlying layer drops remarkably when moving away from the print bed. Additionally, the ink cannot capture the sharp corners of the hexagon due to its inferior rheological properties compared to the composite ink (Figure B4 in Appendix B). As a result, the neat resin ink is mostly suitable for use in the self-sustaining printing strategy.

Fast printing of multi-layer structures can be achieved in the asynchronous, layer-by-layer printing strategy by increasing the print length in each layer. We realize that when depositing the composite ink on a hot substrate ($T \geq 80$ °C), either on the print bed or the last cured layer, it takes maximum 15 seconds for any part of the ink to cure (by linear frontal propagation or through-thickness activation) once it touches the hot substrate (Figure B5 in Appendix B). Therefore, for high-quality printing of multi-layer structures we need to ensure that it will take more than 15 seconds for the printing nozzle to travel along a print path within each layer before starting a new layer, such that the ink is always deposited on an already cured material. Depending on the length of the printing path in each layer, L_{layer}, the print speed, V_p, should be $\leq L_{layer}/15$. For example, in printing the hexagonal structure of Figure 3.4c, which has a perimeter of 60 mm ($L_{layer} = 60$ mm),

the selected print speed, V_p = 3 mm/s, allows for curing any points of each layer before the nozzle finishes the loop that starts from that point and deposits a new layer of ink. When the length of the print path in each layer of a structure increases, higher printing speeds can be used accordingly to accelerate the printing process. We use this criterion to demonstrate printing a composite lattice structure with L_{layer} = 557 mm and V_p = 28 mm/s (Figure 3.4d). This high printing speed enables rapid extrusion of the shear-thinning composite ink followed by frontal curing of the printed material to produce high-quality and high-fidelity composite structures. The asynchronous, layer-by-layer printing strategy is therefore quite versatile for scalable printing of composite structures as long as the deposited ink can capture and maintain the desired geometrical features of a printing design.

3.3.3. Mechanical performance of 3D printed parts

We perform flexural experiments on 3D printed specimens according to the ASTM D790 standard to determine the mechanical performance of the printed materials. Bar specimens containing various concentrations of carbon fibers are prepared by printing the inks along the length (parallel to the length) or the width (transverse to the length) of the bar using a nozzle with an inner diameter of 0.8 mm (Figure 3.5a) (see Appendix B for more details). The self-equilibrating curing strategy is used to cure the inks following the extrusion to ensure that the adjacent roads are already cured for understanding the effect of interlayer properties and also to be able to print neat resin specimens. As a control, bar specimens are also prepared by bulk casting the resin samples in a mold and curing the material via frontal polymerization. We measure the degree-of-cure and glass transition temperature (T_g) of the printed specimens using DSC prior to flexural testing to verify that the materials are properly cured. The 3D-printed samples containing various concentrations of carbon fibers exhibit a high degree of cure (> 98%), comparable to the molded

neat resin sample (Table B2 in Appendix B). Additionally, increasing the concentration of carbon fibers results in a steady increase in the T_g of the material due to the restricted mobility of the crosslinked network caused by stiff carbon fibers (Table B2 in Appendix B).

The results of the flexural tests on specimens printed parallel to the length of the bar reveal that increasing the concentration of carbon fibers leads to an increase in flexural modulus, where a 400% improvement in the modulus of the neat resin sample is obtained by adding 15 vol% of carbon fibers (Figure 3.5b, c). In addition, the flexural modulus of these samples are higher than those of the molded samples with the same CF concentrations. However, the flexural modulus of samples printed in the transverse direction is not affected by the carbon fiber content. A similar trend is observed for the flexural strength of the printed and control samples (Figure B6 in Appendix B); however, the flexural strengths of the samples cannot be thoroughly compared because the neat polymer and 5-vol%-CF specimens do not fail within the 5%-strain range defined

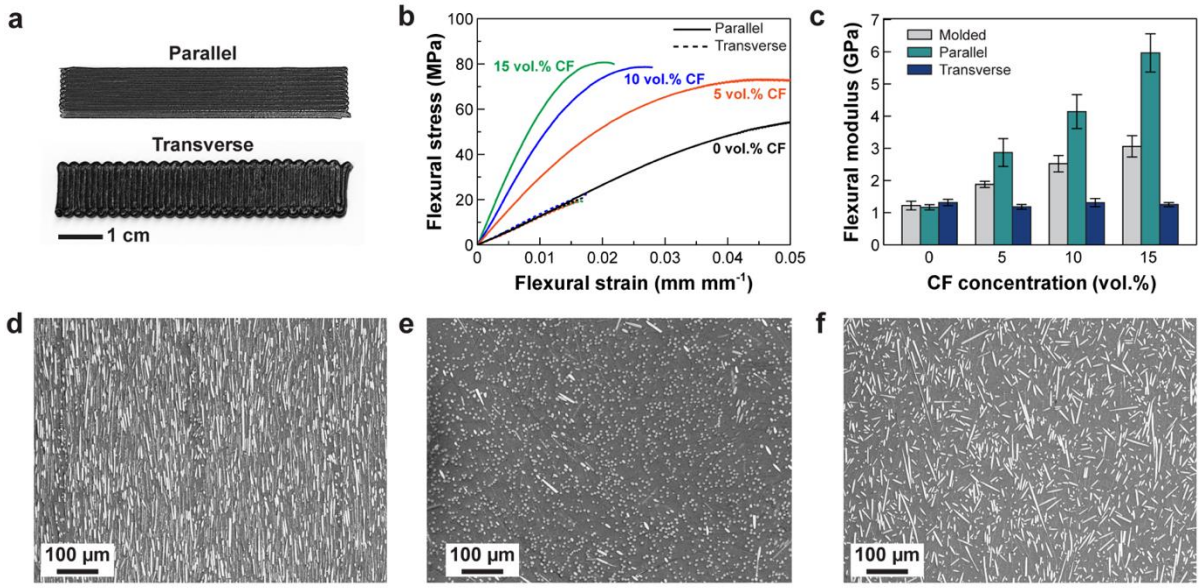

Figure 3.5. Flexural testing of printed samples. (a) Images of bars printed in parallel and transverse directions with respect to the bar length (main axis). (b) Representative flexural test curves for printed samples. (c) Comparison of the flexural modulus of printed samples as well as control, molded samples. (d, e) Optical micrographs from the polished surface and cross-section of a 15-vol%-CF printed bar specimen, respectively, indicating highly aligned fibers and no void formation in the printed composites. (f) An optical micrograph from the cross-section of a 15-vol%-CF molded bar specimen, indicating random alignment and distribution of carbon fibers.

by the ASTM standard. We explain the observed trends in flexural properties by examining the microstructure of produced specimens. In 3D-printed specimens, carbon fibers are highly aligned along the printing direction (Figure 3.5d, e and Figure B7a, b in Appendix B) caused by the high shear forces experienced during printing, whereas a random distribution of fibers is observed in the molded specimens (Figure 3.5f and Figure B7c, d in Appendix B). The alignment of fibers in samples prepared by printing along the length of the bar results in the enhanced reinforcing effect of fibers compared to the molded counterparts with the same concentrations of carbon fibers. In the transverse printing, however, the alignment and concentration of fibers do not play a role on the flexural properties, mainly because the performance of these samples are dictated by the interlayer bonding properties. The interlayer bond strength can be improved by increasing the print speed such that a few deposited layers cure simultaneously as long as the uncured layers do not flow or deform during printing or, alternatively, by adding chemical agents to the ink to enhance the chemical interactions between layers.

A key advantage of our printing technique compared to other composite printing techniques is the manufacture of void-free parts (Figure 3.5d, e). In particular, void formation is one of the main challenges in 3D printing of thermoplastic composites, which is typically detrimental to the performance of produced parts.[50,141] In contrast, our 3D printing technique creates no porosity in the final material, mainly due to the low viscosity of the ink during deposition compared to molten thermoplastics. The relatively low viscosity of the ink allows it to flow easily on the existing surfaces and fill the gaps between different roads during deposition. The effect of void-free printing is evident by the comparable flexural properties of neat samples prepared by 3D printing (both printing directions) and bulk casting.

3.4. Conclusions

In this paper, a novel technique for *in-situ* printing and thermal curing of discontinuous fiber-reinforced thermoset polymer composites is presented. Addition of carbon fibers to the base DCPD resin ink substantially enhances the rheological behavior and thermal conductivity of the frontally polymerizable ink, which are quite useful for fabrication of high-quality composite structures using the developed technique. We demonstrate two printing strategies by controlling the underlying processing conditions. Matching the print speed with the front velocity allows for unsupported, freeform printing of composite structures. The supported printing approach enables faster printing of composite objects with print speeds as high as 28 mm/s. The produced composites are fully cured, are free of voids, and exhibit anisotropic mechanical properties caused by the processed-induced alignment of carbon fibers along the filament length. We envision that this 3D printing technique can be applicable to other frontally polymerizable resin systems and a wide variety of conductive reinforcements, fillers, and particles.

Chapter 4: Frontal Polymerization and 3D Printing of Thermoset Polymers with Tunable Thermomechanical Properties

4.1. Introduction

Three-dimensional (3D) printing of thermoset polymers via direct ink writing (DIW) technique holds a great promise for various applications including load-bearing structures,[142] soft robotics,[143] batteries,[144] sensors,[145] and smart medical devices.[146] However, many thermoset resins used in 3D printing process have sluggish curing rate which makes manufacturing of thermoset components rather challenging. Manufacturing of thermoset polymer components via DIW is generally realized by extrusion of a thermally curable thermoset resin on a substrate followed by curing of the printed part in an oven at elevated temperatures for a few hours. Since the resin is rigidized in an oven after multilayer fabrication process, the printed structure may deform due to the buckling and yielding of ink during printing and curing process, reducing the fidelity of produced parts and limiting the number of layers that can be printed.[55,62] One solution to this problem is using photocurable resin systems, where the resin is extruded and *in-situ* cured by exposure to a UV light as it flows out of the nozzle. While this technique is capable of producing freeform structures, it is not compatible with opaque fillers and reinforcements due to their light screening effect, leads to low conversion of the photocurable resin, requires a second stage thermal curing step, and results in parts with inferior thermal and mechanical properties.[147–149]

A promising approach for addressing the curing issues of thermoset inks during the DIW process is *in-situ* curing via frontal polymerization (FP). FP is a self-sustaining, exothermic polymerization reaction that is activated by applying a local thermal stimulus to the monomer solution. Upon local polymerization, the released exothermic heat activates the polymerization of

more monomers, resulting in the formation of a self-propagating reaction wave that travels through the monomer solution and instantaneously converts available monomers to a solid polymer.[150,151] To date, FP has been demonstrated for a variety of monomers including cyclic olefins,[34] acrylates,[152] epoxies,[153] thiolenes,[90] polyurethanes,[103] and vinyl ethers.[154] Use of FP can produce thermoset polymers with properties comparable to the conventional bulk curing process with ability to speed up the manufacturing process by up to 100 times and reduce the energy consumption by up to 10 orders of magnitude.[36] Owing to the energy-efficiency and rapid curing rate of FP reactions, frontally polymerizable resins can be used in DIW process to enable simultaneous printing and curing of thermosetting parts with a high print fidelity. Recently, FP of dicyclopentadiene (DCPD) resin has been used to demonstrate freeform printing of neat thermoset parts by matching the print speed with the front velocity during ink deposition, leading to one-step printing and curing of thermosets without any post-cure or post-treatment steps.[36,155] The resulting polydicyclopentadiene (pDCPD) polymer is a high-performance thermoset with a good combination of strength and stiffness, fracture toughness, and thermal stability.[156–158] In a recent study, we used FP of DCPD to demonstrate 3D printing of discontinuous fiber-reinforced polymer composites.[159] Adding short carbon fibers to the DCPD ink substantially enhances its rheological properties and thermal conductivity and enables unprecedented DIW of composite structures. Using a similar approach, the print speed can be matched with the front velocity to print freeform composite structures. Although the addition of 15 vol% of carbon fibers increased the printing speed of the DCPD ink from 1.23 to 2.66 mm/s, the printing speed is still limited by the front velocity, making the printing process relatively slow. We exploited the improved yield stress and thermal conductivity of the composite ink to develop an unsynchronized printing and curing

strategy, where the ink is deposited rapidly (28 mm/s) and cured by 3D propagation (i.e., in-plane and through-thickness propagation) of the FP reaction.

The only few demonstrations of FP-assisted DIW of thermosetting structures to date have been limited to printing stiff pDCPD-based structures with fixed thermomechanical properties. This promising printing approach, however, can potentially be used for manufacturing a wide variety of polymers and composites with tunable properties. Here, we present a facile approach for developing frontally polymerizable thermosets based on DCPD with tunable thermomechanical properties and extending the application of FP-assisted DIW to a broader technical field. Our approach for modifying the chemical structure and thermomechanical properties of pDCPD relies on copolymerization of DCPD resin with vegetable oils. Vegetable oils and their derivatives are an emerging source of renewable resins which can be copolymerized with a variety of cyclic olefin resins.[160] Various copolymers have been produced using vegetable oils including soybean,[161] corn,[162] caster,[163] tung,[164] and linseed oil.[165] Vegetable oils have flexible triglycerides units that consist of three fatty acid-based ester chains with a high degree of unsaturation. The presence of unsaturated bonds allows for functionalization with norbornene moieties and creating monomers that can be copolymerized with other strained ring systems via ring-opening metathesis polymerization (ROMP).[166]

Linseed oil is a frequently used vegetable oil, which can be simply modified with DCPD via a Diels-Alder reaction to incorporate highly strained norbornene moieties to the triglyceride chains.[167] DCPD-modified linseed oil (DML) can react with cyclic olefins via ROMP and produce a variety of industrially promising polymers with tunable mechanical properties. For example, glass fiber composites were prepared by ROMP of DML and DCPD in the presence of short or continuous glass fiber to increase the toughness of composite parts.[168–170] In another example, new

rubbers were prepared by ROMP of DML and a norbornene diester that resulted in flexible and stretchable materials.[171] However, previous demonstration on ROMP of modified oil have been carried out based on bulk polymerization using the conventional oven curing process that requires a significant amount of manufacturing energy and time and cannot be extended to emerging manufacturing processes such as 3D printing.

While ROMP of modified linseed oil with DCPD has been previously shown, FP of such resin systems has not been reported. In the present work, we develop a cost-effective and scalable manufacturing process by adding various concentrations of DML into DCPD and exploiting FP to produce thermoset polymers with tailored mechanical properties from stiff and rigid to compliant and stretchable. Exploiting the rapid cure kinetics of new copolymers, we demonstrate DIW of elastomeric objects via *in-situ* printing and frontal curing of inks without any post-curing steps. This concept can be applied for FP-assisted DIW of a wide range of thermosetting parts using various resin systems and functional additives.

4.2. Experimental section

4.2.1. Materials

Dicyclopentadiene (DCPD), 5-ethylidene-2-norbornene (ENB), and second-generation Grubbs catalyst (GC2) were purchased from Sigma Aldrich and used without further purification. DCPD-modified linseed oil (DML) was obtained from Natural Pigments and used as received. Carbon nanotubes (CNTs) were purchased from Nanocyl (Nanocyl NC 7000, Belgium). Tributyl phosphite (TBP) and phenylcyclohexane (PCH) were obtained from TCI America. A 26-Gauge Kanthal resistive wire (diameter = 0.40 mm; resistivity = 0.98 Ω m at room temperature) was used to initiate FP reaction by applying an electric current through the wire. RTV630 silicone rubber was purchased from Momentive and used to make molds.

4.2.2. Preparing DML/DCPD resin solution

First 5 wt% ENB is blended with DCPD (solid at room temperature) to suppress the melting point of DCPD and form a liquid resin at room temperature. All future references to DCPD resin refer to 95:5 DCPD/ENB mixture. FP resin solution is prepared by adding desired amounts of DML to DCPD to create comonomer solutions with DML concentrations ranging from 0 to 50 wt%. For all experiments, 3.21 mg GC2 (100 ppm) is dissolved in 500 μL PCH in a separate vial and then mixed with 1.19 μL TBP (1 molar equivalent with respect to GC2) and sonicated for 10 min. The GC2/TBP solution is then poured into the DML/ DCPD resin and thoroughly mixed. More details are given in Appendix C.

4.2.3. Front temperature and front velocity measurements

The prepared DML/DCPD resin is transferred to a 13 mm × 75 mm borosilicate test tube. FP is triggered by local heating of resin from top using a resistive wire connected to a power supply, which then progresses in a descending mode. Once FP is initiated, the front propagation is monitored using a digital camera. Front velocity is determined by finding the slope of best-fit straight line representing front position versus time. Front temperature is measured using a T-type thermocouple inserted inside the test tube before initiating FP.

4.2.4. Dynamic mechanical analysis

Dynamic mechanical tests are conducted on copolymers using a Dynamic Mechanical Analyzer (DMA, Q800 TA Instruments) in tension testing mode at a constant frequency of 1 Hz and strain rate of 0.1%. Rectangular bar specimens with 15 mm × 5.4 mm × 0.7 mm dimensions are created for analysis (See Appendix C for details of DMA specimens' preparation). Measurements are carried out over the temperature range of 0 °C to 150 °C at a heating rate of 5 °C/min.

4.2.5. Tensile tests

Tensile modulus was calculated as the slop of stress-strain curve in the linear region of 0 - 1% strain. Tensile properties of thermosetting copolymers are measured using a servo-hydraulic material testing system (858 MiniBionix; MTS 16 Systems) at a crosshead speed of 5 mm/min. Tensile dogbone specimens are prepared by FP of DML/DCPD resin in a silicone mold pre-heated to 50 °C based on type IV dimensions specified in the ASTM D638 standard. The silicone mold is fabricated using RTV 630 silicone rubber due to its resistance to front temperatures and thermal insulating properties for preventing heat loss to surrounding. Tensile modulus is calculated as the slope of stress-strain curve in the linear region of 0 - 1% strain.

4.2.6. Preparing 3D printing ink

After preparing the 95:5 DCPD/ENB solution according to the above procedure, desired amount of DML along with 2.5 wt% CNTs is added to the resin solution and stirred using a high-speed homogenizer (IKA-T25, IKA Instruments) at 20,000 rpm for 2 min. The mixture is then processed in a three-roll calendaring mill for eight passes to obtain a homogeneous dispersion of CNTs in the resin. Afterwards, 3.21 mg GC2 catalyst and 1 molar equivalent of TBP inhibitor with respect to GC2 is added to the mixture and mixed for 5 min using a planetary centrifugal mixer (AR-100, Thinky USA). The prepared mixture is used as is or mixed with 50 wt% DML to prepare inks for 3D printing.

4.2.7. Rheological measurements

The rheological properties of 3D printing inks are characterized using a TA instrument discovery HR-2 rheometer with a 40 mm diameter aluminum parallel plates at a reference temperature of -5 °C. Dynamic oscillation stress-sweep tests are conducted using a frequency of 1

Hz and sweeping shear stresses from 0.1 to 7,000 Pa. The viscosity profile of 3D printing inks is measured using a steady-state flow test carried out at shear rates ranging from 0.01 to 100 1/s.

4.2.8. 3D printing via FP

The prepared ink for 3D printing is loaded into a 10 mL syringe barrel and centrifuged for 3 min to remove the trapped bubbles resulting from ink transfer. The loaded syringe is then mounted on a three-axis gantry robot (F5200N, Fisnar). The ink is pumped using a digital high-precision dispenser (DC100, Fisnar) and extruded on a heated glass substrate with an average temperature of 80 °C to enable *in-situ* curing of the ink during the printing process. Printing is performed using a nozzle with an inner diameter of 0.8 mm and a pressure of 70 kPa. The temperature of the ink inside the syringe is reduced to -5 °C using two thermoelectric Peltier coolers installed at the sides of the syringe barrel to minimize background polymerization and maintain a constant viscosity profile during the entire printing process. 3D-printed structures are constructed using G-codes generated by manual coding to control the motion of three-axis gantry robot (See Appendix C).

4.2.9. Differential scanning calorimetry

DSC is used to determine the degree-of-cure (a) of printed samples using a modulated DSC (DSC 2500, TA Instrument). DSC measurements are conducted on 2-3 mg of uncured resin specimens and 5-10 mg of 3D printed cured specimens placed in aluminum hermetic pans at a heating rate of 5 °C/min from 25 to 200 °C under dry nitrogen. The degree of cure (a) is then calculated as,

$$\alpha = 1 - \frac{H_r}{H_t} \quad (1)$$

where H_r is the residual heat of reaction obtained from cured, 3D printed specimens and H_t is the total heat of reaction obtained from uncured resin.

4.2.10. Compression tests on 3D printed lattice structures

The mechanical response of 3D printed lattice structures is assessed by performing large-strain compression tests at a loading rate of 5 mm/min until a compressive strain of 0.5 mm/mm is applied on samples. Compression tests are carried out using a servo-hydraulic material testing system (858 MiniBionix; MTS 16 Systems) equipped with a 5 kN force capacity transducer.

4.3. Results and discussion

4.3.1. Frontal ring opening metathesis polymerization (FROMP)

DML is a triglyceride oil frequently used as a drying oil in surface coating industry. This resin is a commercially available vegetable oil-based monomer modified with one or two norbornene rings attached to the triglyceride chains (Figure 4.1.).[172] The norbornene moieties in DML can undergo FROMP reaction with DCPD to form a thermoset copolymer. Figure 4.1a shows the scheme of FROMP of DCPD and DML comonomer in the presence of the second-generation Grubbs catalyst (GC2) and tributyl phosphite (TBP) inhibitor. Addition of TBP allows for controlling the reactivity of GC2 to make the comonomer solution stable at room temperature. FROMP reaction is activated by applying a small amount of heat to the mixture to trigger an exothermic reaction. The resulting reaction front is a hot localized reaction zone that propagates through unreacted monomers and converts them to a solid thermoset without further energy input. The propagation of FP in a resin solution containing 50 wt% of DML is shown in Figure 4.1b. Following the polymerization, an elastomeric polymer is obtained, which can easily be deformed by twisting, bending, and stretching (Figure 4.1c).

We first study the effect of DML concentration on front temperature and front velocity (Figure 4.2). Norbornene moieties on DML have similar strain energy (100 kJ/mol) compared to DCPC

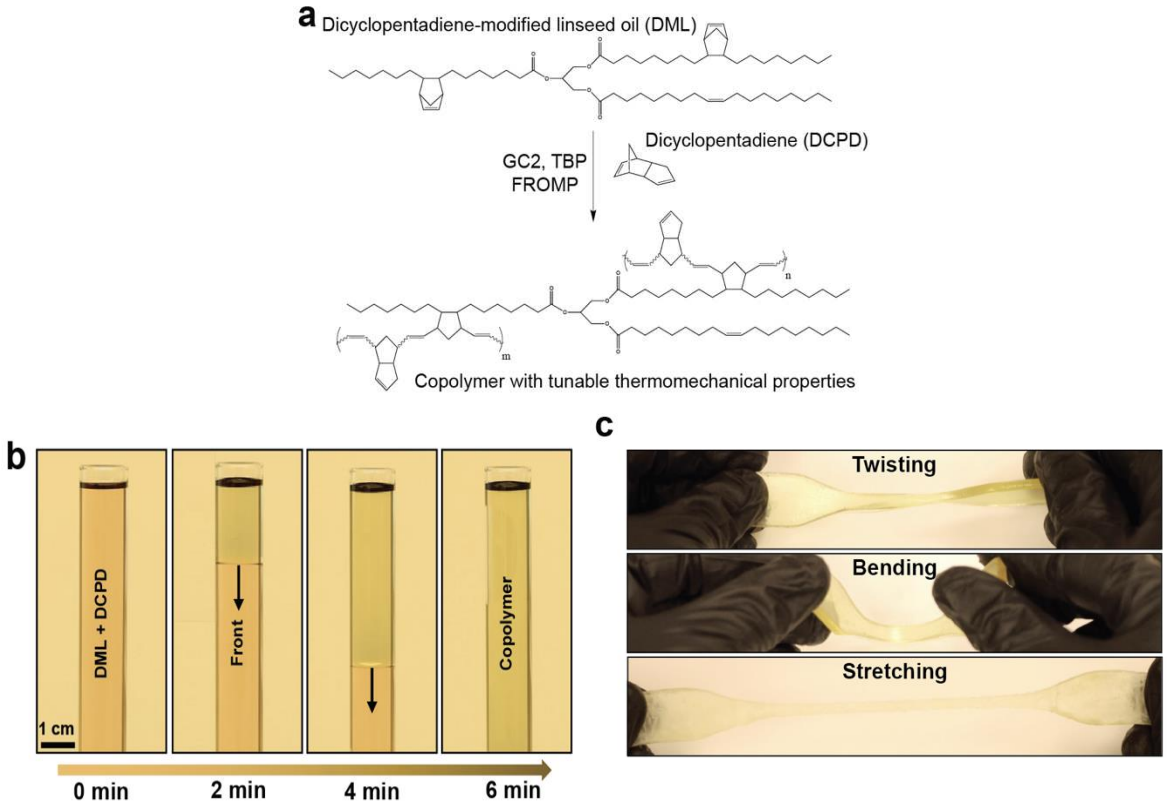

Figure 4.1. Frontal copolymerization of dicyclopentadiene (DCPD) and dicyclopentadiene-modified linseed oil (DML). (a) Scheme of polymerization reaction. (b) Images captured from FROMP of 50 wt% DML in DCPD at various time intervals, showing the propagation of frontal reaction. (c) Manual deformation of a polymer specimen prepared using 50 wt% DML.

(90 kJ/mol).[173,174] However, DML possesses long fatty acid chains, which hinder coordination between the catalyst and norbornene moieties, leading to reduction in the reactivity of DML molecules compared to DCPD.[166] In addition, increasing DML concentration reduces the number of active rings per unit volume, which in turn decreases the overall reactivity of DML/DCPD mixture and suppresses the front temperature and front velocity. Increasing the concentration of DML from 0 to 50 wt% decreases front temperature from 185 °C to 121 °C and front velocity from 1.13 mm/s to 0.12 mm/s (Figure 4.2). At concentrations above 50 wt%, front quenches few seconds after initiation due to insufficient energy density of resin.

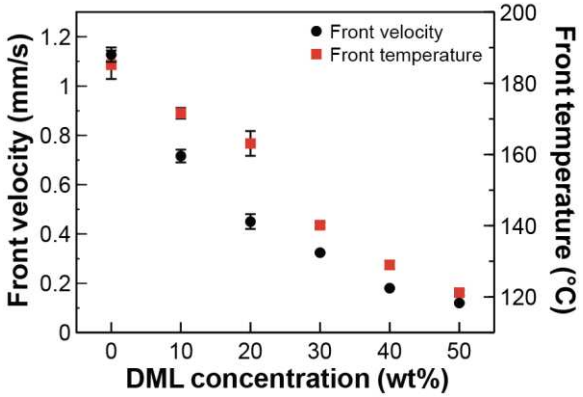

Figure 4.2. Front velocity and maximum front temperature for various concentrations of DML in DCPD. Error bars represent standard deviation from the mean (n = 2).

Dynamic mechanical analysis (DMA) measurements are carried out to understand the underlaying mechanism for transforming the resin from a rigid polymer to a compliant and flexible polymer by changing the DML comonomer content. DMA experiments are performed on various copolymers in the tension mode to determine the storage modulus as a function of temperature (Figure 4.3a). DML/DCPD copolymers exhibit typical reduction in storage modulus upon heating from glassy state to a rubbery plateau. As the DML concentration increases, the storage modulus at the glassy state decreases from 1.8 GPa to 0.7 GPa and shifts to lower temperatures, indicating the plasticizing effect of DML on the thermomechanical properties of produced polymers (Figure 4.3a). This effect can be explained by the fact that linseed oil reduces the degree of crosslinking by introducing a long fatty acid chain between DCPD crosslinks (Figure 4.1a).[172,175] From the theory of rubber elasticity, average molecular weight between crosslinks (M_c) can be calculated from the rubbery plateau of storage modulus at 70 °C above the T_g as,[173]

$$M_c = \frac{3\rho RT}{E'_{T_g+70\ \mathrm{K}}} \tag{2}$$

where ρ is the density of copolymer, R is the universal gas constant, and T is the temperature at 70 °C above the T_g of the copolymer. Polydicyclopentadiene (pDCPD) is a highly crosslinked

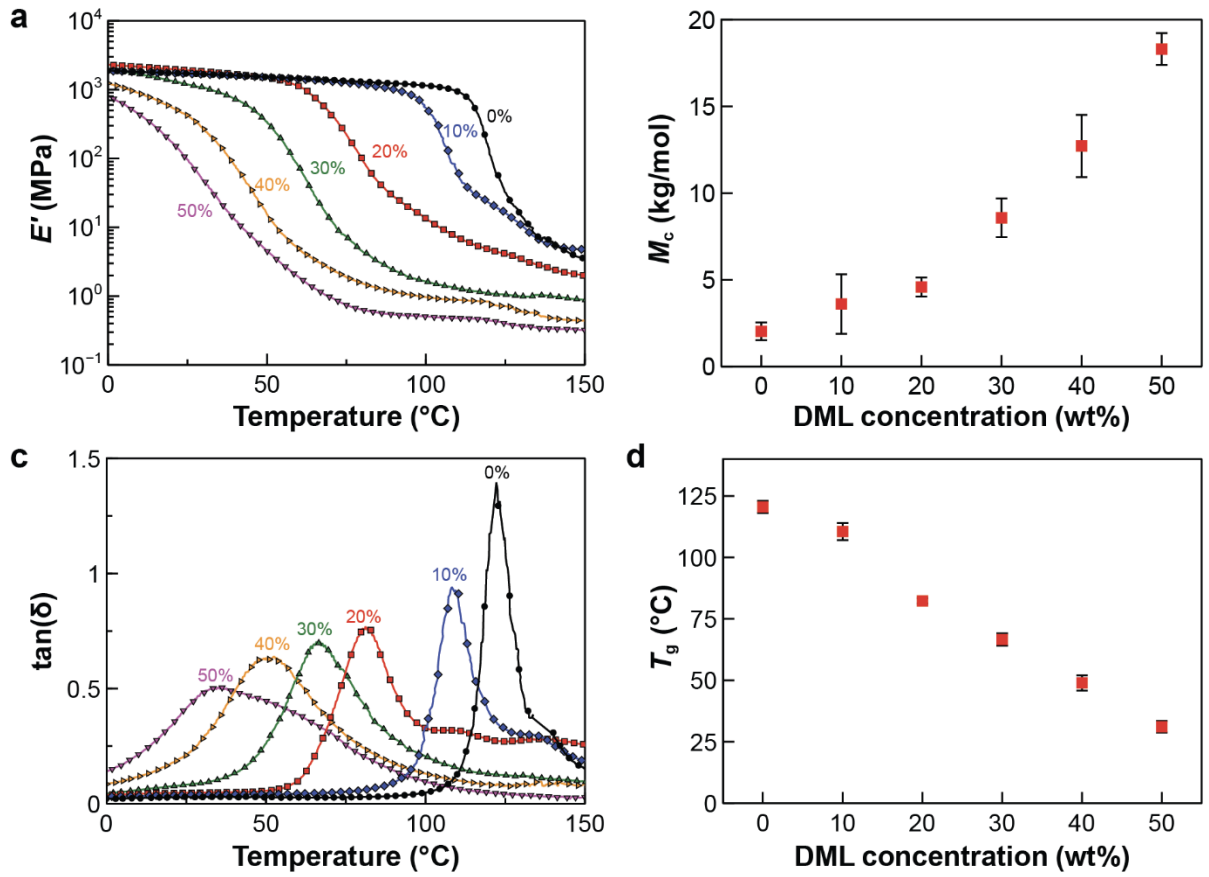

Figure 4.3. DMA measurements on copolymers prepared by FROMP. (a) Temperature-dependence of storage modulus, E', of copolymers containing various weight concentrations of DML. (b) Average molecular weight between crosslinks calculated using E' in the rubbery plateau region. (c, d) tan(δ) curves and glass transition temperature (T_g) of copolymers, respectively. Error bars represent standard deviation from the mean (n = 2).

thermoset polymer as evident from the low M_c in Figure 4.3b. In highly crosslinked pDCPD, chain mobility is severely restricted by crosslinks during deformation, resulting in a high elastic modulus.[176] As DML concentration increases, crosslinking density decreases, allowing chains to dissipate the energy generated by deformation through molecular motion. In addition to reducing the crosslinking density of DCPD, incorporating DML substitutes rigid cyclic DCPD chains for flexible triglyceride, providing an effective lubrication and additional plasticizing effect to the copolymer.[166]

Previous demonstrations on ROMP of DCPD and DML using traditional bulk polymerization have shown reaction-induced phase separation, resulting in micro-aggregation of the oil-rich phase

and property gradient throughout the produced polymer.[177,175] In the DMA plots of tan(δ) curve of these copolymers, two identifiable relaxation peaks related to the microphase-separated regions were typically observed. However, only one peak is observed in the tan(δ) curve of all copolymers produced via FP, which corresponds to the glass transition temperature (T_g) of produced copolymers (Figure 4.3c). The T_g of copolymers monotonically decreases over a wide range of temperature from 120 °C to 31 °C as the concentration of DML is increased from 0 to 50 wt% (Figure 4.3d). The presence of a single tan(δ) peak in the DMA thermograms of produced copolymers indicates that frontal curing produces more homogeneous copolymers compared to the bulk polymerization approach. This observation highlights another advantage of FP, as it limits phase separation by rapidly fixing two components in a metastable condition prior to reaching the thermodynamic equilibrium state.[103,178,179] However, as the concentration of comonomer increases, the tan(δ) peak broadens and its intensity decreases, indicating that the heterogeneity of crosslink networks increases due to random positioning of norbornene groups along the fatty acid chains.[168]

Mechanical properties of copolymers prepared by FROMP can be tuned by controlling the crosslinking density and T_g of copolymers. Copolymers containing 30 wt% or less DML exhibit yielding at small strains (ca. 10%) and irrecoverable plastic deformation until failure (Figure 4.4a, b). In contrast, copolymers prepared using 40 and 50 wt% DML show minimal plastic deformation, and no yielding is observed in their stress-strain curves (inset in Figure 4.4a). These copolymers exhibit an elastomeric behavior with immediate recovery after deformation. Figures 4.4c-e summarize the tensile behavior of copolymers prepared by the FROMP reaction. At room temperature, tensile modulus varies by two orders of magnitude from 1.1 GPa to 5.6 MPa and the tensile strength changes by 90-fold from 45 MPa to 0.5 MPa as the concentration of DML is increased from 0 to 50 wt%. Copolymers prepared using 0 to 20 wt% DML exhibit a slight increase

in elongation at failure from 11% to 18%. Adding 30 wt% DML remarkably enhances elongation at failure to 180% and makes the tensile specimens undergo irrecoverable plastic deformation after

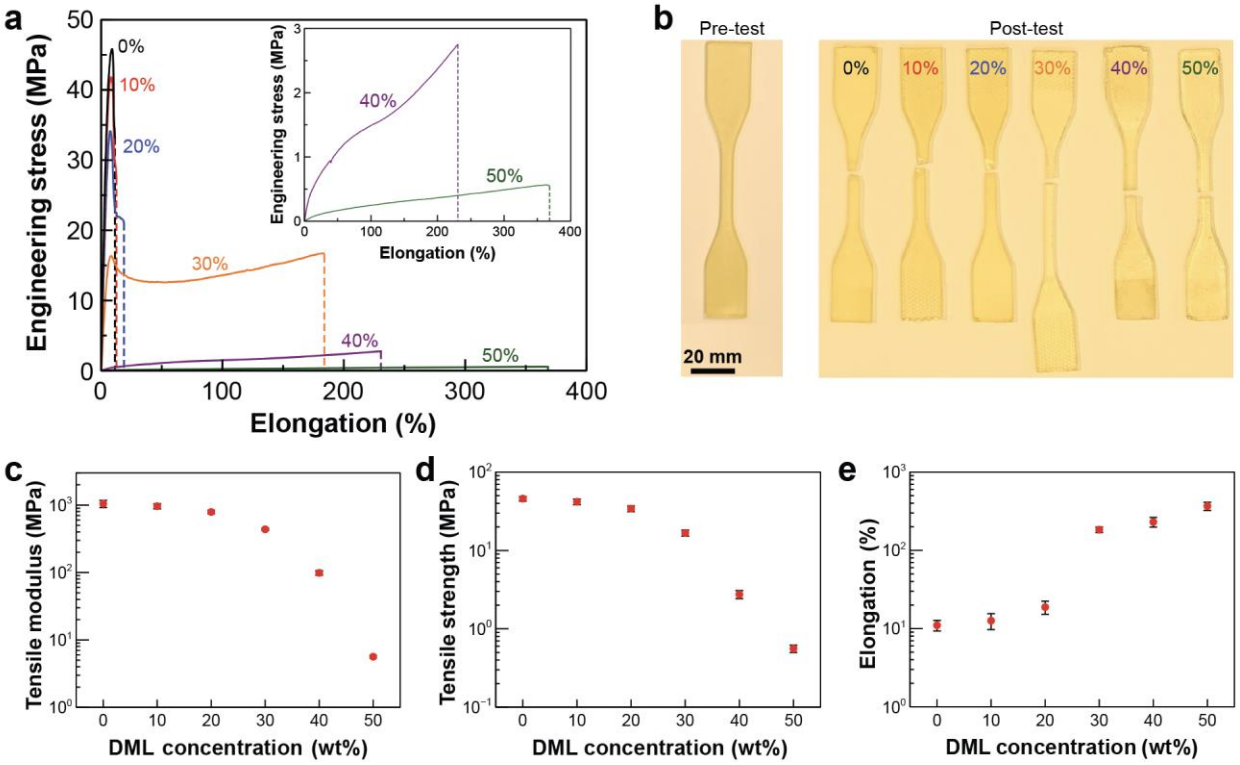

Figure 4.4. Mechanical properties of copolymers prepared by FROMP at room temperature. (a) Engineering stress-strain curves for copolymers containing various concentrations of DML. (b) Image of representative failed samples after tensile tests, showing the difference in deformation behavior of different copolymers. (c-e) Summary of mechanical properties measured for different copolymers: (c) tensile modulus, (d) tensile strength, and (e) elongation at break. Error bars represent standard deviation from the mean (n = 3).

failure. Further increase in the concentration of DML leads to a substantial change in elongation behavior for copolymers containing 40 and 50 wt% DML. These copolymers respectively show a high elongation at failure of 230% and 360% with a highly recoverable elastic deformation after failure (inset in Figure 4.4a). As a result, a series of thermoset copolymers with a wide range of tensile properties can be readily prepared by varying the comonomer content.

4.3.2. 3D printing

The ability to rapidly synthesize thermoset polymers and elastomers with control over their thermomechanical properties simply by changing the DML/ DCPD weight ratio is quite promising

for developing new applications using these polymers. Here, we demonstrate rapid and energy-efficient additive manufacturing of thermoset structures with different stiffness using the developed frontal copolymerization strategy. We print two cellular structures with the same dimensions (30 mm × 30 mm × 7 mm) and infill density using two different inks composed of DCPD resin and 50 wt% DML resin to show the ability of printing thermoset objects with extreme mechanical properties (i.e., relatively stiff and compliant parts).

Inks used in DIW should exhibit a high shear-thinning behavior and high yield stress to easily flow through the printing nozzle and maintain their shape after deposition.[128,129,180] However, the DCPD and 50 wt% DML resin solutions are a Newtonian fluid with a shear-rate-independent viscosity of 0.04 and 0.15 Pa.s, respectively, for the probed range of shear rates from 0.01 to 100 1/s (Figure 4.5a). We prepare printable inks amenable to DIW process by modifying the rheological properties of resin solutions by adding 2.5 wt% of CNTs. Compared to other particles used as a rheology modifier in DIW techniques (e.g., fumed silica, nanoclay), a small concentration of CNTs can create highly thermally conductive printable inks with the desired rheological behavior and a high energy density for FP. Proper dispersion of nanotubes is crucial for achieving a consistent and continuous extrusion of ink without nozzle clogging.[181] A processing protocol is developed to obtain a homogenous dispersion of nanotubes in the composites through a two-step intense shear mixing process. First, nanotubes are introduced to the resin using a homogenizer rotating at 20,000 rpm for two minutes. Following this mixing step, the viscosity of inks is significantly increased; however, the inks still flow under self-weight due to non-uniform dispersion of nanotubes that may lead to the collapse of printed structures (Figure 4.5c). The mixture prepared from the previous step is added to a three-roll calendaring mill and processed for eight passes. Figure 4.5c depicts an image of the CNT-filled DCPD ink processed after 8 milling passes, illustrating no apparent ink

yielding occurring due to gravity. Incorporating 2.5 wt% of CNTs substantially increases the resin viscosity at low shear rates (0.01 1/s) by five orders of magnitude and enhances the shear-thinning behavior of the unfilled resin solutions (Figure 4.5a). The shear-thinning behavior of the resulting 3D printing inks can be modeled by fitting a curve to the measured apparent viscosity, η, values as a function of shear rate, $\dot{\gamma}$, as,

$$\eta = K\dot{\gamma}^{n-1} \tag{3}$$

where K is the flow consistency index and n is the power law exponent index representing the rate-dependence behavior of inks. For a shear-thinning ink, $0 < n < 1$, where a stronger shear-thinning behavior is expected as n approaches zero.[182] For the prepared inks in this study, $n \sim 0.2$ over the

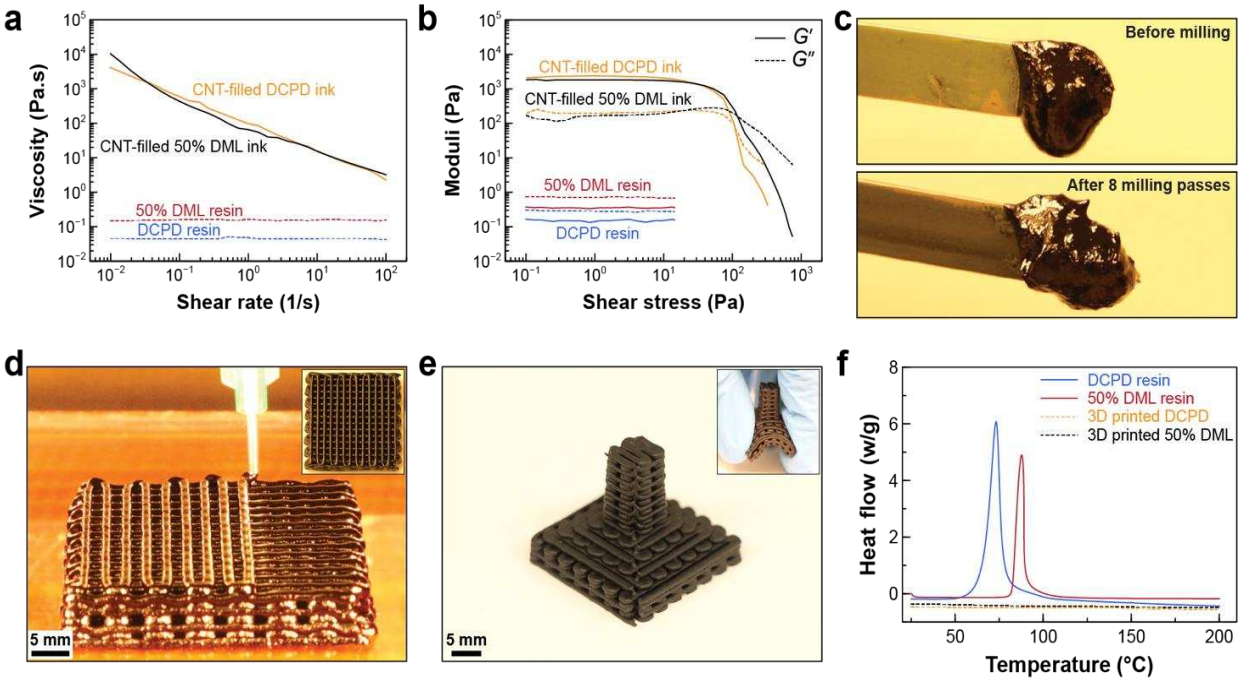

Figure 4.5. FP-assisted 3D printing. (a) Viscosity profile of unfilled and CNT-filled resins as a function of shear rate. (b) Shear storage and loss moduli of unfilled and CNT-filled resins as a function of applied shear stress. (c) Images of 50 wt% DML ink before milling and after 8 passes of milling using a three-roll-mill. (d) Printing and FP curing of a lattice structure using 50 wt% DML ink. The inset shows the image of the final lattice structure. (e) A 3D layered structure printed using 50 wt% DML ink. The inset depicts manual deformation of the printed part. (f) Heat flow curves obtained from DSC measurements, indicating minimal residual heat of reaction in printed samples (degree of cure > 98%).

range of tested shear rates (0.01 to 100 1/s). This value indicates a good shear-thinning behavior

and falls within the range of power law exponents previously reported for several other 3D printing inks.[56,128,142,183]

Results of storage (G') and loss (G'') moduli measurements for unfilled and CNT-filled resins are shown in Figure 4.5b. The shear loss modulus (G'') of the unfilled DCPD and 50 wt% DML resins exhibits a stress-independent response that is approximately three times higher than their storage modulus (G'), indicating the viscous characteristic of the unfilled resins. As CNTs are added to the resins, both storage and loss moduli increase; the storage modulus exceeds the loss modulus by one order of magnitude and the inks exhibit a solid-like behavior at low shear stresses. As the stress increases, the inks yield and flow and their storage modulus steadily drops to a value below that of the loss modulus, resulting in a liquid-like behavior. This transition from solid-like to liquid-like behavior is called yield stress and calculated from the crossover point where the storage modulus drops below the loss modulus.[184] Adding carbon nanotubes results in a high shear yield stress in CNT-filled inks (τ_y ~ 104 and 117 Pa for DCPD and 50 wt% DML inks, respectively), which falls within the range of yield stresses previously reported for DIW techniques ($100 < \tau_y < 6{,}000$ Pa).[57,120,129,185]

Prepared inks with a proper rheological profile are loaded into a syringe barrel and then the barrel is mounted on a 3-axis gantry robotic platform. The ink is controllably deposited on a heated substrate with an average temperature of 80 °C through a nozzle with an inner diameter of 0.8 mm. The ink temperature is maintained at -5 °C during the entire printing process to avoid background polymerization. In our printing process, we rely on the high yield stress and shear-thinning properties of inks to extrude the material on the heated substrate and temporarily maintain the form of the printed part. The extruded ink is then cured by a combination of through-thickness and in-plane propagation of FP according to our recently developed printing strategy (Figure 4.5d).[159]

The enhanced thermal conductivity of inks by adding CNTs is crucial for transferring heat via conduction from the heated substrate to the top, uncured layers. The result is a solid lattice comprised of 10 stacking layers of alternating vertically and horizontally printed lines. Similarly, controlling the printing process allows for printing and *in-situ* curing of tall, layered structures (Figure 4.5e). Once the printing is complete, the part is fully cured, eliminating the need for any post-curing step ($\alpha > 98\%$) (Figure 4.5f).

4.3.3. Large-strain compression tests on 3D printed cellular structures

Large-strain compression tests (engineering strain up to 0.5 mm/mm) are carried out on printed lattices to understand the mechanical performance of printed parts. The compressive engineering strain-stress curves of the nanocomposite lattices and representative images from tested samples after 0.5 mm/mm strain are shown in Figure 4.6. The stress-strain curve of the part printed using CNT-filled DCPD ink shows a brittle behavior with a relatively low compressive failure strain (ε_y = -0.064 mm/mm) (Figure 4.6a, b). Multiple yielding points are observed during the compression test, which are due to the delamination of stacking layers caused by the buckling deformation. Delamination initiates at the interface of printed layers caused by shear stresses and then propagates along the specimen length, splitting the part into separate layers (Figure 4.6b). In contrast, the part made using CNT-filled 50 wt% DML ink does not fail catastrophically and exhibits out-of-plane buckling when subjected to a large compressive strain (Figure 4.6a, c). Following the test, the original shape of the lattice is recovered and no major delamination is observed, owing to the compliant nature of the printed layers as well as good adhesion between layers (Figure 4.6c). In addition to high compressibility, the lattice structure printed using the highly stretchable elastomer has 264 times lower compression modulus than the part printed using the DCPD-based ink formulation. Higher compressibility and lower stiffness allow for better

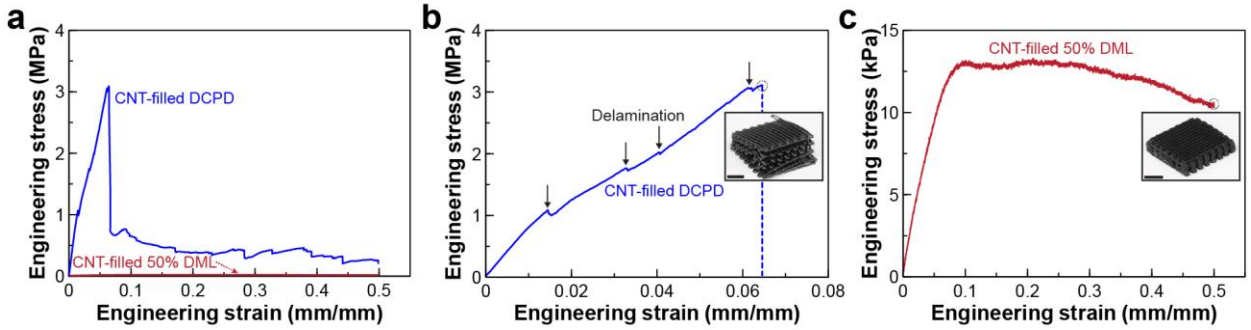

Figure 4.6. Compression testing of 3D printed lattice structures. (a) Comparison of CNT-filled DCPD and CNT-filled 50 wt% DML lattices. Major delamination failure is observed in DCPD sample at a strain of 0.064 mm/mm. CNT-filled DML sample exhibits a flexible behavior compared with DCPD sample. (b) Compression response of CNT-filled sample prior to failure. (c) Magnified response of CNT-filled 50 wt% DML sample, showing large-scale deformation without failure. Inset images in (b) and (c) depict samples after compression testing until 0.5 mm/mm strain. Scale bars in these images represent 1 cm.

distribution of stress at large deformations and circumventing the premature failure of printed structures.[186] This concept can be implemented to print heterogeneous composites with damage-tolerant mechanical behavior and tunable failure.

4.4. Conclusions

In this work, we have demonstrated a new approach for rapid and energy-efficient manufacturing of thermoset polymers with a wide range of thermomechanical properties using FROMP of DCPD and DML comonomers. The results of experimental studies show that the front properties (i.e., front velocity and front temperature) and the mechanical and thermal properties of resulting polymers can be tailored by changing the weight ratio of DCPD and DML comonomers. Adding 0 to 50 wt% DML comonomer to DCPD resin results in a substantial change in mechanical properties with increased propensity for recoverable elastic deformation at room temperature and altered T_g from 120 °C to 31 °C. The new resin formulations are promising for additive manufacturing of compliant and stretchable elastomers via the developed *in-situ* printing and curing approach. Two lattice structures with extreme mechanical behaviors are printed using two different inks to demonstrate the ability of printing highly stiff to compliant structures.

Chapter 5: Fast and Scalable Additive Manufacturing of Carbon Fiber-Reinforced Thermoset Polymer Composites

5.1. Introduction

Fiber-reinforced polymer composites (FRPCs) have been widely adopted in various industries from aerospace to automotive to energy sectors due to the combination of their superior thermal and mechanical properties and high stability at elevated temperatures.[187] FRPCs are conventionally manufactured using expensive molds or tooling to shape the resin and fibers. Design and manufacturing of molds is a labor-intensive and expensive process, which imparts a significant economic barrier for creation of complicated molds or changing the design of composite products. In marked contrast, additive manufacturing (AM) allows to readily fabricate composite parts with minimal tooling at a lower cost and higher design flexibility.[188]

The most ubiquitous additive technology that can create 3D structures with a high resolution and rapid production time is direct ink writing (DIW).[39] DIW has been demonstrated to fabricate various FRPC parts with continuous or discontinuous fiber reinforcements.[57,105] DIW of thermoset polymer composites consists of extruding a viscoelastic ink from a nozzle on a substrate to form layer-by-layer 3D structures. The viscoelastic ink used in DIW must exhibit a shear thinning behavior to facilitate extrusion from the nozzle and retaining its filamentary shape.[189] The most convenient method to achieve a shear thinning behavior is adding particles, including fumed silica, nanoclay, carbon nanotubes, graphene, boron nitrides, or short carbon fibers to thermoset resins to modify its rheological profile and achieve desired thermal, electrical, and mechanical properties.[52,56,190]

While considerable progress has been made in AM of thermoset composites, the use of DIW is mainly limited to small structures with sluggish printing rates and substantial energy needs.[63,119] Most AM technologies utilize thermal curing resin systems that require the printed material to be cured in an oven at elevated temperatures for a few hours. Since the composite ink is thermally cured in an oven after the multi-layer fabrication process, this approach prevents printing tall or freeform structures due to the buckling or yielding of the ink.[55,120,121,191] In addition, the printed parts should be placed in an appropriately sized oven, making it difficult to fabricate large parts.

In contrast, *in-situ* curing enables scalable manufacturing processes and offers greater flexibility in creating freestanding or unsupported structures. Most methods utilizing *in-situ* curing are based on UV-curable resin systems, in which the ink is printed and immediately solidified as it is exposed to UV light. The use of UV partially cures the ink which allows the ink to capture the print geometry. After printing the composite, the components are additionally treated by UV irradiation and/or heating to achieve a complete cure.[114,116] Therefore, the existing UV-curing AM technologies struggle with lengthy post-treatment and energy-intensive processes. In addition, these technologies are not suitable to manufacture carbon fiber reinforced composites, where the presence of fiber attenuates UV irradiation and significantly lowers the reaction rate, resulting in poor mechanical properties.[192]

Recently, frontal polymerization (FP) has been introduced as a promising curing strategy to fabricate thermoset polymers and composites. In FP, a local thermal stimulus initiates a propagating reaction front that rapidly converts the unreacted monomer to a solid polymer.[34] When FP is coupled with DIW, it can enable *in-situ* printing and curing of high-quality structures without requiring any post-treatments.[36] To enable DIW printing, the resin is transformed to a high-viscosity gel in the presence of a catalyst and inhibitor. FP is initiated at the beginning of printing

using a heated substrate that produces a self-sustaining propagating front. Matching the rate of the propagating reactive front with print speed allows printing freeform structures. Previous demonstration of FP printing has shown than the rate of propagating front is quite low to be applicable to manufacture of large composite structures.[36,69,119] In addition, the rate of polymerization greatly depends on ambient temperature and boundary conditions, making FP printing quite challenging and unpredictable due to the existent temperature gradient through the building envelope.

The previously developed AM methods have unattainable rates of polymerization for rapid DIW of FRPCs. Thus, there is a need for a new AM technique that can print and simultaneously cure any part size at high speeds in any ambient condition without the need for any post-curing steps. In this chapter, a new DIW approach is presented that rapidly builds high-fidelity, freeform architectures in space. We have shown that the printing speed can reach up to 1.5 m/min in conventional layer-by-layer printing process which is 8.3 times faster than the highest printing speeds previously reported for *in-situ* printing and curing strategies.[193] The new method is based on using a thermal stimulus as a localized heat supply to instantaneously cure the composite ink filled with short carbon fibers (CFs) as extruded from a nozzle. In our printing process, dicyclopentadiene (DCPD) is used as a thermally curable thermoset resin which rapidly undergoes ring-opening metathesis polymerization (ROMP) when exposed to a thermal stimulus. The resin is modified with short carbon fibers (CFs) to tailor the rheological profile of the ink. When coupled with *in-situ* curing process, it allows unprecedented printing speeds and fabrication of high-quality composite parts. Given the high printing speeds, scalability, and commercial availability of reagents, our new printing method can be quite attractive for composite and AM industries.

5.2. Experimental section

5.2.1. Materials

Dicyclopentadiene (DCPD), 5-ethylidene-2-norbornene (ENB), and second-generation Grubbs' catalyst (GC2) were purchased from Sigma-Aldrich and used as received without further purification. Tributyl phosphite inhibitor (TBP, 93%) was obtained from TCI Chemicals. Cyclohexylbenzene (Acros Organics, 98%) was used to dissolve GC2. Short carbon fibers (CF) used in all experiments were kindly donated by Zoltek Corporation. Hexcel AS4 12K carbon fibers were kindly donated by Hexcel Corporation.

5.2.2. Preparation of 3D printing ink

The inks used for printing process were prepared based on the procedure described in chapter 3. Given that DCPD is solid at room temperature, DCPD was first melted in an oven at 60 °C and mixed with 5 wt% ENB to suppress the melting point of DCPD. The solution was stirred for one hour to obtain a homogenous mixture and degassed at 20 kPa overnight. All subsequent references to DCPD resin herein refer to the 95:5 DCPD/ENB solution. For all specimens, 6.42 mg GC2 (100 ppm with respect to DCPD) and 2.38 μL TBP (1 molar equivalent with respect to GC2) were completely dissolved in 500 μL cyclohexylbenzene by sonication for 10 minutes, followed by mixing the solution with 12 g of DCPD. The freshly prepared DCPD solution was transferred to an oven to partially cure the resin at 30 °C for one hour to increase the resin viscosity for effective mixing of CFs and preventing precipitation of dispersed fibers. CFs (15 vol%) were added to the resin solution and mixed for 5 minutes using a planetary centrifugal mixer (AR-100, Thinky USA) to obtain a uniform suspension. The resulting ink was then placed in an oven at 30 °C for another 20 minutes to allow further cross linking and pre-curing of the DCPD resin to form a highly viscous

ink amenable to 3D printing. The prepared ink was transferred to a 10 mL syringe barrel and centrifuged at 2000 rpm for 5 minutes to remove any bubbles.

5.2.3. 3D printing procedure

The syringe barrel containing the ink was placed inside an aluminum syringe holder mounted on a three-axis gantry robot. We maintained the ink temperature at -5 °C using two thermoelectric Peltier coolers embedded inside the aluminum syringe holder to avoid further crosslinking of the resin and achieve a constant viscosity profile during printing process (Figure D1 in Appendix D). The ink was pneumatically dispensed by a high-precision dispenser using an air pressure of 40 kPa and *in-situ* cured using a 450 nm blue laser light with output power of 4.5 W. The laser diode was installed on a custom-designed holder attached to the robot to steadily deliver light to the point of extrusion. The composite ink was controllably extruded through a micronozzle with an inner diameter of 1.6 mm and instantaneously cured upon exposure to laser. For printing unsupported spiral structures and supported tall cylinder, the ink was extruded on a custom-designed rotating platform spinning at a constant speed of 6.5 rpm. A print speed of 0.5 m/min was used for the bracket and the flexural samples. The printing paths to create 3D structures are provided in Appendix D.

5.2.4. Degree of cure measurements

Differential scanning calorimetry (DSC) measurements were carried out using a modulated DSC (DSC 2500, TA Instrument) to measure the degree of cure for printed samples. An uncured resin specimen (2-3 mg) and cured specimens (5-10 mg) were placed in aluminum hermetic pans, sealed, and heated from 25 to 250 °C at a heating rate of 5 °C/min to measure the total heat of reaction (H_t) and residual heat of reaction (H_r), respectively. The degree of cure (a) was calculated as,

$$\alpha = 1 - \frac{H_r}{H_t} \quad (1)$$

5.2.5. Flexural tests

Three-point flexural tests were conducted using a servo-hydraulic material testing system (858 MiniBionix; MTS 16 Systems) equipped with a 5-kN force capacity transducer. The flexural strength and modulus of printed and control samples were determined according to the ASTM D790 standard at ambient temperature, crosshead speed of 1.5 mm/min, and span length of 52 mm. Specimens were printed in a rectangular geometry with dimensions of 65 mm × 12 mm × 3 mm. For each ink formulation, at least three specimens were tested. The flexural strain, ε, on the outer surface of test specimens at midspan was calculated as,

$$\varepsilon = \frac{6dD}{L^2} \quad (2)$$

where D is the crosshead displacement, d is the thickness of the beam, and L is the support span length. Flexural stress, σ, was calculated as,

$$\sigma = \frac{3PL}{2bd^2} \quad (3)$$

where P is the applied load at the center of the beam and b is the width of the beam. It is assumed that the beam fails at the midspan of the beam. Flexural modulus and strength were estimated as the slope of the flexural stress-strain curve and the maximum stress sustained by the test specimens according to ASTM D790 standard, respectively.

To compare the flexural properties of printed samples, control specimens were produced using the traditional casting method, where the composite ink was transferred to a silicone mold with a 65 mm × 12 mm × 3 mm cavity sandwiched between two glass plates and cured via FP at room

temperature using a hot soldering iron. All samples were prepared using the same resin formulation and 15 vol% of carbon fibers.

5.2.6. Optical microscopy

Optical microscopy was used to visually assess the quality of printed parts as well as the orientation of fibers in the printed filaments. Microscopy specimens were cast in a mounting epoxy resin and polished using a polisher machine (PACE Technologies). Polished specimens were then imaged using a digital microscope (VHX-6000, Keyence).

5.3. Results and discussion

5.3.1. 3D printing of short carbon fiber-reinforced composites

Previous demonstrations on *in-situ* printing and curing of FRPCs rely on photopolymerization, which is not suitable for creation of large composite structures. Fundamentally, the above challenge caused by unattainable full cure conversion of light sensitive resins in the presence of light absorbing fibers requires post-curing steps, and results in inferior mechanical performance and thermal stability compared with thermally curable systems. In the present work, we introduce a new *in-situ* printing technique based on photothermal curing method to rapidly create solid polymers for rapid and scalable prototyping and production of FRPCs. This approach includes using a thermal stimulus to speed up the rate of polymerization or crosslinking. An increase in the rate of polymerization enhances printing speed and improves the fidelity of printed parts. Such high rates of polymerization can be realized by delivering an external localized energy supply to the portion of the composite ink extruded from the nozzle. Figure 5.1 depicts the curing procedure of our printing method. The thermal stimulus used here is a 450 nm laser beam,

which is directed toward the point of extrusion and that rapidly heats up the surface of the filament due to the photothermal conversion effect.[194]

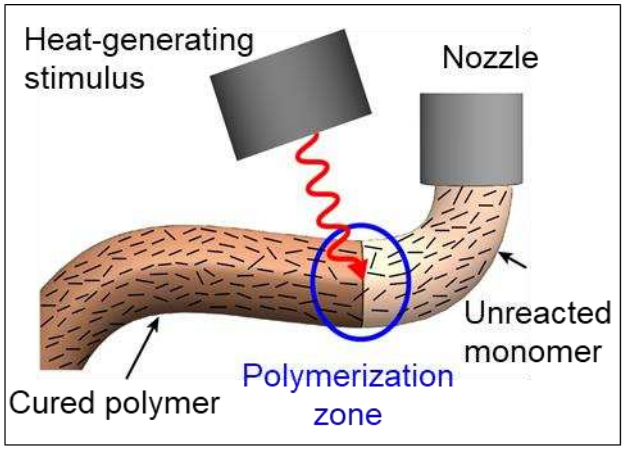

Figure 5.1. Schematic representation of our novel *in-situ* printing and curing technique.

The use of an external thermal stimulus for generating highly localized thermal effects has been previously exploited in photothermal cancer therapy, cell imaging, micropatterning, and self-healing materials.[195–197] To date, various types of thermal stimulus implementation has been demonstrated including laser light, plasma, microwave, electro-magnetic field, electro-resistive heating, and ultrasonic waves.[17,97,198–201] While all of these methods are capable of instantaneous localized heating, we utilize a laser beam in this study because of accessibility, facile operation and easy integration with the DIW process.

The photothermal heating achieved by the laser is sufficiently short to provide effective *in-situ* curing of the composite ink. Upon laser-induced polymerization, the composite ink is rigidified instantaneously, allowing for freeform writing in mid air. A bracket with sharp corners is made using the laser curing system that spans 40 mm and requires no additional support material to manufacture (Figure 5.2a). The bracket is printed in two layers where the second layer is deposited and *in-situ* cured on the previously cured layer, demonstrating the capability of this approach for freeform fabrication of multilayer objects. The laser curing method is not limited to

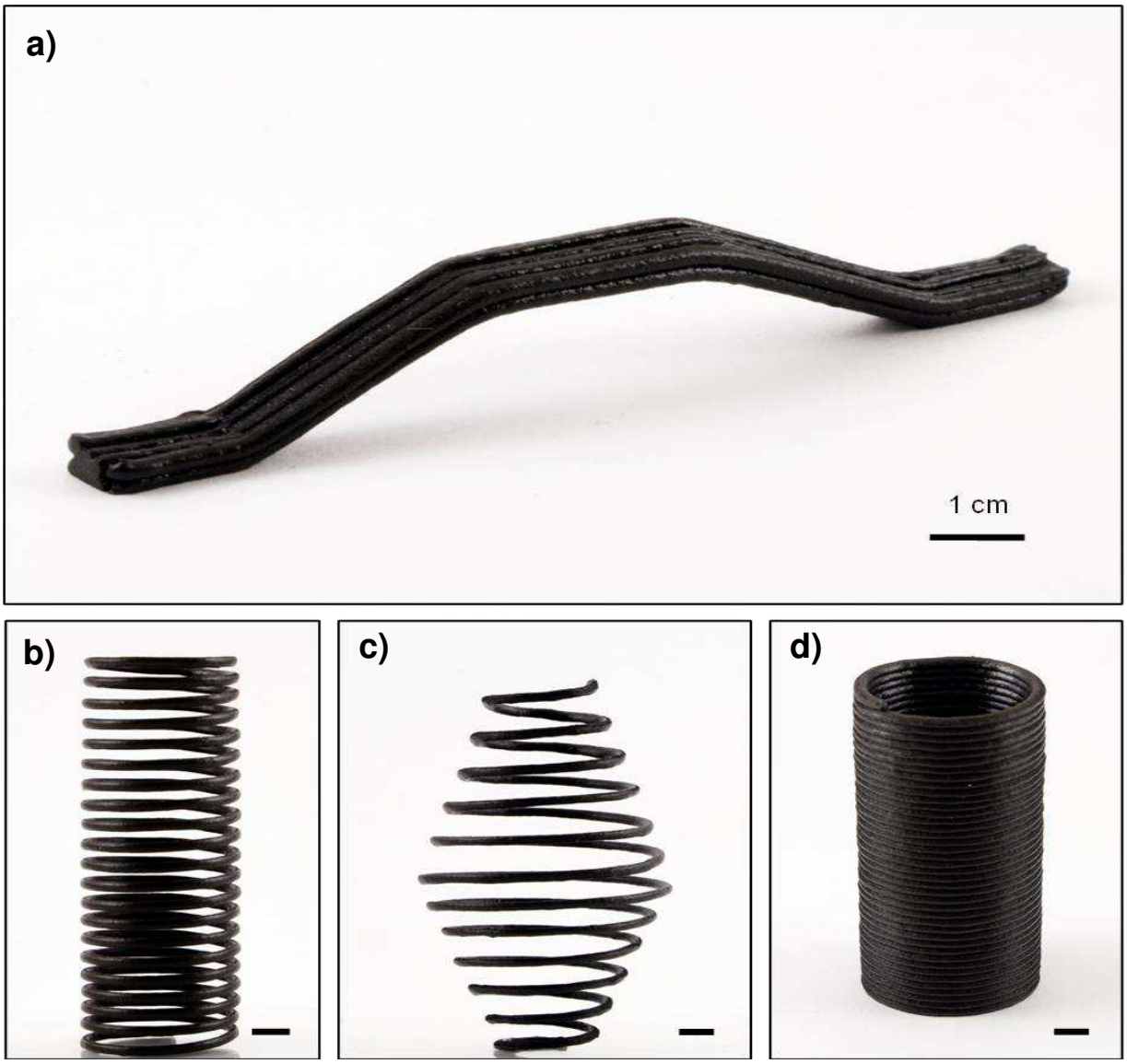

Figure 5.2. Additive manufacturing of complex geometries using the developed laser assisted printing technique with the ink containing 15 vol% CF. (a) An example of a multi-layer object printed linearly in the air. (b, c, d) Samples were printed on a rotating platform while the nozzle moved in the x-z plane at varying speeds. Scale bar in b–c represents 5 cm.

a traditional X-Y stage; a rotating platform is also used to freeform print symmetric objects like unsupported spiral structures (Figure 5.2b, 5.2c). In addition to enhancing the manufacturability of complex shapes, this printing technique can facilitate the manufacturing of high aspect ratio printed parts not previously accessible in layer-by-layer printing of thermoset resins. As a proof of concept, we demonstrate printing of a tall cylinder (average height = 45 mm) without ink distortion

as printing height increases (Figure 5.2d). The results indicate scalability of the printing process to create large composite structures.

5.3.2. Effect of printing parameters on in-situ curing process

Successful *in-situ* 3D printing process greatly depends on curing of the composite ink, which can be affected by power density of laser beam. We designed a simple experiment by printing 100-mm straight filaments using a laser diode system with a constant output power of 4.5 W to examine the influence of power density on the photothermal curing process. In all experiments, composite inks filled with 15 vol% CFs are extruded on a glass substrate using various printing speeds (i.e., 0.5, 1, and 1.5 m/min) and immediately exposed to the laser with tuned power density. The power density of laser beam is controlled by adjusting spot size of the laser. When the composite ink is irradiated with the laser, the light is absorbed by CFs embedded within the composite ink and its energy is transformed to heat, resulting in a rapid increase in ink temperature.[202] The heat generated is then consumed by the surrounding matrix to locally polymerize the resin. Printing at high speeds reduces the amount of heat generation due to reduced exposure time of resin leading to incomplete curing of the composite ink; hence, it is essential to tune the power density of laser beam when using higher printing speeds. Figure 5.3 displays the power density values exploited to achieve a hot spot temperature of 240 °C at various printing speeds to ensure the maximum amount of heat is delivered to 3D printing inks without potential occurrence of defects caused by overexposure of resin. Figure 5.3 shows that the power density linearly increases with printing speed which is adjusted by reducing the laser spot size to concentrate the energy of beam on the extruded material.

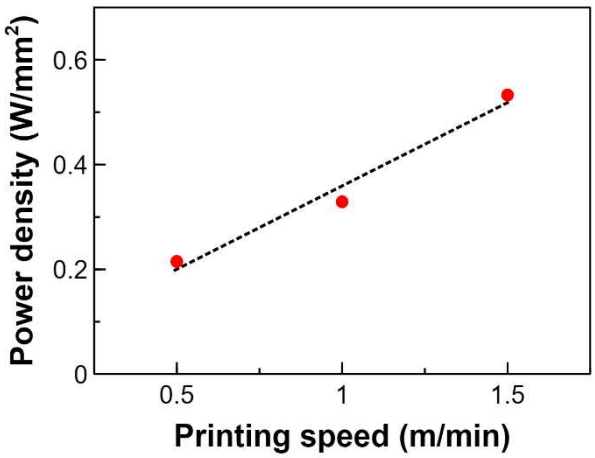

Figure 5.3. The power density used to print composite inks at various printing speeds.

Using the power density values obtained from the previously described procedure, degree of cure is measured by printing straight composite filaments at various printing speeds and nozzle diameter. The measurements obtained from DSC tests reveal that the degree of cure drops as printing speed increases due to reduced exposure time of resin (Figure 5.4a). Also, the maximum allowable printing speed while the composite fully cures ($\alpha > 95\%$) is around 1.5 m/min. This speed is the highest printing speed reported to date for simultaneous printing and curing of a thermally curable thermoset composite. Further experiments on the effect of nozzle size show that the degree of cure almost remains constant as the nozzle diameter increases (Figure 5.4b).

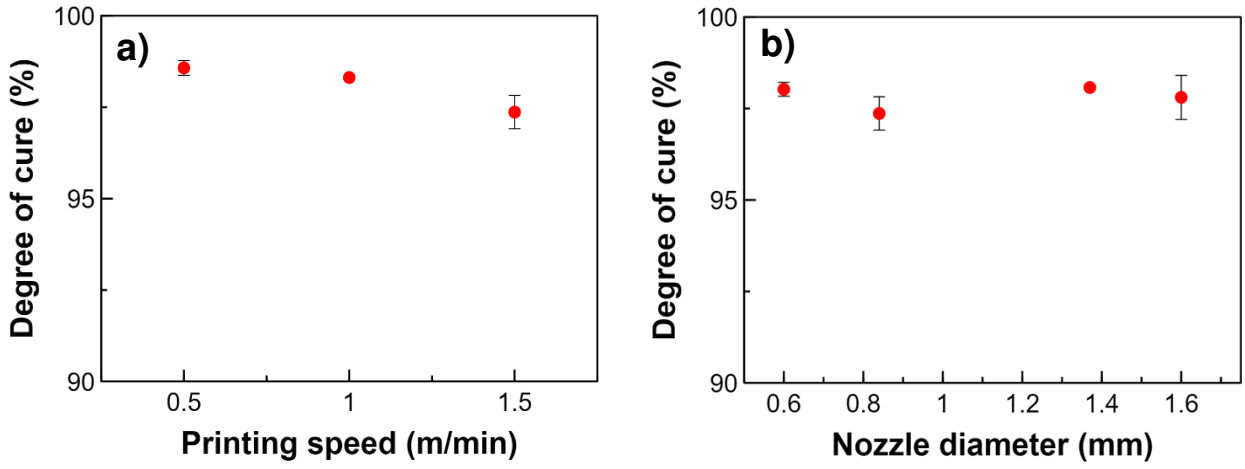

Figure 5.4. Effect of printing speed and nozzle diameter on degree of cure measured by DSC experiments.

5.3.3. Mechanical and microstructure characterization

Flexural experiments are performed on 3D printed specimens according to the ASTM D790 standard to determine the mechanical performance of printed parts. Using laser curing system, bar specimens containing 15 vol% CF are printed by printing the ink in parallel and transverse to the length of the bar. As a control, additional bar specimens are also fabricated by conventional molding and subsequent curing by FP. We found that flexural modulus and flexural strength of samples printed in parallel direction are significantly higher than those prepared by the conventional molding process (Figure 5.5a, 5.5b). However, printing in transverse direction results in inferior mechanical properties compared to the molded counterparts with the same

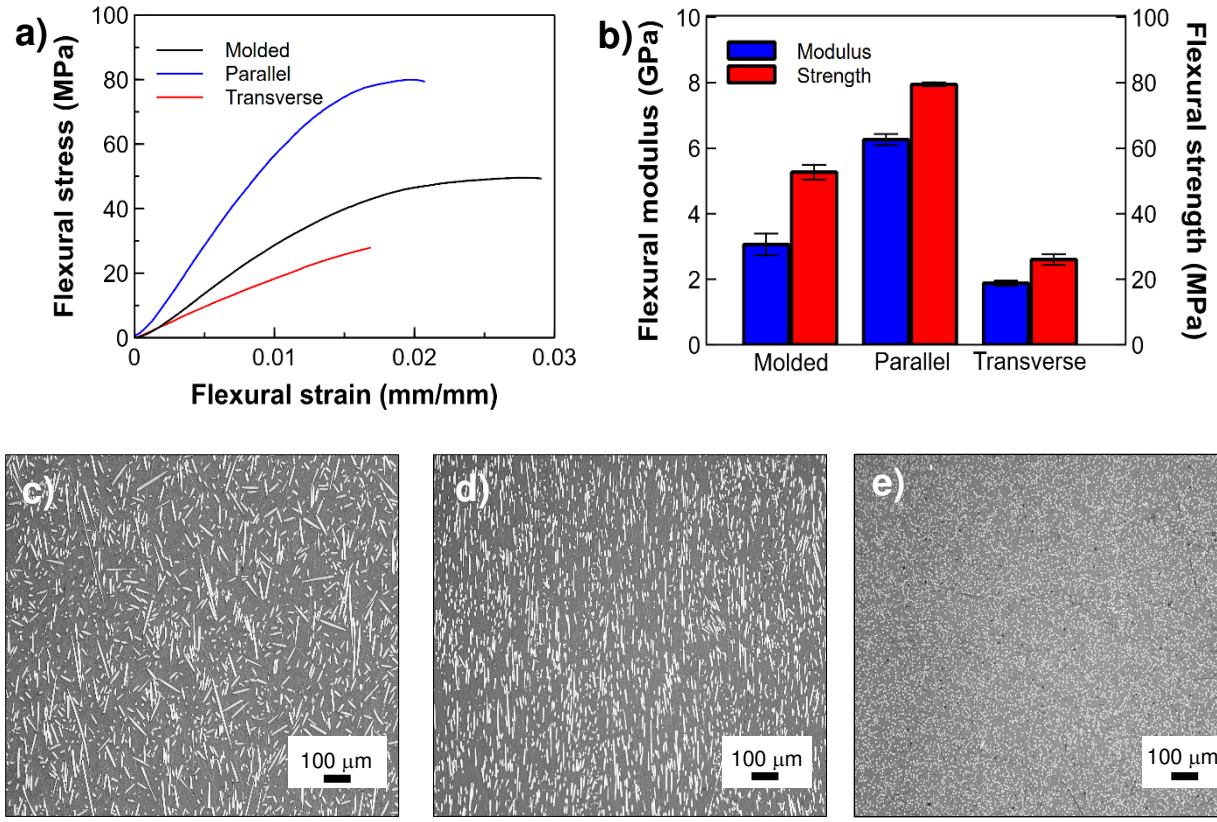

Figure 5.5. (a) Representative flexural test curves for printed and molded samples. (b) Comparison of flexural modulus and flexural strength of samples printed in parallel and transverse as well as control, molded samples. (c, d) Optical micrographs from the polished surface of molded and 3D printed bar specimens, respectively, indicating fiber orientation induced by 3D printing process. (e) Optical micrograph from polished cross-section of 3D printed bar specimen.

concentrations of carbon fibers. This observation can be attributed to the alignment of CFs caused by the printing process that plays a critical role in directional reinforcement of fibers (Figure 5.5c-d).[133] Further microstructure characterization from the surface of printed samples shows no defect formation by degassing or boiling of monomers in the photothermal curing process (Figure 5.5e and Figure D2 in Appendix D).

5.3.4. 3D printing of continuous carbon fiber-reinforced composites

A key advantage of 3D printing via laser is to manufacture continuous carbon fiber-reinforced composites which cannot be achieved by FP-assisted 3D printing technique due to the lower energy density of resin at high fiber volume concentrations. Figure 5.6a represents details of the printing process. A dry continuous carbon fiber is guided into a syringe barrel filled with DCPD resin, impregnated, and then extruded through a squeezing nozzle to remove the excess amount of resin. The impregnated fiber is then placed on a glass substrate using a 6-axis robot and compacted with assistance of a soft roller and immediately cured by the laser. Figure 5.6b shows a composite loop printed and *in-situ* cured via a 4.5 W laser diode using a 12K carbon fiber tow. This simple yet powerful manufacturing technique opens new opportunities for rapid manufacturing of multiscale fiber-reinforced composites for a wide range of applications.

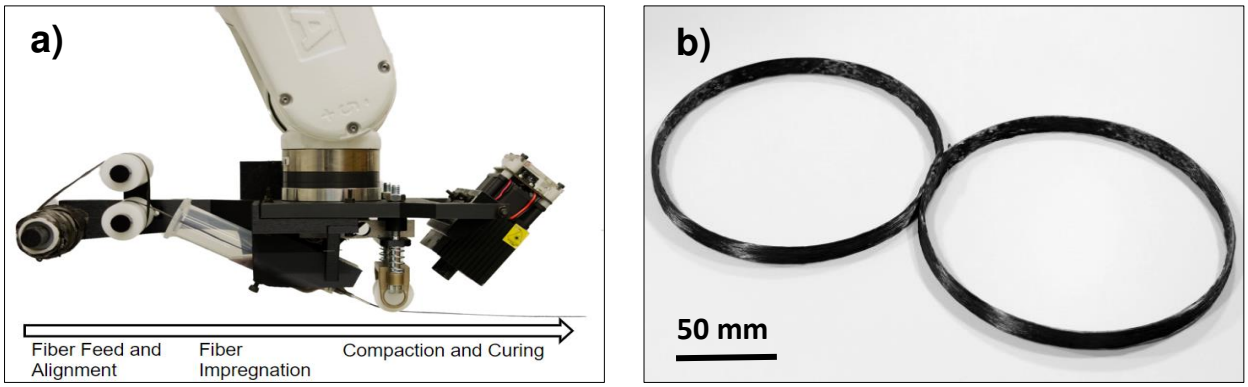

Figure 5.6. (a) Experimental setup used for continuous fiber 3D printing via a laser. (b) A continuous carbon fiber-reinforced composite structure produced via the developed 3D printing technique using printing speed of 0.5 m/min.

5.4. Conclusions

A novel AM technique for the manufacture of high-performance and high-quality FRPC parts is developed. The overarching goal of this study is to print FRPC parts at high speeds and with high degrees of cure. Previous demonstrations on AM of FRPCs use bulk curing of thermal curable resin systems which are not applicable to creation of large composite structures. Instead of relying on bulk polymerization of printed parts, *in-situ* printing and curing technique is suitable for large-scale manufacturing and enables printing freeform structures. In this work, we use a thermal stimulus to deliver the required energy for controlled and rapid heating at the reaction site for *in-situ* printing and curing of composite structures at high speeds which cannot be achieved using any other methods. The thermal stimulus is a 450 nm laser beam to rapidly heat up and cure the extruded ink. Our laser-assisted printing method is suitable for manufacturing large composite structures with much less consumed energy (six orders of magnitude less energy) compared to conventional autoclave/oven curing methods.

Chapter 6: Bubble-Free Free Radical Frontal Polymerization Using Redox Initiators

6.1. Introduction

Thermosetting polymers and composites are widely used in many industrial applications from aerospace to automotive to prosthetics due to combination of excellent specific mechanical properties, good resistance to elevated temperatures and corrosive environments, and their flexibility in use in various manufacturing processes.[203,204] However, conventional manufacturing of thermosetting polymers and composites is slow, expensive, energy-inefficient, produces a significant amount of carbon footprints, and requires expensive autoclaves or ovens for curing of resin.[2,3,79] Alternatively, frontal polymerization (FP) is a promising curing strategy that can drastically reduce the energy consumption and overall manufacturing time, offering a sustainable solution for larger scale production of thermosetting polymers and composites. FP is a mode of polymerization in which a resin filled with a thermal latent initiator cures on demand at room temperature through activation via a hot trigger. Once FP is started by activation of the initiator, a self-sustaining reaction wave is produced and propagates through the monomers by coupling of thermal diffusion and the Arrhenius kinetic of the exothermic reaction to convert unreacted monomers to a solid polymer.[151]

An early demonstration of FP was carried out on methyl methacrylate using benzoyl peroxide as a thermal laten initiator in a closed reaction vessel under a high pressure (3500 atm) to promote the rate of polymerization and eliminate convective instabilities in front propagation.[20,205] Since FP at this extreme condition is hard and cannot be easily integrated in many manufacturing

processes, FP research has been extended to multifunctional acrylate systems. Compared with methacrylate monomer, FP of multifunctional acrylates can be performed at ambient pressure due to their higher reactivity,[29,152] produce a thermoset polymer with enhanced mechanical properties,[206] and mitigate Rayleigh–Taylor instability that is detrimental to the traveling front.[207] Considering the advantage of multifunctional acrylates over methacrylate monomers, a great deal of work has been conducted on using these monomer systems for various applications including development of new adhesives and coatings for wood substrates,[208] fabrication of foams with varying porosity,[209] and rapid manufacturing of microfluidic endoskeletons.[28]

The most common types of thermal initiators used for FP of multifunctional acrylates are peroxide and nitril initiators including benzoyl peroxide (BPO), tert-butylperoxide (t-BPO), cumene hydroperoxide (CHP), 1,1-Di-(tert-butylperoxy)-3,3,5-trimethylcyclohexane (Luperox 231), and 2,2-azobis(isobutyronitrile) (AIBN).[102,206,210,211] Among these initiators, Luperox 231 is a more stable thermal initiator that can be easily dissolved in acrylate systems and allows high conversion of monomers (< 92%) upon FP.[212] However, FP using the above initiators generates volatile components upon initiator decomposition that can substantially reduce the mechanical performance of produced polymers.[213] In addition, FP of multifunctional acrylates is highly exothermic and lacks sufficient control over the front temperature. For example, FP of diacrylate and triacrylate monomers results in front temperatures above 300 °C leading to boiling of monomers and collapse of propagating front.[29] Also, polymerization at such high temperatures can potentially result in degradation of cured polymer or even a burnout of the initiator leading to a very low conversion of monomers, which greatly limits its practical application.[214]

Several methods have been developed to address the problems related to FP of acrylate monomers by reducing the front temperature. One approach is FP in the presence of peracrylates

that decomposes upon copolymerization with acrylate monomers allowing FP to occur at lower temperatures.[215] This method can reduce bubble formation, but it adversely affects the stability of polymerizing front. In addition, inert fillers or nonvolatile deep eutectic solvents have been utilized to absorb the heat of polymerization and reduce front temperature.[216,217] In another work, frontal copolymerization of acrylate monomers with thiol-acrylate systems was performed to lower the enthalpy of polymerization.[90] Addition of thiol-ene monomers can decrease the front temperature and make produced polymer more flexible but significantly shortens the pot life of resin.

Compared with the above techniques, FP using redox initiators has shown to be very effective in performing bubble-free free-radical FP under controlled reaction condition. However, use of thermally activated redox initiated systems are mainly limited to synthesis of hydrogels while FP of multifunctional acrylates has not been reported to date.[218–222] Therefore, in this study we aim to study FP of acrylate monomers with various functionality including methyl methacrylate (MMA), 1,6-hexanediol diacrylate (HDDA) and trimethylolpropane triacrylate (TMPTA) using *N,N*-dimethylaniline/ benzoyl peroxide (DMA/BPO) redox initiator at room temperature and compare their front properties and pot life with the front behavior and the pot life obtained by a conventional peroxide initiator based on Luperox 231.

6.2. Experimental section

6.2.1. Materials

Methyl methacrylate (MMA, 99%), 1,6-hexanediol diacrylate (HDDA, 90%), and trimethylolpropane triacrylate (TMPTA, 88%) were used as mono to trifunctional monomers and obtained from Fisher Scientific, TCI America, and Alfa Aesar, respectively. The redox couple was composed of benzoyl peroxide (BPO, 97%) and *N,N*-dimethylaniline (DMA, 99%), purchased from Fisher Scientific. Luperox 231 (1,1-Bis(tert-butylperoxy) 3,3,5-trimethylcyclohexane) was

used as a peroxide initiator and obtained from Sigma-Aldrich. All chemicals are commercially available and used as received without further purification. The chemical structures of the monomers and initiators are presented in Figure 6.1.

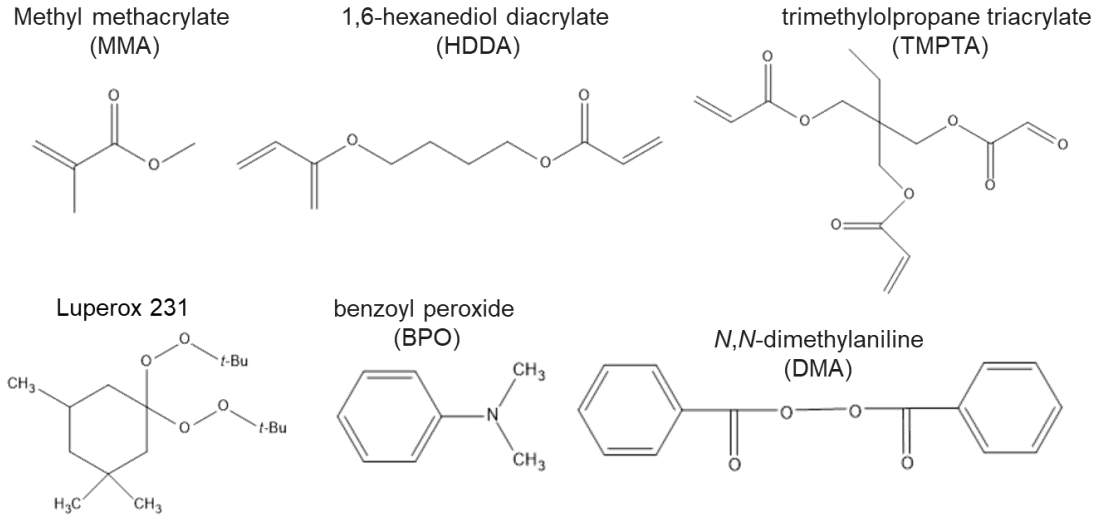

Figure 6.1. Reagents used in this study.

6.2.2. Preparation of reactant solutions

In all experiments, 12 g of monomers were weighed out into a 100 mL disposable cup using the Sartorius Quintix balance. FP solutions using peroxide initiator were prepared by measuring 0.4 phr (parts per hundred resin) Luperox 231 on the Mettler-Toledo microbalance and mixing it with the resins using the planetary centrifugal mixer (AR-100, Thinky USA) for 2 min. For FP experiments using the redox initiator, 0.2 phr BPO was measured on the Mettler-Toledo microbalance and mixed with the resins using the centrifugal mixer for 2 min. After adding BPO, DMA with various molar ratios with respect to BPO (i.e., 0, 4, 8, 16 and 32 mol/mol) was pipetted into the prepared mixtures using the Ergonomic High-Performance micropipette and centrifuged for 1 min. The resulting mixtures were then transferred to a 10 mL glass test tube (15 mm

diameter), and FP reaction was triggered by applying heat via touching a hot soldering iron to the upper side of mixtures.

6.2.3. Measurements of front behavior

Once FP was formed, the heat source was removed, and front propagation was monitored using a Canon EOS 90D DSLR (Figure 6.2a). The front velocity was calculated by plotting front position as a function of time and finding the slope of the best fit straight line (Figure 6.2b). Temperature profile of resin during FP experiments was continuously measured using a K-type thermocouple connected to a thermocouple reader (Phidgets Inc., model 1048) and recorded by a custom LabVIEW code (National Instrument) at 3 Hz. The maximum temperature obtained from the thermocouple was identified as a front temperature (Figure 6.2c). Activation time was determined as the time required for the hot trigger to initiate self-propagating front. All experiments were carried out three times.

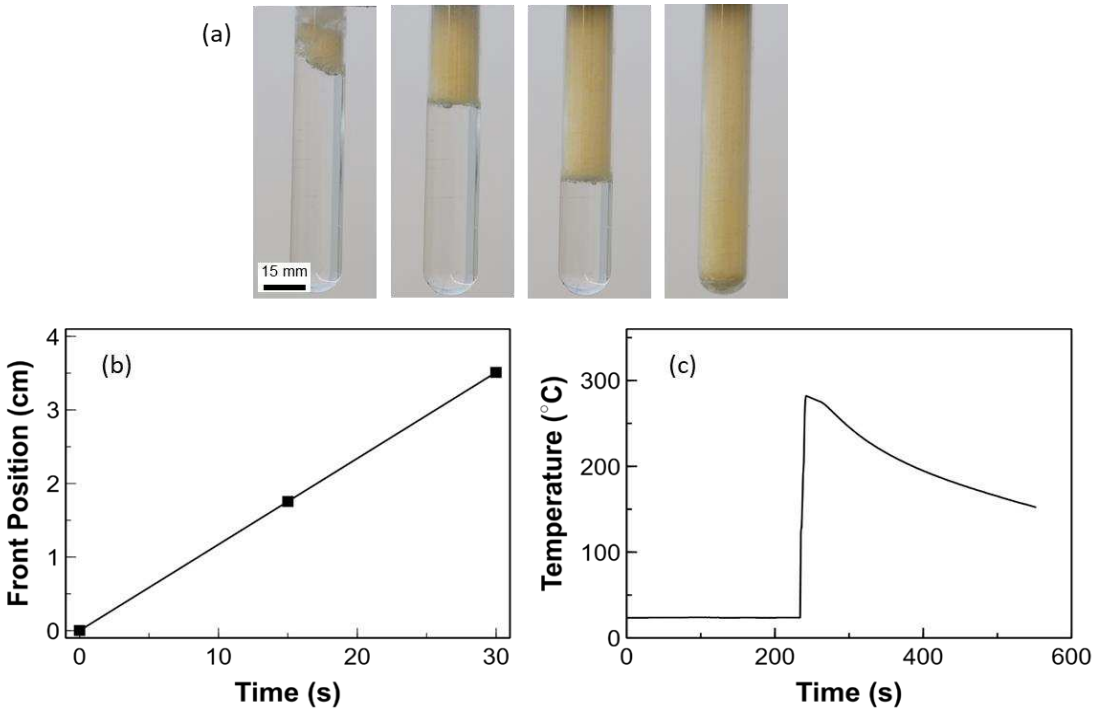

Figure 6.2. a) Sequential images captured from FP of HDDA monomer using 0.4 phr Luperox 231. b) Front position vs. time. c) The temperature profile of the resin collected by a thermocouple during FP.

6.2.4. Optical imaging

The samples frontally polymerized in the test tube were cut via a precision saw (PACE Technologies, PICO 155P) operating at low speed (900 rpm), and images of their surface were captured using a digital microscope (Dino-Lite Edge 5 MP) to qualitatively evaluate the effect of DMA concentration on the amount of bubble formation.

6.3. Results and discussion

6.3.1. Frontal polymerization using peroxide initiator

Luperox 231 is the most common type of thermal initiator used for free-radical frontal polymerization of varying vinyl monomers due to its high stability at room temperature, high solubility in organic media, and less gas production per radical upon decomposition compared to most peroxides and nitriles.[223–225] Thus, motivated by these essential requirements, FP of diacrylate monomers was first examined using Luperox 231. Figure 6.2a displays sequential snapshots captured from front propagation in HDDA monomer using 0.4 phr Luperox 231 as an FP initiator. FP experiments reveal significant bubble formation in the test tube that is mainly caused by the initiator decomposition. Upon decomposition of Luperox 231, volatile compounds including acetone and methyl radicals are produced that lead to generation of bubbles with various sizes in the sample (Figure 6.3a).[226] The presence of small bubbles scatters the light and makes the material opaque, whereas the polymer itself is transparent.[214]

Another source of bubble in FP of diacrylate monomers is attributed to the highly exothermic nature of the reaction. In thermal FP, increase in exothermic heat of polymerization promotes the rate of reaction and helps the front propagate faster; however, it can induce nucleation of bubbles via boiling of monomers at the reaction front.[227] Measurements of front behavior for diacrylate monomer reveals that the front propagates as high as 7.02 cm/min, which is relatively fast

compared to other frontally curable monomer systems; however, it results in front temperatures up to 282.33 °C that can result in nucleation of bubbles.

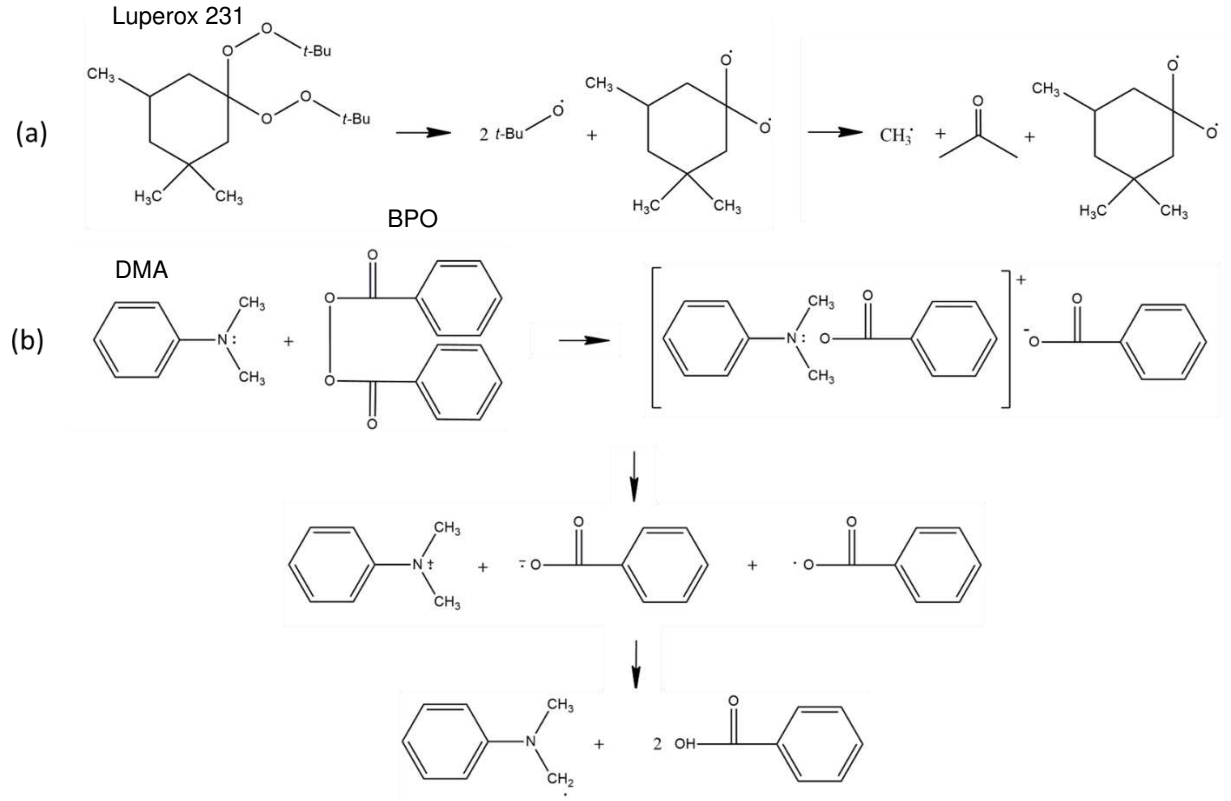

Figure 6.3. Initiation mechanism for a) Luperox 231, and b) DMA/BPO redox initiator.

6.3.2. Frontal polymerization using redox initiator

Previous studies have shown that redox initiators can be used to suppress bubble formation in free-radical FP of vinyl monomers, which is not possible by Luperox 231 alone.[228,229] A redox initiator contains the oxidant BPO and the reductant DMA that enables FP to proceed through oxidation-reduction reaction activation mechanism. The initiation mechanism in DMA/BPO system involves an electron transfer from the nitrogen of aniline to the peroxide leading to dissociation of oxygen-oxygen bond and generation of free radicals (Figure 6.3b).[230] As opposed to Luperox 231, use of the redox initiator prevents bubble formation in FP of HDDA monomers by eliminating production of volatile components (Figure 6.4a). We observed that some bubbles

are formed at the beginning of front propagation, which can be caused by the preheating of monomer and higher initial temperature of resin at the top of the test tube (Figure 6.4a). However, as the front propagates toward the end of the test tube, no visible bubbles are formed, allowing bubble-free propagation of FP.

Interestingly, FP in HDDA monomers using the redox initiator produces periodic patterns on the surface of product (Figure 6.4b). These periodic patterns are formed due to Rayleigh-Taylor instability or double-diffusive instability where a molten polymer diffuses into the monomer ahead of descending front, leaving interesting patterns in the product.[231] The instability results in non-uniform curing across the material and can be harnessed to autonomously produce functionally patterned materials.[232]

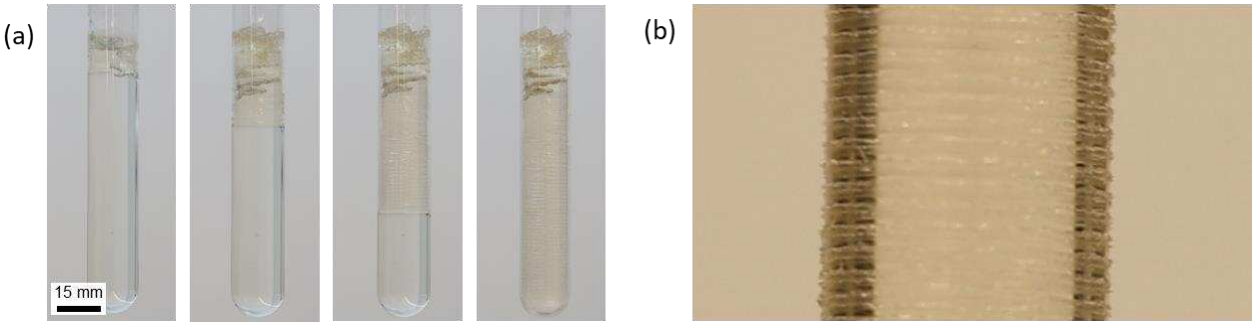

Figure 6.4. a) Sequential images captured from FP of HDDA monomer using 0.2 phr BPO and DMA/BPO molar ratio of 32. b) A spontaneous pattern is formed during FP of diacrylate monomer.

6.3.3. Effect of DMA/BPO ratio

Previous studies have shown that the efficiency of a redox system greatly depends on the oxidant (BPO) and reductant (DMA) ratio, and it can influence the amount of bubble formation and front behavior.[228] We carried out a series of FP experiments using HDDA as frontally curable monomer with various DMA/BPO molar ratio to elucidate this effect on various parameters including bubble formation, front velocity, front temperature, and activation time. FP tests were performed at a constant concentration of oxidant, BPO = 0.2 phr, while DMA/BPO ratio was

varied from 0 to 32 mol/mol. We found that by increasing DMA concentration the amount of bubble formation is suppressed. Figure 6.5b shows the cross-section images of FP-cured samples prepared by various concentrations of DMA, which are fractured roughly from the location indicated in figure 6.5a. The cross-section views illustrate that a relatively smoother fracture surface can be obtained when using more DMA, indicating less bubble formation. Interestingly, bubble formation is completely prevented when DMA/BPO molar ratio is 32. The reason for this behavior is that at low DMA concentrations, FP activation is mostly derived from the decomposition of peroxide initiator leading to liberation of carbon dioxide, whereas at high DMA concentrations free radicals produced by decomposition of peroxide initiator are reduced to anions in the presence of excess DMA that further activates the FP reaction.[228]

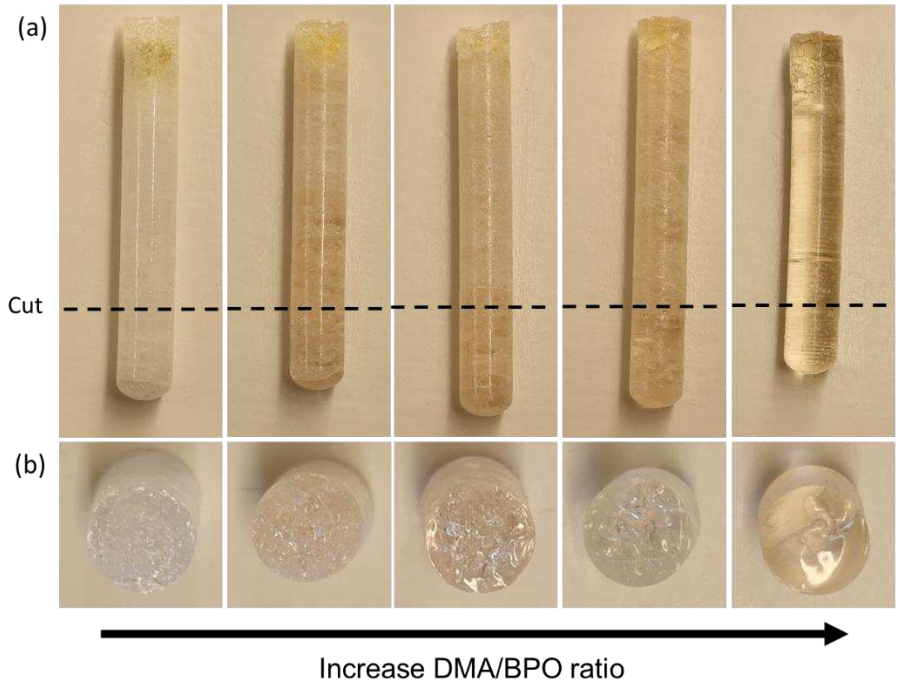

Figure 6.5. Images captured from of a) frontally cured HDDA monomers in the test tube using the redox initiator at a fixed 0.2 phr BPO and various DMA concentrations, and b) the cross sections approximately cut from the location indicated by the dotted line. From left to right DMA/BPO molar ratio are 0, 4, 8, 16, 32.

In addition to reducing gas byproducts, our experiments with FP of diacrylate monomer demonstrates that the front propagates slower at a higher DMA/BPO ratio, which is related to the inhibiting effect of excess DMA on the rate of polymerization (Figure 6.6a). It is observed that the front velocity decreases from 4.89 to 1.96 cm/min when DMA/BPO molar ratio is increased from 0 to 32 mol/mol. Reduction in front velocity prolongs the time of heat loss through boundaries, which can reduce front temperature. Our measurements confirm that the front temperature monotonically decreases from 277.7 °C to 234.9 °C with increasing DMA/BPO molar ratio, allowing to perform FP under a milder reaction condition (Figure 6.6b).

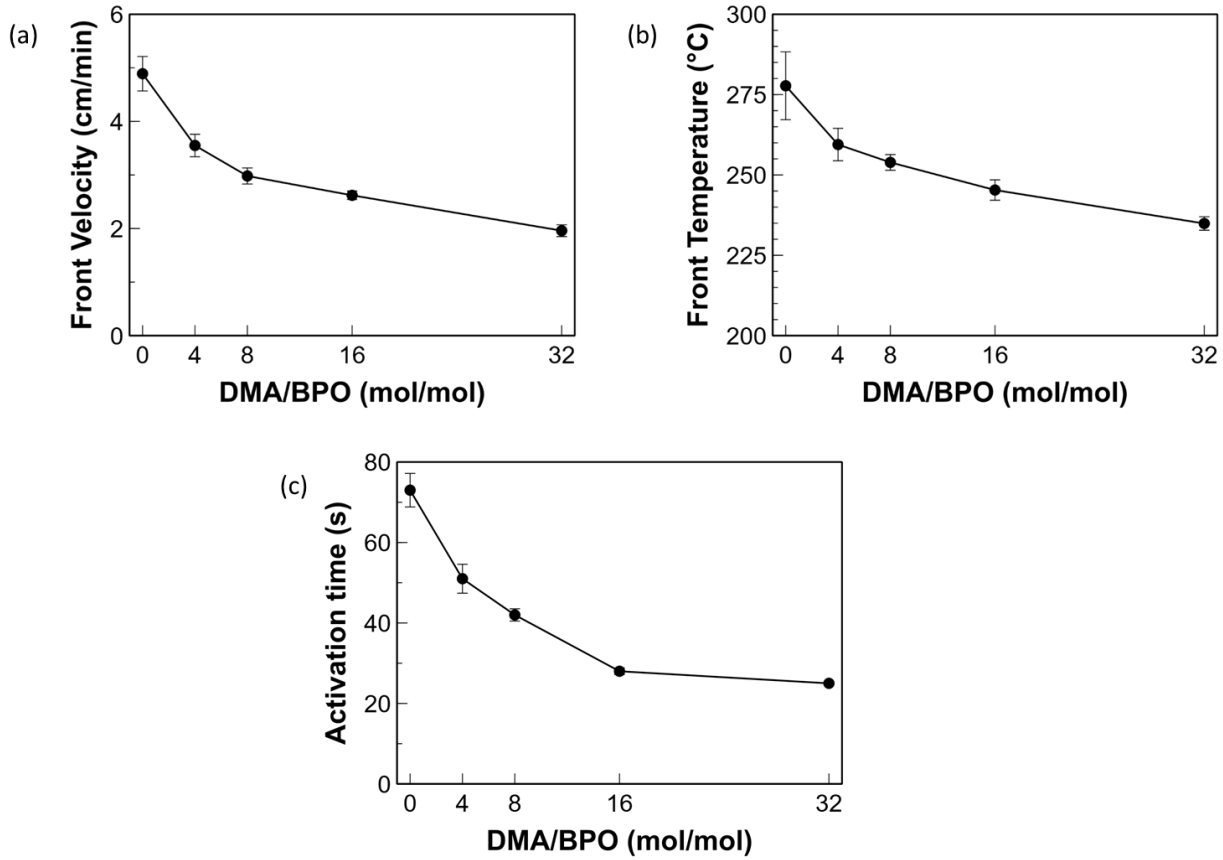

Figure 6.6. a) Front velocity, b) front temperature, and c) activation time measured for the redox-initiated diacrylate system with various DMA concentrations.

Another advantage of redox initiator systems is that they have lower activation energy compared to peroxide initiators, which enables faster triggering of FP without overheating of the monomer.[233,234] The results of activation time measurements, defined as the time required to apply the hot trigger to the formation of self-propagating front, are shown in Figure 6.6c. The activation time of FP reaction in diacrylate monomer continuously decreases when using a higher DMA concentration. A high DMA concentration promotes decomposition of peroxide caused by the excess amount of aniline that results in a faster FP activation. For example, the system containing only BPO takes 73 s to initiate FP that can cause overheating and potential degradation of the produced polymer at the location where FP is initiated. This can be confirmed by the change in color at the upper part of the produced polymer where the hot trigger is applied (Figure 6.5a). However, this problem can be mitigated using higher DMA/BPO ratios and completely avoided using a DMA/BPO ratio of 32.

6.3.4. Pot life

The essential criterion for FP system is that it should be stable at room temperature and have enough work time to be usable for various manufacturing processes. Table 6.1 compares the pot life of diacrylate resin systems obtained by Luperox 231 and the redox initiator with various DMA/BPO molar ratios. The pot life was determined by adding the initiator to the monomer and storing the resin solution at room temperature and observing whether the resin can still be frontally polymerized at different periods of time. A key advantage of using Luperox 231 is that it has extended pot life compared to the redox initiator due to its larger activation energy. The resin solution obtained by 0.4 phr Luperox 231 can be cured by FP at least after 24 h storage at room temperature and becomes unreactive to FP after this period due to the reduced reactivity of reagents. We also observed that the FP solution prepared with 0.2 phr BPO in the absence of DMA

exhibits a pot life of at least 24 h. However, with increasing the DMA concentration the pot life is significantly reduced, and the resin spontaneously polymerizes within a few minutes to hours of storage at room temperature. For the resin formulation containing DMA/BPO ratio of 32, where no bubble is formed, the pot life is approximately 15 min. Although the pot life achieved by this resin formulation is short, future studies are required to investigate other types of redox initiator

Table 6.1. Comparing pot life measured for diacrylate systems prepared by Luperox 231 and redox initiator with various DMA concentrations. Scale bar represents 5 mm.

Initiator	**DMA/BPO (mol/mol)**	**Pot life**	**Cross section of FP-cured samples**
Luperox 231	-	>24 h	
Redox	0	> 24 h	
	4	> 5 h	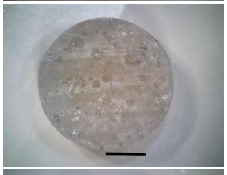
	8	2 h	
	16	1 h	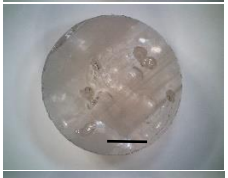
	32	15 min	

systems with a higher activation energy compared to DMA/BPO to obtain a FP system with an extended pot life.

6.3.5. Effect of acrylate functionality on front properties

FP of monomer systems with various functionality is very interesting for rapid manufacturing of thermoplastic and thermoset polymers with controlled mechanical properties. For example, FP of monofunctional monomers can pave the way toward rapid manufacturing of thermoplastic polymers with the advantage of being able to be recycled,[235] whereas FP of multifunctional monomers produces thermoset polymers with enhanced thermomechanical properties.[152] Thus, motivated by this fact, a series of FP experiments were also carried out on methyl methacrylate (MMA) and trimethylolpropane triacrylate (TMPTA) monomers using Luperox and DMA/BPO redox initiators. For Luperox initiator system, FP solutions were prepared by mixing the monomers with 0.4 phr Luperox initiator, and for redox initiator system the monomers were mixed by 0.2 phr BPO and various DMA concentrations (i.e., 4, 8, 16, and 32 mol/mol with respect to BPO) in order to compare their front properties with the front behavior previously measured for diacrylate monomer. FP experiments on MMA reveal that this monofunctional monomer cannot support FP reaction at ambient condition, irrespective of the type of initiator due to its low intrinsic reactivity.[29] While MMA cannot be frontally polymerized, TMPTA is highly reactive to thermal FP reaction (Figure 6.7a). Front velocity measurements obtained from TMPTA using Luperox initiator indicates that TMPTA produces a higher front velocity, 11.42 cm/min, and front temperature, 319.53 °C, compared to diacrylate monomer due to a higher acrylate group concentration and increased crosslinking (Figure 6.7b, c).[29] However, similar to FP of diacrylate monomer, a significant amount of bubbles are formed upon FP of triacrylate (Figure 6.7a). FP runs on triacrylate monomer were also performed using DMA/BPO redox initiator to prevent bubble

formation by eliminating gaseous byproducts caused by initiator decomposition. The results show that triacrylate monomer system is highly unstable and spontaneously polymerizes upon addition of redox initiator, irrespective of DMA concentrations, indicating on-demand polymerization of triacrylate monomer cannot be achieved using DMA/BPO redox initiator (Figure 6.8).

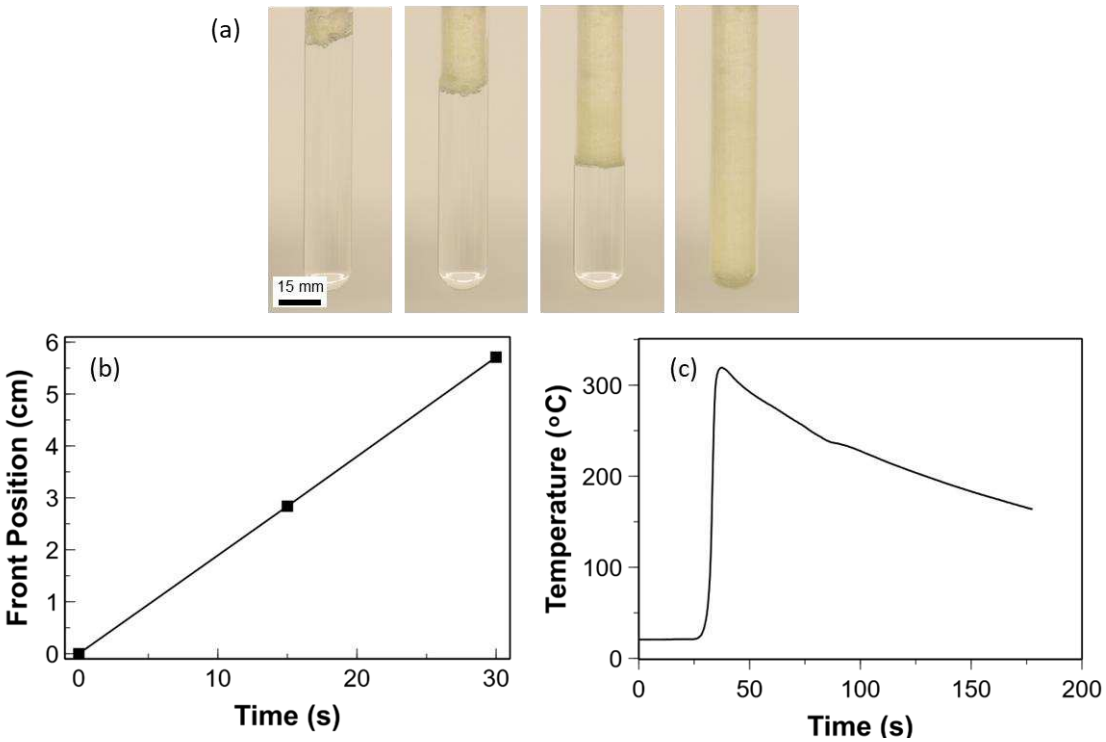

Figure 6.7. a) Sequential images captured from FP of TMPTA monomer using 0.4 phr Luperox 231. b) Front position vs. time. c) The temperature profile of the resin collected by a thermocouple during FP.

Figure 6.8. a) TMPTA monomer containing 0.2 phr BPO and DMA/BPO of 4 mol/mol spontaneously polymerized upon addition of redox initiator.

6.4. Conclusions

This study reports the effect of Luperox 231 and DMA/BPO redox initiator on the synthesis of 1,6 hexanediol diacrylate monomer by free-radical FP at ambient condition. The experimental results indicate that while FP solution containing Luperox 231 exhibits a longer pot life and a faster front propagation, a significant amount of bubble formation occurs during the FP reaction. The main reason for bubble formation is attributed to production of volatile byproducts including acetone and methane upon decomposition of Luperox 231. The gaseous byproducts can be avoided using DMA/BPO redox initiator that allows to perform bubble-free FP. It is found that bubble formation and front behavior can be controlled by changing the reductant concentration. An increase in reductant concentration reduces the amounts of bubble formation and enables FP at a lower front temperature, but it significantly reduces the pot life of resin. While FP of diacrylate monomer using the redox initiator results in a thermoset polymer, the results of this study can be extended to other vinyl monomer systems for future design of thermoplastic polymers.

Chapter 7: Conclusions

This chapter summarizes the results of this research work, presents the main contributions of the research, and provides new topics for future studies.

7.1. Concluding remarks

The objective of this dissertation was to develop advanced manufacturing techniques to rapidly fabricate thermosetting polymers and composites with minimal tooling and energy requirements. Such new manufacturing techniques are designed by combining novel thermosensitive resin systems with extrusion-based additive manufacturing for simultaneous printing and curing of high-quality thermoset parts. The inks used for additive manufacturing (AM) are developed by staging the resin at an elevated temperature to transform the low viscosity resin to a viscoelastic gel useful for 3D printing. A comprehensive study was first conducted to understand the effect of staging on resin reactivity and pot life of resin which are important factors for printability. The insights gained from this study were applied for developments of 3D printing inks and used to fabricate short-fiber reinforced composites and stretchable polymers with tunable mechanical properties. The printing technique was further improved by adding an external energy source to accelerate *in-situ* curing rate and achieve a more robust manufacturing process. Finally, another thermosensitive resin was introduced as a new feedstock material for this novel AM technique. In what follows, the concluding remarks from this research are presented.

1) Frontal polymerization (FP) is a time- and temperature-dependent reaction and is greatly affected by staging conditioning. A systematic study was designed to experimentally characterize the influence of inhibitor concentration, staging time, and staging temperature on front behavior including front velocity, front temperature, and activation time in frontal ring opening metathesis

polymerization (FROM) of dicyclopentadiene (DCPD) in the presence of second-generation Grubbs catalyst. The results indicate that the front behavior is highly affected by several parameters including available energy density of resin, stability of catalyst-inhibitor complex, and resin viscosity. It was found that an increase in staging temperature accelerates the gelation process and leads to hotter and faster fronts and lower activation times, but it substantially limits the resin pot life. Also, an increase in inhibitor concentration results in longer resin pot lives, slower fronts, higher activation times, and front temperatures.

2) A new 3D printing technique is developed for *in-situ* printing and curing short fiber-reinforced thermoset composites without requiring any post-curing step. In this technique, the composite ink is extruded from a printing nozzle and deposited on a heated substrate and *in-situ* cured following the extrusion via FP. It is shown that addition of short carbon fibers enhances the thermal conductivity and rheological behavior of 3D printing ink, which enables rapid manufacturing of high-quality multilayer composite structures via through-thickness curing of deposited inks. Also, unsupported, freeform 3D printing of composite parts is demonstrated by matching printing speed with front velocity, and it is found that increasing carbon fiber concentration from 0 to 15 vol% results in a higher front velocity and printing speed. The new printing process produces void-free composite parts with anisotropic mechanical properties caused by shear-induced fiber orientation along the printing direction.

3) A new FP formulation is introduced for rapid AM of thermoset polymers with a wide range of thermomechanical properties. The new resin system consists of DCPD and dicyclopentadiene-modified linseed oil (DML), which can be frontally polymerized to solid parts at room temperature. Rigid polymers and soft elastomers are obtained by varying DML concentrations. The experimental results show that addition of DML comonomer results in slower fronts by

reducing energy density of resin, but results in polymers with higher elastomeric properties. For example, FP of resin formulations containing up to 50 wt% of DML commoner produces a polymer with a robust elastomeric behavior with ultimate elongation of 360%. As a demonstration for capability of this resin formulation, elastomeric parts with substantial flexibility and compressibility were produced via FP-assisted 3D printing approach.

4) While 3D printing via FP offers a new opportunity for rapid manufacturing of thermoset composite structures, the printing process is limited by cure kinetics of FP resin systems, low concentrations of heat absorbing fillers and reinforcements, and boundary conditions of surrounding environment. These limitations are addressed using an external energy source for on-demand curing of thermoset composite extrudate. In this technique, a blue laser diode is configured to rapidly heat up and rigidize the composite material upon extrusion from the printing nozzle. This technique is demonstrated for simultaneous printing and curing of freestanding and tall multilayer composite structures at a constant printing speed, irrespective of boundary condition and allows for rapid manufacturing of continuous carbon fiber-reinforced composites which is hard to achieve using FP-assisted 3D printing technique. Using the novel printing technique, discontinuous and continuous carbon fiber-reinforced composites were manufactured at unprecedented printing speed of 1.5 m/min without requiring any post-curing steps.

5) Motivated by a desire to print recyclable composite materials, the last part of this research focuses on FP of polyacrylates as a new feedstock for the laser-assisted 3D printing technique. A series of FP experiments are carried out on 1,6-hexanediol diacrylate monomer using a peroxide and a redox initiator in a test tube. Compared with the peroxide initiator, FP of diacrylate monomer using the redox initiator prevents undesired bubble formation during FP reaction. Furthermore, the effect of reductant ratio on the bubble formation and the front behavior is studied at a fixed oxidant

concentration, and the results reveal that bubble formation, front velocity, and front temperature are reduced when using higher reductant concentrations. While FP of 1,6 hexanediol diacrylate monomer using DMA/BPO redox initiator produces a thermoset polymer, the insight gained from this study can be exploited for future design of recyclable thermoplastic polymers using modified resin formulation system.

7.2. Thesis contributions

In this research, the following contributions have been added to the literature.

1) A systematic study on the effect of ambient conditioning on thermal frontal polymerization was performed. The results obtained from this study can be used to design new manufacturing processes based on FP where an exquisite control over resin viscosity, resin reactivity, and pot life are required.

2) 3D printing via FP was developed to rapidly manufacture short carbon fiber-reinforced thermoset composite parts. Using this *in-situ* printing technique and controlling underlying printing process, unsupported and supported tall composite structures were created, which is hard or even impossible to achieve using other AM techniques. Also, mechanical characterization on 3D printed parts elucidated the impact of shear-induced fiber alignments on directional reinforcement of carbon fibers.

3) DML was identified as a comonomer that can be frontally polymerized with DCPD to produce polymers with tunable mechanical properties. Using this resin formulation, parts from highly rigid to soft and flexible elastomers were printed via FP to demonstrate the capability of developed 3D printing technique to creation of thermoset components with controlled mechanical properties.

4) The first-ever *in-situ* printing and curing of thermally curable thermoset composites via a laser stimulus was developed to manufacture discontinuous and continuous carbon fiber-reinforced thermoset composites. This novel 3D printing technique offers great flexibility in rapid additive manufacturing of larger composite components, which can be highly interesting for composite and AM industries.

5) The ability to perform bubble-free FP at ambient condition is quite challenging, as most commercially available peroxide and nitril initiators used for free-radical FP produce gas upon decomposition. Inspired by previous works on free-radical FP of hydrogels, the DMA/BPO redox initiator was used to perform FP of a diacrylate monomer and achieve a bubble-free rigid polymer.

7.3. Recommendations for future work

The overall goal of this dissertation was to develop new techniques for rapid AM of thermoset polymers and composites. In what follows, some limitations of the work are discussed and new topics for future studies are presented.

- In layer-by-layer 3D printing via FP, printing speed is inversely proportional to the contact-to-cure time. Contact-to-cure time was experimentally measured on a heated print bed with an average temperature of 80 °C, and it was assumed that the temperature of the underlying substrate for the new, deposited ink remains at 80 °C as more layers are deposited. However, there is a temperature gradient perpendicular to the build platform as the number of layers increases, affecting the contact-to-cure time in various layers. Developing a model that predicts substrate temperature for new, deposited layers will further advance this technique to predict process parameters for manufacturing large-scale composites structures.
- Warpage was found to be a main problem in FP-assisted 3D printing process because of the temperature gradient caused by the FP reaction. Future studies are required to suppress

warpage by controlling the ambient temperature and reducing the temperature variation in the printed part.

- The developed frontally polymerizable resin systems with tunable thermomechanical properties based on DML/DCPD enable *in-situ* 3D printing of functional heterogenous materials for novel applications. A micromixer equipped with programmable dispensers can be added to the print head to control local composition of the printed part as the printing ink is deposited.
- In laser-assisted 3D printing technique, mechanical properties should be examined at various printing conditions including laser power density, printing speed, and nozzle diameter, and be compared with conventionally cured samples. The interfacial bonding strength of 3D printed parts can be evaluated by mechanical testing at these various printing conditions. Understanding the influence of these parameters is crucial to optimize the printing process and achieve more robust composite structures.
- Microscopic voids were formed in 3D printing of continuous fiber-reinforced composite (CFRC) parts due to improper impregnation of dry fiber in the syringe barrel. A potential solution to this problem is using fiber with a proper sizing compatible with the resin to properly wet the dry fiber and reduce void contents. In the next step of this research, the effect of laser and printing speed can be explored on the fiber sizing and the interfacial adhesion between the carbon fiber and the polymer matrix.
- 3D printing via laser was carried out using a 450 nm blue laser diode to simultaneously print and cure thermoset composite parts. A blue laser diode produces a Gaussian beam, where its intensity decays exponentially moving away from the center of the beam. In addition to this problem, the blue laser diode has low penetration depth in the presence of light absorbing

carbon fibers leading to potential decay of light intensity through the thickness of filament. The non-uniform light exposure caused by the blue laser diode results in non-uniform heating and curing of resin within the composite filament. The spatial gradient in degree of cure requires limiting the printing speed to increase the exposure time of resin and achieve a greater depth of cure. In 3D printing via laser, the printing speed is limited to 1.5 m/min, which can further be improved by replacing the blue laser diode with other remote irradiation techniques such as infrared and microwave heating sources.

- Redox initiators have shown to be effective in bubble-free FP of polyacrylates. This resin can be used for rapid *in-situ* printing and curing of high-quality thermoset polymers and composites; however, its manufacturing process is limited due to its very short pot life. This problem can be addressed by microencapsulating one component of the redox initiator and separating it from the other component to prevent any radical formation caused by oxidation-reduction reaction. Since the components of initiator are sequestered, the polymerization does not take place until the capsule is burst by heating. Another possible solution to circumvent the short pot life of resin is designing a new print head where the redox initiator is mixed with the resin using a static mixer immediately before extrusion. This print head design enables rapid *in-situ* mixing and printing of thermoset polymer, irrespective of the pot life of the resin system.
- Frontal polymerization of diacrylate monomer produces a crosslinked thermoset polymer with thermomechanical properties inferior to pDCPD. Mechanical properties of the polymer can be improved by adding a trifunctional acrylate comonomer to increase crosslinking density and achieve a copolymer with a higher level of strength. Alternatively, diacrylate monomer can be incorporated to other frontally curable resin systems such as dicyclopentadiene to

achieve interpenetrating polydicyclopentadiene/polyacrylate networks. Furthermore, the effect of miscibility of two resin systems can be explored on front behavior and mechanical properties of welded thermoset materials.

References

(1) Khan, A.; Bhawani, S. A.; Asiri, A. M.; Khan, I. *Thermoset Composites: Preparation, Properties and Applications*; Materials Research Forum LLC, 2018.

(2) Abliz, D.; Duan, Y.; Steuernagel, L.; Xie, L.; Li, D.; Ziegmann, G. Curing Methods for Advanced Polymer Composites - A Review. *Polymers and Polymer Composites* **2013**, *21* (6), 341–348.

(3) Witik, R. A.; Gaille, F.; Teuscher, R.; Ringwald, H.; Michaud, V.; Månson, J.-A. E. Economic and Environmental Assessment of Alternative Production Methods for Composite Aircraft Components. *Journal of Cleaner Production* **2012**, *29–30*, 91–102.

(4) Timmis, A. J.; Hodzic, A.; Koh, L.; Bonner, M.; Soutis, C.; Schäfer, A. W.; Dray, L. Environmental Impact Assessment of Aviation Emission Reduction through the Implementation of Composite Materials. *Int J Life Cycle Assess* **2015**, *20* (2), 233–243.

(5) Li, Y.; Xiao, Y.; Yu, L.; Ji, K.; Li, D. A Review on the Tooling Technologies for Composites Manufacturing of Aerospace Structures: Materials, Structures and Processes. *Composites Part A: Applied Science and Manufacturing* **2022**, *154*, 106762.

(6) Kamae, T.; Tanaka, G.; Oosedo, H. A Rapid Cure Epoxy Resin System for a RTM Process. In *Proc. of the 12th US-Japan Conference on Composite materials, Michigan*; 2006; pp 390–397.

(7) Kamae, T.; Oosedo, H.; Tanaka, G.; Iwasawa, S. Epoxy Resin Composition, Process for Producing Fiber-Reinforced Composite Materials and Fiber-Reinforced Composite Materials. US7148294B2, December 12, 2006.

(8) Wang, C. R.; Gu, Y. Z.; Zhang, K. M.; Li, M.; Zhang, Z. G. Rapid Curing Epoxy Resin and Its Application in Carbon Fibre Composite Fabricated Using Vartm Moulding. *Polymers and Polymer Composites* **2013**, *21* (5), 315–324.

(9) Abliz, D.; Duan, Y.; Zhao, X.; Li, D. Low-Energy Electron Beam Cured Tape Placement for out-of-Autoclave Fabrication of Advanced Polymer Composites. *Composites Part A: Applied Science and Manufacturing* **2014**, *65*, 73–82.

(10) Guasti, F.; Rosi, E. Low Energy Electron Beam Curing for Thick Composite Production. *Composites Part A: Applied Science and Manufacturing* **1997**, *28* (11), 965–969.

(11) Osada, T.; Mizoguchi, M.; Nakai, A.; Hamada, H. Interfacial Properties of EB Cured Composite. In *JISSE-7: Seventh Japan International Sampe Symposium*; 2001; pp 761–764.

(12) Berejka, A. J.; Cleland, M. R.; Galloway, R. A.; Gregoire, O. X-Ray Curing of Composite Materials. *Nuclear Instruments and Methods in Physics Research Section B: Beam Interactions with Materials and Atoms* **2005**, *241* (1), 847–849.

(13) Dispenza, C.; Alessi, S.; Spadaro, G. Carbon Fiber Composites Cured by γ-Radiation-Induced Polymerization of an Epoxy Resin Matrix. *Advances in Polymer Technology* **2008**, *27* (3), 163–171.

(14) Endruweit, A.; Johnson, M. S.; Long, A. C. Curing of Composite Components by Ultraviolet Radiation: A Review. *Polymer Composites* **2006**, *27* (2), 119–128.

(15) Atif, M.; Yang, J.; Yang, H.; Jun, N.; Bongiovanni, R. Effect of Novel UV-Curing Approach on Thermo-Mechanical Properties of Colored Epoxy Composites in Outsized Dimensions. *Journal of Composite Materials* **2016**, *50* (22), 3147–3156.

(16) Kumar, P. K.; Raghavendra, N. V.; Sridhara, B. K. Effect of Infrared Cure Parameters on the Mechanical Properties of Polymer Composite Laminates. *Journal of Composite Materials* **2012**, *46* (5), 549–556.
(17) Odom, M. G. B.; Sweeney, C. B.; Parviz, D.; Sill, L. P.; Saed, M. A.; Green, M. J. Rapid Curing and Additive Manufacturing of Thermoset Systems Using Scanning Microwave Heating of Carbon Nanotube/Epoxy Composites. *Carbon* **2017**, *120*, 447–453.
(18) Kim, N. D.; Metzger, A.; Hejazi, V.; Li, Y.; Kovalchuk, A.; Lee, S.-K.; Ye, R.; Mann, J. A.; Kittrell, C.; Shahsavari, R.; Tour, J. M. Microwave Heating of Functionalized Graphene Nanoribbons in Thermoset Polymers for Wellbore Reinforcement. *ACS Appl. Mater. Interfaces* **2016**, *8* (20), 12985–12991.
(19) Zhao, B.; Hardiman, M.; M. Ryan, K.; O'Reilly, E.; McCarthy, C. Formation of Reworkable Nanocomposite Adhesives by Dielectric Heating of Epoxy Resin Embedded Fe 3 O 4 Hollow Spheres. *CrystEngComm* **2016**, *18* (32), 6096–6101.
(20) Li, Q.; Shen, H.-X.; Liu, C.; Wang, C.-F.; Zhu, L.; Chen, S. Advances in Frontal Polymerization Strategy: From Fundamentals to Applications. *Progress in Polymer Science* **2022**, *127*, 101514.
(21) Pojman, J. Frontal Polymerization. *Polymer Science: A Comprehensive Reference* **2012**, *4*, 957–980.
(22) Masere, J.; Lewis, L. L.; Pojman, J. A. Optical Gradient Materials Produced via Low-Temperature Isothermal Frontal Polymerization. *Journal of Applied Polymer Science* **2001**, *80* (4), 686–691.
(23) Lewis, L. L.; DeBisschop, C. S.; Pojman, J. A.; Volpert, V. A. Isothermal Frontal Polymerization: Confirmation of the Mechanism and Determination of Factors Affecting the Front Velocity, Front Shape, and Propagation Distance with Comparison to Mathematical Modeling. *Journal of Polymer Science Part A: Polymer Chemistry* **2005**, *43* (23), 5774–5786.
(24) Cabral, J. T.; Hudson, S. D.; Harrison, C.; Douglas, J. F. Frontal Photopolymerization for Microfluidic Applications. *Langmuir* **2004**, *20* (23), 10020–10029.
(25) Klikovits, N.; Liska, R.; D'Anna, A.; Sangermano, M. Successful UV-Induced RICFP of Epoxy-Composites. *Macromolecular Chemistry and Physics* **2017**, *218* (18), 1700313.
(26) Sangermano, M.; D'Anna, A.; Marro, C.; Klikovits, N.; Liska, R. UV-Activated Frontal Polymerization of Glass Fibre Reinforced Epoxy Composites. *Composites Part B: Engineering* **2018**, *143*, 168–171.
(27) Potzmann, P. M.; Lopez Villanueva, F. J.; Liska, R. UV-Initiated Bubble-Free Frontal Polymerization in Aqueous Conditions. *Macromolecules* **2015**, *48* (24), 8738–8745.
(28) Robertson, I. D.; Hernandez, H. L.; White, S. R.; Moore, J. S. Rapid Stiffening of a Microfluidic Endoskeleton via Frontal Polymerization. *ACS Appl. Mater. Interfaces* **2014**, *6* (21), 18469–18474.
(29) Bynum, S.; Tullier, M.; Morejon-Garcia, C.; Guidry, J.; Runnoe, E.; Pojman, J. A. The Effect of Acrylate Functionality on Frontal Polymerization Velocity and Temperature. *Journal of Polymer Science Part A: Polymer Chemistry* **2019**, *57* (9), 982–988.
(30) Vallons, K. A. M.; Drozdzak, R.; Charret, M.; Lomov, S. V.; Verpoest, I. Assessment of the Mechanical Behaviour of Glass Fibre Composites with a Tough Polydicyclopentadiene (PDCPD) Matrix. *Composites Part A: Applied Science and Manufacturing* **2015**, *78*, 191–200.

(31) Jr, C. S. W.; Grubbs, R. H. Polymeric Composites Including Dicyclopentadiene and Related Monomers. US6310121B1, October 30, 2001.
(32) Mariani, A.; Fiori, S.; Chekanov, Y.; Pojman, J. A. Frontal Ring-Opening Metathesis Polymerization of Dicyclopentadiene. *Macromolecules* **2001**, *34* (19), 6539–6541.
(33) Alzari, V.; Nuvoli, D.; Sanna, D.; Ruiu, A.; Mariani, A. Effect of Limonene on the Frontal Ring Opening Metathesis Polymerization of Dicyclopentadiene. *Journal of Polymer Science Part A: Polymer Chemistry* **2016**, *54* (1), 63–68.
(34) Robertson, I. D.; Dean, L. M.; Rudebusch, G. E.; Sottos, N. R.; White, S. R.; Moore, J. S. Alkyl Phosphite Inhibitors for Frontal Ring-Opening Metathesis Polymerization Greatly Increase Pot Life. *ACS Macro Lett.* **2017**, *6* (6), 609–612.
(35) Garg, M.; Aw, J. E.; Zhang, X.; Centellas, P. J.; Dean, L. M.; Lloyd, E. M.; Robertson, I. D.; Liu, Y.; Yourdkhani, M.; Moore, J. S.; Geubelle, P. H.; Sottos, N. R. Rapid Synchronized Fabrication of Vascularized Thermosets and Composites. *Nat Commun* **2021**, *12* (1), 2836.
(36) Robertson, I. D.; Yourdkhani, M.; Centellas, P. J.; Aw, J. E.; Ivanoff, D. G.; Goli, E.; Lloyd, E. M.; Dean, L. M.; Sottos, N. R.; Geubelle, P. H.; Moore, J. S.; White, S. R. Rapid Energy-Efficient Manufacturing of Polymers and Composites via Frontal Polymerization. *Nature* **2018**, *557* (7704), 223–227.
(37) Alzate-Sanchez, D. M.; Cencer, M. M.; Rogalski, M.; Kersh, M. E.; Sottos, N.; Moore, J. S. Anisotropic Foams via Frontal Polymerization. *Advanced Materials* **2022**, *34* (8), 2105821.
(38) Peng, T.; Kellens, K.; Tang, R.; Chen, C.; Chen, G. Sustainability of Additive Manufacturing: An Overview on Its Energy Demand and Environmental Impact. *Additive Manufacturing* **2018**, *21*, 694–704.
(39) Truby, R. L.; Lewis, J. A. Printing Soft Matter in Three Dimensions. *Nature* **2016**, *540* (7633), 371–378.
(40) Sun, C.; Fang, N.; Wu, D. M.; Zhang, X. Projection Micro-Stereolithography Using Digital Micro-Mirror Dynamic Mask. *Sensors and Actuators A: Physical* **2005**, *121* (1), 113–120.
(41) Zheng, X.; Deotte, J.; Alonso, M. P.; Farquar, G. R.; Weisgraber, T. H.; Gemberling, S.; Lee, H.; Fang, N.; Spadaccini, C. M. Design and Optimization of a Light-Emitting Diode Projection Micro-Stereolithography Three-Dimensional Manufacturing System. *Review of Scientific Instruments* **2012**, *83* (12), 125001.
(42) Zak, G.; Sela, M. N.; Yevko, V.; Park, C. B.; Benhabib, B. Layered-Manufacturing of Fiber-Reinforced Composites. *Journal of Manufacturing Science and Engineering* **1999**, *121* (3), 448–456.
(43) Karalekas, D. E. Study of the Mechanical Properties of Nonwoven Fibre Mat Reinforced Photopolymers Used in Rapid Prototyping. *Materials & Design* **2003**, *24* (8), 665–670.
(44) Gupta, A.; Ogale, A. A. Dual Curing of Carbon Fiber Reinforced Photoresins for Rapid Prototyping. *Polymer Composites* **2002**, *23* (6), 1162–1170.
(45) Tamez, M. B. A.; Taha, I. A Review of Additive Manufacturing Technologies and Markets for Thermosetting Resins and Their Potential for Carbon Fiber Integration. *Additive Manufacturing* **2021**, *37*, 101748.
(46) Sugioka, K.; Cheng, Y. Femtosecond Laser Three-Dimensional Micro- and Nanofabrication. *Applied Physics Reviews* **2014**, *1* (4), 041303.
(47) Klosterman, D.; Chartoff, R.; Agarwala, M.; Fiscus, I.; Murphy, J.; Cullen, S.; Yeazell, M. Direct Fabrication of Polymer Composite Structures with Curved LOM; 1999.

(48) Klosterman, D.; Chartoff, R.; Graves, G.; Osborne, N.; Priore, B. Interfacial Characteristics of Composites Fabricated by Laminated Object Manufacturing. *Composites Part A: Applied Science and Manufacturing* **1998**, *29* (9), 1165–1174.
(49) Blok, L. G.; Longana, M. L.; Yu, H.; Woods, B. K. S. An Investigation into 3D Printing of Fibre Reinforced Thermoplastic Composites. *Additive Manufacturing* **2018**, *22*, 176–186.
(50) Yang, D.; Zhang, H.; Wu, J.; McCarthy, E. D. Fibre Flow and Void Formation in 3D Printing of Short-Fibre Reinforced Thermoplastic Composites: An Experimental Benchmark Exercise. *Additive Manufacturing* **2021**, *37*, 101686.
(51) Dickson, A. N.; Abourayana, H. M.; Dowling, D. P. 3D Printing of Fibre-Reinforced Thermoplastic Composites Using Fused Filament Fabrication—A Review. *Polymers* **2020**, *12* (10), 2188.
(52) Guo, Y.; Liu, Y.; Liu, J.; Zhao, J.; Zhang, H.; Zhang, Z. Shape Memory Epoxy Composites with High Mechanical Performance Manufactured by Multi-Material Direct Ink Writing. *Composites Part A: Applied Science and Manufacturing* **2020**, *135*, 105903.
(53) Zhang, Y.; Shi, G.; Qin, J.; Lowe, S. E.; Zhang, S.; Zhao, H.; Zhong, Y. L. Recent Progress of Direct Ink Writing of Electronic Components for Advanced Wearable Devices. *ACS Appl. Electron. Mater.* **2019**, *1* (9), 1718–1734.
(54) Chen, Q.; Sukmanee, T.; Rong, L.; Yang, M.; Ren, J.; Ekgasit, S.; Advincula, R. A Dual Approach in Direct Ink Writing of Thermally Cured Shape Memory Rubber Toughened Epoxy. *ACS Appl. Polym. Mater.* **2020**, *2* (12), 5492–5500.
(55) Romberg, S. K.; Islam, M. A.; Hershey, C. J.; DeVinney, M.; Duty, C. E.; Kunc, V.; Compton, B. G. Linking Thermoset Ink Rheology to the Stability of 3D-Printed Structures. *Additive Manufacturing* **2021**, *37*, 101621.
(56) Hmeidat, N. S.; Kemp, J. W.; Compton, B. G. High-Strength Epoxy Nanocomposites for 3D Printing. *Composites Science and Technology* **2018**, *160*, 9–20.
(57) Compton, B. G.; Lewis, J. A. 3D-Printing of Lightweight Cellular Composites. *Advanced Materials* **2014**, *26* (34), 5930–5935.
(58) Li, V. C.-F.; Kuang, X.; Hamel, C. M.; Roach, D.; Deng, Y.; Qi, H. J. Cellulose Nanocrystals Support Material for 3D Printing Complexly Shaped Structures via Multi-Materials-Multi-Methods Printing. *Additive Manufacturing* **2019**, *28*, 14–22.
(59) Jiang, Z.; Diggle, B.; Tan, M. L.; Viktorova, J.; Bennett, C. W.; Connal, L. A. Extrusion 3D Printing of Polymeric Materials with Advanced Properties. *Advanced Science* **2020**, *7* (17), 2001379.
(60) Ahmad, H. M.; Kamal, M. S.; Al-Harthi, M. A. High Molecular Weight Copolymers as Rheology Modifier and Fluid Loss Additive for Water-Based Drilling Fluids. *Journal of Molecular Liquids* **2018**, *252*, 133–143.
(61) Martín-Alfonso, J. E.; Valencia, C.; Sánchez, M. C.; Franco, J. M.; Gallegos, C. Evaluation of Different Polyolefins as Rheology Modifier Additives in Lubricating Grease Formulations. *Materials Chemistry and Physics* **2011**, *128* (3), 530–538.
(62) Lei, D.; Yang, Y.; Liu, Z.; Chen, S.; Song, B.; Shen, A.; Yang, B.; Li, S.; Yuan, Z.; Qi, Q.; Sun, L.; Guo, Y.; Zuo, H.; Huang, S.; Yang, Q.; Mo, X.; He, C.; Zhu, B.; Jeffries, E. M.; Qing, F.-L.; Ye, X.; Zhao, Q.; You, Z. A General Strategy of 3D Printing Thermosets for Diverse Applications. *Mater. Horiz.* **2019**, *6* (2), 394–404.
(63) Uitz, O.; Koirala, P.; Tehrani, M.; Seepersad, C. C. Fast, Low-Energy Additive Manufacturing of Isotropic Parts via Reactive Extrusion. *Additive Manufacturing* **2021**, *41*, 101919.

(64) Levenhagen, N. P.; Dadmun, M. D. Reactive Processing in Extrusion-Based 3D Printing to Improve Isotropy and Mechanical Properties. *Macromolecules* **2019**, *52* (17), 6495–6501.
(65) Zhu, J.; Zhang, Q.; Yang, T.; Liu, Y.; Liu, R. 3D Printing of Multi-Scalable Structures via High Penetration near-Infrared Photopolymerization. *Nat Commun* **2020**, *11* (1), 3462.
(66) Tu, R.; Sodano, H. A. Additive Manufacturing of High-Performance Vinyl Ester Resin via Direct Ink Writing with UV-Thermal Dual Curing. *Additive Manufacturing* **2021**, *46*, 102180.
(67) Ji, Z.; Jiang, D.; Zhang, X.; Guo, Y.; Wang, X. Facile Photo and Thermal Two-Stage Curing for High-Performance 3D Printing of Poly(Dimethylsiloxane). *Macromolecular Rapid Communications* **2020**, *41* (10), 2000064.
(68) Zhang, Z.; Gao, C.; Liu, R.; Li, W.; Qiu, J.; Wang, S. Catalyzed Frontal Polymerization-Aided 3D Printing of Epoxy Thermosets. *Additive Manufacturing Letters* **2022**, *2*, 100030.
(69) Zhang, Z.; Liu, R.; Li, W.; Liu, Y.; Luo, H.; Zeng, L.; Qiu, J.; Wang, S. Direct Writing of Continuous Carbon Fibers/Epoxy Thermoset Composites with High-Strength and Low Energy-Consumption. *Additive Manufacturing* **2021**, *47*, 102348.
(70) Zhang, Z.; Liu, R.; Li, W.; Liu, Y.; Pei, Z.; Qiu, J.; Wang, S. Frontal Polymerization-Assisted 3D Printing of Short Carbon Fibers/Dicyclopentadiene Composites. *Journal of Manufacturing Processes* **2021**, *71*, 753–762.
(71) Shimamoto, D.; Tominaga, Y.; Imai, Y.; Hotta, Y. Fiber Orientation and Flexural Properties of Short Carbon Fiber/Epoxy Composites. *Journal of the Ceramic Society of Japan* **2016**, *124* (1), 125–128.
(72) van de Werken, N.; Tekinalp, H.; Khanbolouki, P.; Ozcan, S.; Williams, A.; Tehrani, M. Additively Manufactured Carbon Fiber-Reinforced Composites: State of the Art and Perspective. *Additive Manufacturing* **2020**, *31*, 100962.
(73) He, X.; Ding, Y.; Lei, Z.; Welch, S.; Zhang, W.; Dunn, M.; Yu, K. 3D Printing of Continuous Fiber-Reinforced Thermoset Composites. *Additive Manufacturing* **2021**, *40*, 101921.
(74) Ming, Y.; Xin, Z.; Zhang, J.; Duan, Y.; Wang, B. Fabrication of Continuous Glass Fiber-Reinforced Dual-Cure Epoxy Composites via UV-Assisted Fused Deposition Modeling. *Composites Communications* **2020**, *21*, 100401.
(75) Rahman, M. A.; Islam, M. Z.; Gibbon, L.; Ulven, C. A.; La Scala, J. J. 3D Printing of Continuous Carbon Fiber Reinforced Thermoset Composites Using UV Curable Resin. *Polymer Composites* **2021**, *42* (11), 5859–5868.
(76) Shi, B.; Shang, Y.; Zhang, P.; Cuadros, A. P.; Qu, J.; Sun, B.; Gu, B.; Chou, T.-W.; Fu, K. (Kelvin). Dynamic Capillary-Driven Additive Manufacturing of Continuous Carbon Fiber Composite. *Matter* **2020**, *2* (6), 1594–1604.
(77) Pascault, J.-P.; Sautereau, H.; Verdu, J.; Williams, R. J. J. *Thermosetting Polymers*; CRC Press: New York, USA, 2002.
(78) Daniel, I. M.; Ishai, O. *Engineering Mechanics of Composite Materials*; Oxford University Press: New York, USA, 2006; Vol. 3.
(79) Li, Y.; Li, N.; Zhou, J.; Cheng, Q. Microwave Curing of Multidirectional Carbon Fiber Reinforced Polymer Composites. *Composite Structures* **2019**, *212*, 83–93.
(80) Pojman, J. A. Frontal Polymerization. In *Polymer Science: A Comprehensive Reference*; Matyjaszewski, K., Möller, M., Eds.; Elsevier: Amsterdam, Netherlands, 2012; Vol. 4, pp 957–980.

(81) Tsegay, N. M.; Du, X.-Y.; Liu, S.-S.; Wang, C.-F.; Chen, S. Frontal Polymerization for Smart Intrinsic Self-Healing Hydrogels and Its Integration with Microfluidics. *J. Polym. Sci., Part A: Polym. Chem.* **2018**, *56* (13), 1412–1423.
(82) Sanna, D.; Alzari, V.; Nuvoli, D.; Nuvoli, L.; Rassu, M.; Sanna, V.; Mariani, A. β-Cyclodextrin-Based Supramolecular Poly (N-Isopropylacrylamide) Hydrogels Prepared by Frontal Polymerization. *Carbohydr. Polym.* **2017**, *166*, 249–255.
(83) Irfan, M.; Du, X.; Xu, X. R.; Shen, R. Q.; Chen, S.; Xiao, J. J. Synthesis and Characterization of PH-sensitive Poly(IA- *Co* -AAc- *Co* -AAm) Hydrogels via Frontal Polymerization. *J. Polym. Sci., Part A: Polym. Chem.* **2019**, *57* (22), 2214–2221.
(84) Nuvoli, D.; Alzari, V.; Pojman, J. A.; Sanna, V.; Ruiu, A.; Sanna, D.; Malucelli, G.; Mariani, A. Synthesis and Characterization of Functionally Gradient Materials Obtained by Frontal Polymerization. *ACS Appl. Mater. Interfaces* **2015**, *7* (6), 3600–3606.
(85) Gary, D. P.; Bynum, S.; Thompson, B. D.; Groce, B. R.; Sagona, A.; Hoffman, I. M.; Morejon-Garcia, C.; Weber, C.; Pojman, J. A. Thermal Transport and Chemical Effects of Fillers on FREE-RADICAL Frontal Polymerization. *J. Polym Sci.* **2020**, *58* (16), 2267–2277.
(86) Bynum, S.; Tullier, M.; Morejon-Garcia, C.; Guidry, J.; Runnoe, E.; Pojman, J. A. The Effect of Acrylate Functionality on Frontal Polymerization Velocity and Temperature. *J. Polym. Sci. Part A: Polym. Chem.* **2019**, *57* (9), 982–988.
(87) Mariani, A.; Bidali, S.; Fiori, S.; Malucelli, G.; Sanna, E. Synthesis and Characterization of a Polyurethane Prepared by Frontal Polymerization. *e-Polymers* **2003**, *3* (1).
(88) Bomze, D.; Knaack, P.; Liska, R. Successful Radical Induced Cationic Frontal Polymerization of Epoxy-Based Monomers by C–C Labile Compounds. *Polymer Chemistry* **2015**, *6* (47), 8161–8167.
(89) Tran, A. D.; Koch, T.; Knaack, P.; Liska, R. Radical Induced Cationic Frontal Polymerization for Preparation of Epoxy Composites. *Compos. Part A Appl. Sci. Manuf.* **2020**, *132*, 105855.
(90) Pojman, J. A.; Varisli, B.; Perryman, A.; Edwards, C.; Hoyle, C. Frontal Polymerization with Thiol−Ene Systems. *Macromolecules* **2004**, *37* (3), 691–693.
(91) Mariani, A.; Fiori, S.; Chekanov, Y.; Pojman, J. A. Frontal Ring-Opening Metathesis Polymerization of Dicyclopentadiene. *Macromolecules* **2001**, *34* (19), 6539–6541.
(92) Dean, L. M.; Wu, Q.; Alshangiti, O.; Moore, J. S.; Sottos, N. R. Rapid Synthesis of Elastomers and Thermosets with Tunable Thermomechanical Properties. *ACS Macro Lett.* **2020**, *9* (6), 819–824.
(93) Delaude, L.; Noels, A. F. METATHESIS. In *Kirk-Othmer Encyclopedia of Chemical Technology*; Kroschwitz, J. I., Seidel, A., Eds.; John Wiley & Sons., 2007; Vol. 26, pp 920–958.
(94) Vallons, K. A. M.; Drozdzak, R.; Charret, M.; Lomov, S. V.; Verpoest, I. Assessment of the Mechanical Behaviour of Glass Fibre Composites with a Tough Polydicyclopentadiene (PDCPD) Matrix. *Compos. Part A Appl. Sci. Manuf.* **2015**, *78*, 191–200.
(95) Kovačič, S.; Slugovc, C. Ring-Opening Metathesis Polymerisation Derived Poly(Dicyclopentadiene) Based Materials. *Materials Chemistry Frontiers* **2020**, *4* (8), 2235–2255.
(96) Goli, E.; Parikh, N. A.; Yourdkhani, M.; Hibbard, N. G.; Moore, J. S.; Sottos, N. R.; Geubelle, P. H. Frontal Polymerization of Unidirectional Carbon-Fiber-Reinforced Composites. *Composites Part A: Applied Science and Manufacturing* **2020**, *130*, 105689.

(97) Dean, L. M.; Ravindra, A.; Guo, A. X.; Yourdkhani, M.; Sottos, N. R. Photothermal Initiation of Frontal Polymerization Using Carbon Nanoparticles. *ACS Appl. Polym. Mater.* **2020**, *2* (11), 4690–4696.
(98) Stawiasz, K. J.; Paul, J. E.; Schwarz, K. J.; Sottos, N. R.; Moore, J. S. Photoexcitation of Grubbs' Second-Generation Catalyst Initiates Frontal Ring-Opening Metathesis Polymerization. *ACS Macro Lett.* **2020**, *9* (11), 1563–1568.
(99) Liu, H.; Wei, H.; Moore, J. S. Frontal Ring-Opening Metathesis Copolymerization: Deviation of Front Velocity from Mixing Rules. *ACS Macro Lett.* **2019**, *8*, 846–851.
(100) Robertson, I. D.; Pruitt, E. L.; Moore, J. S. Frontal Ring-Opening Metathesis Polymerization of Exo-Dicyclopentadiene for Low Catalyst Loadings. *ACS Macro Lett.* **2016**, *5* (5), 593–596.
(101) Bantreil, X.; Schmid, T. E.; Randall, R. A.; Slawin, A. M.; Cazin, C. S. Mixed N-Heterocyclic Carbene/Phosphite Ruthenium Complexes: Towards a New Generation of Olefin Metathesis Catalysts. *Chem. Commun.* **2010**, *46* (38), 7115–7117.
(102) Mariani, A.; Fiori, S.; Bidali, S.; Alzari, V.; Malucelli, G. Frontal Polymerization of Diurethane Diacrylates. *Journal of Polymer Science Part A: Polymer Chemistry* **2008**, *46* (10), 3344–3352.
(103) Fiori, S.; Mariani, A.; Ricco, L.; Russo, S. First Synthesis of a Polyurethane by Frontal Polymerization. *Macromolecules* **2003**, *36* (8), 2674–2679.
(104) Mallick, P. K. *Fiber-Reinforced Composites: Materials, Manufacturing, and Design, Third Edition*; CRC Press, 2007.
(105) He, Q.; Wang, H.; Fu, K.; Ye, L. 3D Printed Continuous CF/PA6 Composites: Effect of Microscopic Voids on Mechanical Performance. *Composites Science and Technology* **2020**, *191*, 108077.
(106) Ueda, M.; Kishimoto, S.; Yamawaki, M.; Matsuzaki, R.; Todoroki, A.; Hirano, Y.; Le Duigou, A. 3D Compaction Printing of a Continuous Carbon Fiber Reinforced Thermoplastic. *Composites Part A: Applied Science and Manufacturing* **2020**, *137*, 105985.
(107) Liao, G.; Li, Z.; Cheng, Y.; Xu, D.; Zhu, D.; Jiang, S.; Guo, J.; Chen, X.; Xu, G.; Zhu, Y. Properties of Oriented Carbon Fiber/Polyamide 12 Composite Parts Fabricated by Fused Deposition Modeling. *Materials & Design* **2018**, *139*, 283–292.
(108) Maqsood, N.; Rimašauskas, M. Characterization of Carbon Fiber Reinforced PLA Composites Manufactured by Fused Deposition Modeling. *Composites Part C: Open Access* **2021**, *4*, 100112.
(109) Tekinalp, H. L.; Kunc, V.; Velez-Garcia, G. M.; Duty, C. E.; Love, L. J.; Naskar, A. K.; Blue, C. A.; Ozcan, S. Highly Oriented Carbon Fiber–Polymer Composites via Additive Manufacturing. *Composites Science and Technology* **2014**, *105*, 144–150.
(110) Luo, B.; Wei, Y.; Chen, H.; Zhu, Z.; Fan, P.; Xu, X.; Xie, B. Printing Carbon Nanotube-Embedded Silicone Elastomers via Direct Writing. *ACS Appl. Mater. Interfaces* **2018**, *10* (51), 44796–44802.
(111) Mahmoudi, M.; Burlison, S. R.; Moreno, S.; Minary-Jolandan, M. Additive-Free and Support-Free 3D Printing of Thermosetting Polymers with Isotropic Mechanical Properties. *ACS Appl. Mater. Interfaces* **2021**, *13* (4), 5529–5538.
(112) Wang, B.; Zhang, Z.; Pei, Z.; Qiu, J.; Wang, S. Current Progress on the 3D Printing of Thermosets. *Adv Compos Hybrid Mater* **2020**, *3* (4), 462–472.

(113) Chen, K.; Kuang, X.; Li, V.; Kang, G.; Jerry Qi, H. Fabrication of Tough Epoxy with Shape Memory Effects by UV-Assisted Direct-Ink Write Printing. *Soft Matter* **2018**, *14* (10), 1879–1886.
(114) Mantelli, A.; Romani, A.; Suriano, R.; Diani, M.; Colledani, M.; Sarlin, E.; Turri, S.; Levi, M. UV-Assisted 3D Printing of Polymer Composites from Thermally and Mechanically Recycled Carbon Fibers. *Polymers* **2021**, *13* (5), 726.
(115) Lebel, L. L.; Aissa, B.; Khakani, M. A. E.; Therriault, D. Ultraviolet-Assisted Direct-Write Fabrication of Carbon Nanotube/Polymer Nanocomposite Microcoils. *Advanced Materials* **2010**, *22* (5), 592–596.
(116) Griffini, G.; Invernizzi, M.; Levi, M.; Natale, G.; Postiglione, G.; Turri, S. 3D-Printable CFR Polymer Composites with Dual-Cure Sequential IPNs. *Polymer* **2016**, *91*, 174–179.
(117) Wu, T.; Jiang, P.; Zhang, X.; Guo, Y.; Ji, Z.; Jia, X.; Wang, X.; Zhou, F.; Liu, W. Additively Manufacturing High-Performance Bismaleimide Architectures with Ultraviolet-Assisted Direct Ink Writing. *Materials & Design* **2019**, *180*, 107947.
(118) Guo, Y.; Ji, Z.; Zhang, Y.; Wang, X.; Zhou, F. Solvent-Free and Photocurable Polyimide Inks for 3D Printing. *J. Mater. Chem. A* **2017**, *5* (31), 16307–16314.
(119) Leguizamon, S. C.; Cook, A. W.; Appelhans, L. N. Employing Photosensitizers for Rapid Olefin Metathesis Additive Manufacturing of Poly(Dicyclopentadiene). *Chem. Mater.* **2021**, *33* (24), 9677–9689.
(120) Talley, S. J.; Branch, B.; Welch, C. F.; Park, C. H.; Watt, J.; Kuettner, L.; Patterson, B.; Dattelbaum, D. M.; Lee, K.-S. Impact of Filler Composition on Mechanical and Dynamic Response of 3-D Printed Silicone-Based Nanocomposite Elastomers. *Composites Science and Technology* **2020**, *198*, 108258.
(121) Bakarich, S. E.; Gorkin, R.; Gately, R.; Naficy, S.; in het Panhuis, M.; Spinks, G. M. 3D Printing of Tough Hydrogel Composites with Spatially Varying Materials Properties. *Additive Manufacturing* **2017**, *14*, 24–30.
(122) Muth, J. T.; Vogt, D. M.; Truby, R. L.; Mengüç, Y.; Kolesky, D. B.; Wood, R. J.; Lewis, J. A. Embedded 3D Printing of Strain Sensors within Highly Stretchable Elastomers. *Advanced Materials* **2014**, *26* (36), 6307–6312.
(123) Rios, O.; Carter, W.; Post, B.; Lloyd, P.; Fenn, D.; Kutchko, C.; Rock, R.; Olson, K.; Compton, B. 3D Printing via Ambient Reactive Extrusion. *Materials Today Communications* **2018**, *15*, 333–336.
(124) Pojman, J. A. 4.38 - Frontal Polymerization. In *Polymer Science: A Comprehensive Reference*; Matyjaszewski, K., Möller, M., Eds.; Elsevier: Amsterdam, 2012; pp 957–980.
(125) Ruiu, A.; Sanna, D.; Alzari, V.; Nuvoli, D.; Mariani, A. Advances in the Frontal Ring Opening Metathesis Polymerization of Dicyclopentadiene. *Journal of Polymer Science Part A: Polymer Chemistry* **2014**, *52* (19), 2776–2780.
(126) Kirk, R. E.; Othmer, D. F. Encyclopedia of Chemical Technology. *Encyclopedia of chemical technology* **1947**.
(127) Ziaee, M.; Yourdkhani, M. Effect of Resin Staging on Frontal Polymerization of Dicyclopentadiene. *Journal of Polymer Science* **2021**, *59* (15), 1732–1739.
(128) Hmeidat, N. S.; Pack, R. C.; Talley, S. J.; Moore, R. B.; Compton, B. G. Mechanical Anisotropy in Polymer Composites Produced by Material Extrusion Additive Manufacturing. *Additive Manufacturing* **2020**, *34*, 101385.
(129) Chen, Z.; Zhao, D.; Liu, B.; Nian, G.; Li, X.; Yin, J.; Qu, S.; Yang, W. 3D Printing of Multifunctional Hydrogels. *Advanced Functional Materials* **2019**, *29* (20), 1900971.

(130) Chandrasekaran, S.; Yao, B.; Liu, T.; Xiao, W.; Song, Y.; Qian, F.; Zhu, C.; B. Duoss, E.; M. Spadaccini, C.; Li, Y.; A. Worsley, M. Direct Ink Writing of Organic and Carbon Aerogels. *Materials Horizons* **2018**, *5* (6), 1166–1175.
(131) Sultan, S.; P. Mathew, A. 3D Printed Scaffolds with Gradient Porosity Based on a Cellulose Nanocrystal Hydrogel. *Nanoscale* **2018**, *10* (9), 4421–4431.
(132) Ajinjeru, C.; Kishore, V.; Chen, X.; Hershey, C.; Lindahl, J.; Kunc, V.; Hassen, A. A.; Duty, C. Rheological Survey of Carbon Fiber-Reinforced High-Temperature Thermoplastics for Big Area Additive Manufacturing Tooling Applications. *Journal of Thermoplastic Composite Materials* **2021**, *34* (11), 1443–1461.
(133) Jiang, G.; Turner, T. A.; Pickering, S. J. The Shear Viscosity of Carbon Fibre Suspension and Its Application for Fibre Length Measurement. *Rheol Acta* **2016**, *55* (1), 1–10.
(134) Courtial, E.-J.; Perrinet, C.; Colly, A.; Mariot, D.; Frances, J.-M.; Fulchiron, R.; Marquette, C. Silicone Rheological Behavior Modification for 3D Printing: Evaluation of Yield Stress Impact on Printed Object Properties. *Additive Manufacturing* **2019**, *28*, 50–57.
(135) Jin, Y.; Liu, C.; Chai, W.; Compaan, A.; Huang, Y. Self-Supporting Nanoclay as Internal Scaffold Material for Direct Printing of Soft Hydrogel Composite Structures in Air. *ACS Appl. Mater. Interfaces* **2017**, *9* (20), 17456–17465.
(136) Raney, J. R.; Compton, B. G.; Mueller, J.; Ober, T. J.; Shea, K.; Lewis, J. A. Rotational 3D Printing of Damage-Tolerant Composites with Programmable Mechanics. *PNAS* **2018**, *115* (6), 1198–1203.
(137) Nawafleh, N.; Celik, E. Additive Manufacturing of Short Fiber Reinforced Thermoset Composites with Unprecedented Mechanical Performance. *Additive Manufacturing* **2020**, *33*, 101109.
(138) Pojman, J. A. Cure-on-Demand Composites by Frontal Polymerization. In *Reference Module in Materials Science and Materials Engineering*; Elsevier, 2022.
(139) Duty, C.; Ajinjeru, C.; Kishore, V.; Compton, B.; Hmeidat, N.; Chen, X.; Liu, P.; Hassen, A. A.; Lindahl, J.; Kunc, V. What Makes a Material Printable? A Viscoelastic Model for Extrusion-Based 3D Printing of Polymers. *Journal of Manufacturing Processes* **2018**, *35*, 526–537.
(140) Hansen, C. J.; Wu, W.; Toohey, K. S.; Sottos, N. R.; White, S. R.; Lewis, J. A. Self-Healing Materials with Interpenetrating Microvascular Networks. *Advanced Materials* **2009**, *21* (41), 4143–4147.
(141) Ferreira, R. T. L.; Amatte, I. C.; Dutra, T. A.; Bürger, D. Experimental Characterization and Micrography of 3D Printed PLA and PLA Reinforced with Short Carbon Fibers. *Composites Part B: Engineering* **2017**, *124*, 88–100.
(142) Hmeidat, N. S.; Elkins, D. S.; Peter, H. R.; Kumar, V.; Compton, B. G. Processing and Mechanical Characterization of Short Carbon Fiber-Reinforced Epoxy Composites for Material Extrusion Additive Manufacturing. *Composites Part B: Engineering* **2021**, *223*, 109122.
(143) Yirmibesoglu, O. D.; Simonsen, L. E.; Manson, R.; Davidson, J.; Healy, K.; Menguc, Y.; Wallin, T. Multi-Material Direct Ink Writing of Photocurable Elastomeric Foams. *Commun Mater* **2021**, *2* (1), 1–14.
(144) Wei, T.-S.; Ahn, B. Y.; Grotto, J.; Lewis, J. A. 3D Printing of Customized Li-Ion Batteries with Thick Electrodes. *Advanced Materials* **2018**, *30* (16), 1703027.
(145) Guo, S.-Z.; Qiu, K.; Meng, F.; Park, S. H.; McAlpine, M. C. 3D Printed Stretchable Tactile Sensors. *Advanced Materials* **2017**, *29* (27), 1701218.

(146) Wei, H.; Zhang, Q.; Yao, Y.; Liu, L.; Liu, Y.; Leng, J. Direct-Write Fabrication of 4D Active Shape-Changing Structures Based on a Shape Memory Polymer and Its Nanocomposite. *ACS Appl. Mater. Interfaces* **2017**, *9* (1), 876–883.
(147) Jiang, F.; Wörz, A.; Romeis, M.; Drummer, D. Analysis of UV-Assisted Direct Ink Writing Rheological Properties and Curing Degree. *Polymer Testing* **2022**, *105*, 107428.
(148) Rau, D. A.; Herzberger, J.; Long, T. E.; Williams, C. B. Ultraviolet-Assisted Direct Ink Write to Additively Manufacture All-Aromatic Polyimides. *ACS Appl. Mater. Interfaces* **2018**, *10* (41), 34828–34833.
(149) Tu, R.; Sodano, H. A. Additive Manufacturing of High-Performance Vinyl Ester Resin via Direct Ink Writing with UV-Thermal Dual Curing. *Additive Manufacturing* **2021**, *46*, 102180.
(150) Li, Q.; Shen, H.-X.; Liu, C.; Wang, C.-F.; Zhu, L.; Chen, S. Advances in Frontal Polymerization Strategy: From Fundamentals to Applications. *Progress in Polymer Science* **2022**, *127*, 101514.
(151) Pojman, J. A. Frontal Polymerization. *Polymer Science: A Comprehensive Reference, 10 Volume Set* **2010**, *4*.
(152) Nason, C.; Roper, T.; Hoyle, C.; Pojman, J. A. UV-Induced Frontal Polymerization of Multifunctional (Meth)Acrylates. *Macromolecules* **2005**, *38* (13), 5506–5512.
(153) Mariani, A.; Bidali, S.; Fiori, S.; Sangermano, M.; Malucelli, G.; Bongiovanni, R.; Priola, A. UV-Ignited Frontal Polymerization of an Epoxy Resin. *Journal of Polymer Science Part A: Polymer Chemistry* **2004**, *42* (9), 2066–2072.
(154) Groce, B. R.; Gary, D. P.; Cantrell, J. K.; Pojman, J. A. Front Velocity Dependence on Vinyl Ether and Initiator Concentration in Radical-Induced Cationic Frontal Polymerization of Epoxies. *Journal of Polymer Science* **2021**, *59* (15), 1678–1685.
(155) Aw, J. E.; Zhang, X.; Nelson, A. Z.; Dean, L. M.; Yourdkhani, M.; Ewoldt, R. H.; Geubelle, P. H.; Sottos, N. R. Self-Regulative Direct Ink Writing of Frontally Polymerizing Thermoset Polymers. *Advanced Materials Technologies n/a* (n/a), 2200230.
(156) Vallons, K. A. M.; Drozdzak, R.; Charret, M.; Lomov, S. V.; Verpoest, I. Assessment of the Mechanical Behaviour of Glass Fibre Composites with a Tough Polydicyclopentadiene (PDCPD) Matrix. *Composites Part A: Applied Science and Manufacturing* **2015**, *78*, 191–200.
(157) Jr, C. S. W.; Grubbs, R. H. Polymeric Composites Including Dicyclopentadiene and Related Monomers. US6310121B1, October 30, 2001.
(158) Delaude, L.; Noels, A. F. Metathesis (2007) Kirk-Othmer Encyclopedia of Chemical Technology, 26. *5th Print Ed, A. Seidel Ed, Wiley, New York* 920–958.
(159) Ziaee, M.; Johnson, J. W.; Yourdkhani, M. 3D Printing of Short-Carbon-Fiber-Reinforced Thermoset Polymer Composites via Frontal Polymerization. *ACS Appl. Mater. Interfaces* **2022**, *14* (14), 16694–16702.
(160) Andjelkovic, D. D.; Valverde, M.; Henna, P.; Li, F.; Larock, R. C. Novel Thermosets Prepared by Cationic Copolymerization of Various Vegetable Oils—Synthesis and Their Structure–Property Relationships. *Polymer* **2005**, *46* (23), 9674–9685.
(161) Xia, Y.; Lu, Y.; Larock, R. C. Ring-Opening Metathesis Polymerization (ROMP) of Norbornenyl-Functionalized Fatty Alcohols. *Polymer* **2010**, *51* (1), 53–61.
(162) Li, F.; Hasjim, J.; Larock, R. C. Synthesis, Structure, and Thermophysical and Mechanical Properties of New Polymers Prepared by the Cationic Copolymerization of Corn Oil, Styrene, and Divinylbenzene. *Journal of Applied Polymer Science* **2003**, *90* (7), 1830–1838.

(163) Ding, R.; Xia, Y.; Mauldin, T. C.; Kessler, M. R. Biorenewable ROMP-Based Thermosetting Copolymers from Functionalized Castor Oil Derivative with Various Cross-Linking Agents. *Polymer* **2014**, *55* (22), 5718–5726.
(164) Li, F.; Larock, R. C. Synthesis, Structure and Properties of New Tung Oil−Styrene−Divinylbenzene Copolymers Prepared by Thermal Polymerization. *Biomacromolecules* **2003**, *4* (4), 1018–1025.
(165) Cui, H.; Kessler, M. R. Composition-Dependent Fracture Toughness of ROMP-Based Dilulin/Dicyclopentadiene Copolymers. *J Mater Sci* **2014**, *49* (14), 4880–4890.
(166) Henna, P.; Larock, R. C. Novel Thermosets Obtained by the Ring-Opening Metathesis Polymerization of a Functionalized Vegetable Oil and Dicyclopentadiene. *Journal of Applied Polymer Science* **2009**, *112* (3), 1788–1797.
(167) Cui, H.; Hanus, R.; Kessler, M. R. Degradation of ROMP-Based Bio-Renewable Polymers by UV Radiation. *Polymer Degradation and Stability* **2013**, *98* (11), 2357–2365.
(168) Henna, P. H.; Kessler, M. R.; Larock, R. C. Fabrication and Properties of Vegetable-Oil-Based Glass Fiber Composites by Ring-Opening Metathesis Polymerization. *Macromolecular Materials and Engineering* **2008**, *293* (12), 979–990.
(169) Cui, H.; Kessler, M. R. Glass Fiber Reinforced ROMP-Based Bio-Renewable Polymers: Enhancement of the Interface with Silane Coupling Agents. *Composites Science and Technology* **2012**, *72* (11), 1264–1272.
(170) Cui, H.; Kessler, M. R. Pultruded Glass Fiber/Bio-Based Polymer: Interface Tailoring with Silane Coupling Agent. *Composites Part A: Applied Science and Manufacturing* **2014**, *65*, 83–90.
(171) Jeong, W.; Mauldin, T. C.; Larock, R. C.; Kessler, M. R. Bio-Based Rubbers by Concurrent Cationic and Ring-Opening Metathesis Polymerization of a Modified Linseed Oil. *Macromolecular Materials and Engineering* **2009**, *294* (11), 756–761.
(172) Haman, K.; Badrinarayanan, P.; Kessler, M. R. Cure Characterization of the Ring-Opening Metathesis Polymerization of Linseed Oil-Based Thermosetting Resins. *Polymer International* **2009**, *58* (7), 738–744.
(173) Dean, L. M.; Wu, Q.; Alshangiti, O.; Moore, J. S.; Sottos, N. R. Rapid Synthesis of Elastomers and Thermosets with Tunable Thermomechanical Properties. *ACS Macro Lett.* **2020**, *9* (6), 819–824.
(174) L. Gringolts, M.; I. Denisova, Y.; A. Shandryuk, G.; B. Krentsel, L.; D. Litmanovich, A.; Sh. Finkelshtein, E.; V. Kudryavtsev, Y. Synthesis of Norbornene–Cyclooctene Copolymers by the Cross-Metathesis of Polynorbornene with Polyoctenamer. *RSC Advances* **2015**, *5* (1), 316–319.
(175) Mauldin, T. C.; Haman, K.; Sheng, X.; Henna, P.; Larock, R. C.; Kessler, M. R. Ring-Opening Metathesis Polymerization of a Modified Linseed Oil with Varying Levels of Crosslinking. *Journal of Polymer Science Part A: Polymer Chemistry* **2008**, *46* (20), 6851–6860.
(176) Nielsen, L. E. Cross-Linking–Effect on Physical Properties of Polymers. *Journal of Macromolecular Science, Part C* **1969**, *3* (1), 69–103.
(177) Thunga, M.; Xia, Y.; Gohs, U.; Heinrich, G.; Larock, R. C.; Kessler, M. R. Influence of Electron Beam Irradiation on the Mechanical Properties of Vegetable-Oil-Based Biopolymers. *Macromolecular Materials and Engineering* **2012**, *297* (8), 799–806.
(178) Washington, R. P.; Steinbock, O. Frontal Polymerization Synthesis of Temperature-Sensitive Hydrogels. *J. Am. Chem. Soc.* **2001**, *123* (32), 7933–7934.

(179) Tredici, A.; Pecchini, R.; Sliepcevich, A.; Morbidelli, M. Polymer Blends by Self-Propagating Frontal Polymerization. *Journal of Applied Polymer Science* **1998**, *70* (13), 2695–2702.
(180) Chandrasekaran, S.; Yao, B.; Liu, T.; Xiao, W.; Song, Y.; Qian, F.; Zhu, C.; Duoss, E. B.; Spadaccini, C. M.; Li, Y.; Worsley, M. A. Direct Ink Writing of Organic and Carbon Aerogels. *Mater. Horiz.* **2018**, *5* (6), 1166–1175.
(181) Ravichandran, D.; Xu, W.; Kakarla, M.; Jambhulkar, S.; Zhu, Y.; Song, K. Multiphase Direct Ink Writing (MDIW) for Multilayered Polymer/Nanoparticle Composites. *Additive Manufacturing* **2021**, *47*, 102322.
(182) Chapman, S. J.; Fitt, A. D.; Please, C. P. Extrusion of Power-Law Shear-Thinning Fluids with Small Exponent. *International Journal of Non-Linear Mechanics* **1997**, *32* (1), 187–199.
(183) Sun, Y.; Peng, C.; Wang, X.; Wang, R.; Yang, J.; Zhang, D. Rheological Behavior of Al2O3 Suspensions Containing Polyelectrolyte Complexes for Direct Ink Writing. *Powder Technology* **2017**, *320*, 223–229.
(184) Liu, J.; Guo, Y.; Weng, C.; Zhang, H.; Zhang, Z. High Thermal Conductive Epoxy Based Composites Fabricated by Multi-Material Direct Ink Writing. *Composites Part A: Applied Science and Manufacturing* **2020**, *129*, 105684.
(185) Siqueira, G.; Kokkinis, D.; Libanori, R.; Hausmann, M. K.; Gladman, A. S.; Neels, A.; Tingaut, P.; Zimmermann, T.; Lewis, J. A.; Studart, A. R. Cellulose Nanocrystal Inks for 3D Printing of Textured Cellular Architectures. *Advanced Functional Materials* **2017**, *27* (12), 1604619.
(186) Kokkinis, D.; Bouville, F.; Studart, A. R. 3D Printing of Materials with Tunable Failure via Bioinspired Mechanical Gradients. *Advanced Materials* **2018**, *30* (19), 1705808.
(187) Mallick, P. K. *Fiber-Reinforced Composites: Materials, Manufacturing, and Design, Third Edition*, 3rd ed.; CRC Press: Boca Raton, 2007.
(188) Goh, G. D.; Yap, Y. L.; Agarwala, S.; Yeong, W. Y. Recent Progress in Additive Manufacturing of Fiber Reinforced Polymer Composite. *Advanced Materials Technologies* **2019**, *4* (1), 1800271.
(189) Lewis, J. A. Direct Ink Writing of 3D Functional Materials. *Advanced Functional Materials* **2006**, *16* (17), 2193–2204.
(190) Liu, M.; Chiang, S.-W.; Chu, X.; Li, J.; Gan, L.; He, Y.; Li, B.; Kang, F.; Du, H. Polymer Composites with Enhanced Thermal Conductivity via Oriented Boron Nitride and Alumina Hybrid Fillers Assisted by 3-D Printing. *Ceramics International* **2020**, *46* (13), 20810–20818.
(191) Romberg, S. K.; Abir, A. I.; Hershey, C. J.; Kunc, V.; Compton, B. G. Structural Stability of Thin Overhanging Walls during Material Extrusion Additive Manufacturing of Thermoset-Based Ink. *Additive Manufacturing* **2022**, *53*, 102677.
(192) Invernizzi, M.; Natale, G.; Levi, M.; Turri, S.; Griffini, G. UV-Assisted 3D Printing of Glass and Carbon Fiber-Reinforced Dual-Cure Polymer Composites. *Materials* **2016**, *9* (7), 583.
(193) Aw, J. E.; Zhang, X.; Nelson, A. Z.; Dean, L. M.; Yourdkhani, M.; Ewoldt, R. H.; Geubelle, P. H.; Sottos, N. R. Self-Regulative Direct Ink Writing of Frontally Polymerizing Thermoset Polymers. *Advanced Materials Technologies* **2022**, *7* (9), 2200230.
(194) Fortenbaugh, R. J.; Carrozzi, S. A.; Lear, B. J. Photothermal Control over the Mechanical and Physical Properties of Polydimethylsiloxane. *Macromolecules* **2019**, *52* (10), 3839–3844.

(195) Lei, T.; Fernandez-Fernandez, A.; Manchanda, R.; Huang, Y.-C.; McGoron, A. J. Near-Infrared Dye Loaded Polymeric Nanoparticles for Cancer Imaging and Therapy and Cellular Response after Laser-Induced Heating. *Beilstein J. Nanotechnol.* **2014**, *5* (1), 313–322.
(196) Zhou, B.; Li, Y.; Niu, G.; Lan, M.; Jia, Q.; Liang, Q. Near-Infrared Organic Dye-Based Nanoagent for the Photothermal Therapy of Cancer. *ACS Appl. Mater. Interfaces* **2016**, *8* (44), 29899–29905.
(197) Pimentel-Domínguez, R.; Velázquez-Benítez, A. M.; Vélez-Cordero, J. R.; Hautefeuille, M.; Sánchez-Arévalo, F.; Hernández-Cordero, J. Photothermal Effects and Applications of Polydimethylsiloxane Membranes with Carbon Nanoparticles. *Polymers* **2016**, *8* (4), 84.
(198) Sharma, S.; Luzinov, I. Ultrasonic Curing of One-Part Epoxy System. *Journal of Composite Materials* **2011**, *45* (21), 2217–2224.
(199) Yu, C.; Wang, C.-F.; Chen, S. Robust Self-Healing Host–Guest Gels from Magnetocaloric Radical Polymerization. *Advanced Functional Materials* **2014**, *24* (9), 1235–1242.
(200) Fortenbaugh, R. J.; J. Lear, B. On-Demand Curing of Polydimethylsiloxane (PDMS) Using the Photothermal Effect of Gold Nanoparticles. *Nanoscale* **2017**, *9* (25), 8555–8559.
(201) Xu, X.; Zhang, Y.; Jiang, J.; Wang, H.; Zhao, X.; Li, Q.; Lu, W. In-Situ Curing of Glass Fiber Reinforced Polymer Composites via Resistive Heating of Carbon Nanotube Films. *Composites Science and Technology* **2017**, *149*, 20–27.
(202) Bonardi, A. heloise; Bonardi, F.; Dumur, F.; Gigmes, D.; Fouassier, J. P.; Lalevée, J. Fillers as Heaters for Photothermal Polymerization upon NIR Light. *Macromolecular Rapid Communications* **2019**, *40* (23), 1900495.
(203) Pascault, J.-P.; Williams, R. J. J. Thermosetting Polymers. In *Handbook of Polymer Synthesis, Characterization, and Processing*; John Wiley & Sons, Ltd, 2013; pp 519–533.
(204) Daniel, I. M.; Ishai, O. *Engineering Mechanics of Composite Materials*, 2nd ed.; Oxford University Press: New York, 2006.
(205) Davtyan, S. P.; Berlin, A. A.; Tonoyan, A. O. Advances and Problems of Frontal Polymerization Processes. *Ref. J. Chem.* **2011**, *1* (1), 56–92.
(206) McFarland, B.; Popwell, S.; Pojman, J. A. Free-Radical Frontal Polymerization with a Microencapsulated Initiator: Characterization of Microcapsules and Their Effect on Pot Life, Front Velocity, and Mechanical Properties. *Macromolecules* **2006**, *39* (1), 55–63.
(207) Pojman, J. A. Nonlinear Chemical Dynamics In Synthetic Polymer Systems. In *Chemomechanical Instabilities in Responsive Materials*; Borckmans, P., De Kepper, P., Khokhlov, A. R., Métens, S., Eds.; NATO Science for Peace and Security Series A: Chemistry and Biology; Springer Netherlands: Dordrecht, 2009; pp 221–240.
(208) Holt, T.; Fazende, K.; Jee, E.; Wu, Q.; Pojman, J. A. Cure-on-Demand Wood Adhesive Based on the Frontal Polymerization of Acrylates. *Journal of Applied Polymer Science* **2016**, *133* (40).
(209) Lessard, J. J.; Kaur, P.; Paul, J. E.; Chang, K. M.; Sottos, N. R.; Moore, J. S. Switching Frontal Polymerization Mechanisms: FROMP and FRaP. *ACS Macro Lett.* **2022**, *11* (9), 1097–1101.
(210) Pujari, N. S.; Vishwakarma, A. R.; Vishwakarma, A. R.; Kelkar, M. K.; Ponrathnam, S. Gel Formation in Frontal Polymerization of 2-Hydroxyethyl Methacrylate. *e-Polymers* **2004**, *4* (1).
(211) Gary, D. P.; Bynum, S.; Thompson, B. D.; Groce, B. R.; Sagona, A.; Hoffman, I. M.; Morejon-Garcia, C.; Weber, C.; Pojman, J. A. Thermal Transport and Chemical Effects of

Fillers on Free-Radical Frontal Polymerization. *Journal of Polymer Science* **2020**, *58* (16), 2267–2277.
(212) Tredici, A.; Pecchini, R.; Morbidelli, M. Self-Propagating Frontal Copolymerization. *Journal of Polymer Science Part A: Polymer Chemistry* **1998**, *36* (7), 1117–1126.
(213) Mariani, A.; Nuvoli, D.; Alzari, V.; Pini, M. Phosphonium-Based Ionic Liquids as a New Class of Radical Initiators and Their Use in Gas-Free Frontal Polymerization. *Macromolecules* **2008**, *41* (14), 5191–5196.
(214) A. Pojman, J.; M. Ilyashenko, V.; M. Khan, A. Free-Radical Frontal Polymerization: Self-Propagating Thermal Reaction Waves. *Journal of the Chemical Society, Faraday Transactions* **1996**, *92* (16), 2825–2837.
(215) Gugg, A.; Gorsche, C.; Moszner, N.; Liska, R. Frontal Polymerization: Polymerization Induced Destabilization of Peracrylates. *Macromolecular Rapid Communications* **2011**, *32* (14), 1096–1100.
(216) Nason, C.; Pojman, J. A.; Hoyle, C. The Effect of a Trithiol and Inorganic Fillers on the Photo-Induced Thermal Frontal Polymerization of a Triacrylate. *Journal of Polymer Science Part A: Polymer Chemistry* **2008**, *46* (24), 8091–8096.
(217) Mota-Morales, J. D.; Gutiérrez, M. C.; Ferrer, M. L.; Sanchez, I. C.; Elizalde-Peña, E. A.; Pojman, J. A.; Monte, F. D.; Luna-Bárcenas, G. Deep Eutectic Solvents as Both Active Fillers and Monomers for Frontal Polymerization. *Journal of Polymer Science Part A: Polymer Chemistry* **2013**, *51* (8), 1767–1773.
(218) Du, X.-Y.; Shen, J.; Zhang, J.; Ling, L.; Wang, C.-F.; Chen, S. Generation of a Carbon Dots/Ammonium Persulfate Redox Initiator Couple for Free Radical Frontal Polymerization. *Polymer Chemistry* **2018**, *9* (4), 420–427.
(219) Liu, S.-S.; Yu, Z.-Y.; Fang, Y.; Yin, S.-N.; Wang, C.-F.; Chen, L.; Chen, S. A Facile Pathway for the Fast Synthesis of Colloidal Crystal-Loaded Hydrogels via Frontal Polymerization. *Journal of Polymer Science Part A: Polymer Chemistry* **2011**, *49* (14), 3121–3128.
(220) Fang, Y.; Yu, H.; Chen, L.; Chen, S. Facile Glycerol-Assisted Synthesis of N-Vinyl Pyrrolidinone-Based Thermosensitive Hydrogels via Frontal Polymerization. *Chem. Mater.* **2009**, *21* (19), 4711–4718.
(221) Tang, W.-Q.; Mao, L.-H.; Zhou, Z.-F.; Wang, C.-F.; Chen, Q.-L.; Chen, S. Facile Synthesis of 4-Vinylpyridine-Based Hydrogels via Laser-Ignited Frontal Polymerization and Their Performance on Ion Removal. *Colloid Polym Sci* **2014**, *292* (10), 2529–2537.
(222) Tu, J.; Zhou, J.; Wang, C.-F.; Zhang, Q.; Chen, S. Facile Synthesis of N-Vinylimidazole-Based Hydrogels via Frontal Polymerization and Investigation of Their Performance on Adsorption of Copper Ions. *Journal of Polymer Science Part A: Polymer Chemistry* **2010**, *48* (18), 4005–4012.
(223) McCaughey, B.; Pojman, J. A.; Simmons, C.; Volpert, V. A. The Effect of Convection on a Propagating Front with a Liquid Product: Comparison of Theory and Experiments. *Chaos* **1998**, *8* (2), 520–529.
(224) Bazile Jr., M.; Nichols, H. A.; Pojman, J. A.; Volpert, V. Effect of Orientation on Thermoset Frontal Polymerization. *Journal of Polymer Science Part A: Polymer Chemistry* **2002**, *40* (20), 3504–3508.
(225) Masere, J.; Stewart, F.; Meehan, T.; Pojman, J. A. Period-Doubling Behavior in Frontal Polymerization of Multifunctional Acrylates. *Chaos* **1999**, *9* (2), 315–322.

(226) Masere, J.; Chekanov, Y.; Warren, J. R.; Stewart, F. D.; Al-Kaysi, R.; Rasmussen, J. K.; Pojman, J. A. Gas-Free Initiators for High-Temperature Free-Radical Polymerization. *Journal of Polymer Science Part A: Polymer Chemistry* **2000**, *38* (21), 3984–3990.
(227) Alam, S.; Manzur, T.; Banjara, A.; Eklund, S.; Radadia, A.; Johnston, W.; Hashm, H.; Williams, J.; Matthews, J. Rapid Curing Prospects of Geopolymer Cementitious Composite Using Frontal Polymerization of Methyl Methacrylate Monomer. *Construction and Building Materials* **2021**, *309*, 125198.
(228) Yu, H.; Fang, Y.; Chen, L.; Chen, S. Investigation of Redox Initiators for Free Radical Frontal Polymerization. *Polymer International* **2009**, *58* (8), 851–857.
(229) Chen, S.; Hu, T.; Tian, Y.; Chen, L.; Pojman, J. A. Facile Synthesis of Poly(Hydroxyethyl Acrylate) by Frontal Free-Radical Polymerization. *Journal of Polymer Science Part A: Polymer Chemistry* **2007**, *45* (5), 873–881.
(230) Zhou, Z.-F.; Yu, C.; Wang, X.-Q.; Tang, W.-Q.; Wang, C.-F.; Chen, S. Facile Access to Poly(NMA- Co -VCL) Hydrogels via Long Range Laser Ignited Frontal Polymerization. *Journal of Materials Chemistry A* **2013**, *1* (25), 7326–7331.
(231) Suslick, B.; Hemmer, J.; Groce, B.; Stawiasz, K.; Geubelle, P.; Malucelli, G.; Mariani, A.; Moore, J.; Pojman, J.; Sottos, N. Frontal Polymerizations: From Chemical Perspectives to Macroscopic Properties and Applications. **2022**.
(232) Lloyd, E. M.; Feinberg, E. C.; Gao, Y.; Peterson, S. R.; Soman, B.; Hemmer, J.; Dean, L. M.; Wu, Q.; Geubelle, P. H.; Sottos, N. R.; Moore, J. S. Spontaneous Patterning during Frontal Polymerization. *ACS Cent. Sci.* **2021**.
(233) Essawy, H. A. Poly(Methyl Methacrylate)-Kaolinite Nanocomposites Prepared by Interfacial Polymerization with Redox Initiator System. *Colloid Polym Sci* **2008**, *286* (6), 795–803.
(234) Lee, K. E.; Morad, N.; Teng, T. T.; Poh, B. T. Kinetics and *In-Situ* Rheological Behavior of Acrylamide Redox Polymerization. *Journal of Dispersion Science and Technology* **2012**, *33* (3), 387–395.
(235) Pojman, J. A. Traveling Fronts of Methacrylic Acid Polymerization. *J. Am. Chem. Soc.* **1991**, *113* (16), 6284–6286.

Appendix A

GC2 storage

GC2 is sensitive to temperature and air; it must be stored in a refrigerator at temperature of 2–8 °C under an inert gas. Using GC2 without proper storage reduces the resin reactivity and degree of cure of produced polymer. Since GC2 is frequently used in this dissertation, a new protocol for proper storage of GC2 has been developed to reduce the exposure of GC2 to air. In this protocol, as-received GC2 is divided into a few baches of 100 mg and each batch is transferred to a 20 mL storage vial and purged with a dry nitrogen gas for 1 min. After purging the gas, the vials are immediately sealed with a cap and covered with parafilm and stored in the refrigerator. Vials should be purged with the nitrogen gas and stored in the refrigerator after each use. Once each vial is opened, the catalyst remains usable for about 4 months.

TBP storage

TBP is a moisture-sensitive material and undergoes hydrolysis in the presence of air. This hydrolysis reduces its inhibiting performance leading to faster gelation and lower reactivity of resin and prevents reliable measurements of front properties. To preserve TBP quality and consistency, small quantities (up to 1 mL) of as-received TBP are transferred to several 5 mL glass vials and purged with dry nitrogen gas for 1 min. The vials are then caped and sealed with parafilm and stored in a desiccator at room temperature for a month. Each vial can be used for up to 3 days under ambient condition after opening.

Preparation of DCPD/ENB solution

DCPD/ENB solution is prepared by placing a 2.5 kg bottle of solid DCPD inside the refrigerated incubator (Heratherm Thermo Scientific) at 60 °C for 2 h to melt the resin. 1 kg of

melted DCPD resin is weighed out using a balance (Sartorius Quintix, precision 0.01 g) and poured into a 2.4 L amber glass bottle. After transferring the liquid DCPD resin, 52.63 g of ENB is measured by the Sartorius Quintix balance and added to the DCPD and thoroughly mixed using a magnetic stirrer for 3 h to obtain a homogeneous 95:5 DCPD/ENB solution. The DCPD/ENB solution is then slowly passed through a 60 mL Buchner filtering funnel filled with aluminum oxide (basic activated Brockmann I, Sigma-Aldrich) via vacuum to remove the butyl hydroxytoluene (BHT) (0.05 wt%) stabilizer from the resin.

Preparation of FP solution

For all FP experiments, 3.21 mg of GC2 is weighed using a microbalance (Mettler-Toledo, precision 0.01 mg) and transferred to a 1.5 mL Eppendorf tube using a disposable propylene spatula. The Eppendorf is filled with 400 μl of PCH using a 1 mL micropipette (Ergonomic High-Performance, precision 100 μL) to dissolve GC2. Various concentrations of TBP inhibitor (1-4 M equiv. with respect to GC2) are added to the solution using a volumetric syringe (Hamilton, precision 0.01 μL) by submerging its tip and releasing the inhibitor in the PCH. The catalyst/inhibitor solution is sonicated (Barsonic cleaner) at room temperature for 10 min to change its color from dark pink to light pink, indicative of TBP- coordinated catalyst species. The prepared catalyst/inhibitor solution is then added to 5 g of DCPD/ENB using a disposable glass pipette and gently swirled for 30 s to achieve a uniform FP solution.

FP experiments

The FP solution prepared from previous step is transferred to a glass test tube inside a preheated incubator (Heratherm Thermo Scientific, precision 0.5 °C) and staged at various temperatures (i.e., 25, 35, and 45 °C) for different time intervals (Figure A1). FP is performed in a descending mode by passing a constant 2.5 A electrical current for 2 min through the resistive

wire immersed about 5 mm below the free surface of resin solution. Once the front is observed, its propagation is monitored using a FLIR T540 infrared camera and its position is measured by finding the location of sharp thermal gradients at different time intervals. Front velocities are then calculated based on the slope of a best-fit straight line for front position versus time. The temperature of resin is also recorded using a T-type thermocouple (MN Measurements Instruments, USA) positioned roughly in the middle of test tube. The temperature data is collected using a thermocouple reader (Phidgets Inc., model 1048) and recorded using a custom LabVIEW code (National Instrument) at 3 Hz.

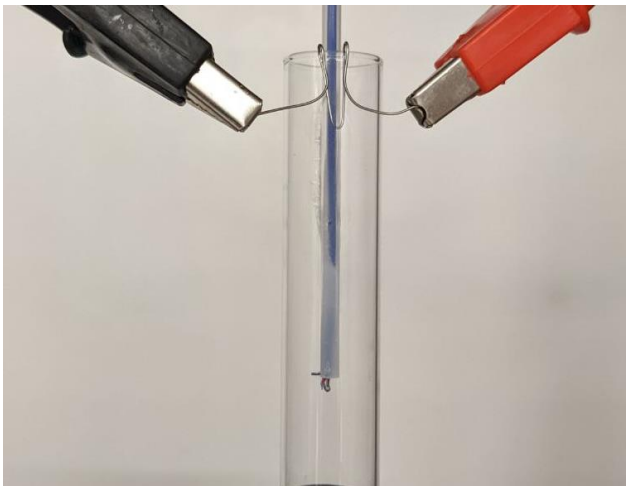

Figure A1. Experimental setup used for FP experiments.

Appendix B

Preparation of 3D printing milled carbon fiber-reinforced inks

6.42 mg of GC2 is weighed on the Mettler-Toledo microbalance using a disposable plastic spatula and transferred to a 1.5 mL Eppendorf tube. In a separate Eppendorf tube, 500 μL of PCH solvent is measured using the Ergonomic High-Performance micropipette and filled with 2.38 μL of TBP inhibitor (1 M equiv. with respect to GC2) via the volumetric syringe (Hamilton, precision 0.01 μL). The TBP inhibitor is hand mixed for about 2 min and the resulting solution is added to the GC2. The catalyst/inhibitor solution is sonicated (Barsonic cleaner) at room temperature for 10 min and added to 12 g of DCPD/ENB using a disposable glass pipette. The solution is then transferred to the refrigerated incubator (Heratherm Thermo Scientific, precision 0.5 °C) to stage the resin at 30 °C for 60 min to increase its viscosity and make it suitable for mixing with CFs. It should be noted that staging the neat resin less than 60 min leads to precipitation of CFs due to low viscosity of resin and staging the neat resin more than 70 min reduces the mixing performance, leading to formation of CF aggregates. In both scenarios, a nonhomogeneous mixture is obtained that later causes nozzle clogging and inconsistent flow of ink during printing process. After the staging is completed, various concentrations of CFs (0, 5, 10, and 15 vol%) are measured using the Mettler Toledo balance (ME204, precision 0.1 g) and added to the resin and mixed for 5 min by the planetary centrifugal mixer (AR-100, Thinky USA). The resulting ink still has a low viscosity and should be staged for additional 20 min at 30 °C in the incubator oven to further increase its viscosity (Figure B1). The ink is then transferred to a 10 mL syringe barrel using a disposable plastic spatula and centrifuged via Thinky mixer for 5 min to remove any trapped bubbles.

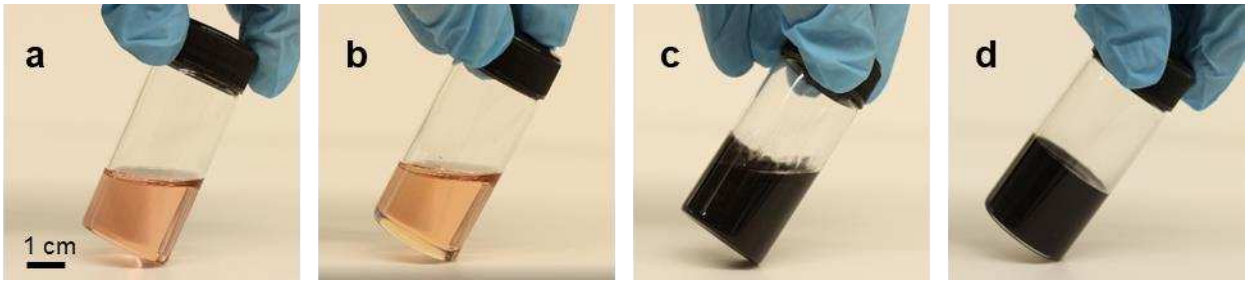

Figure B1. Comparing viscosity of the resin system in different preparation steps. (a) Neat DCPD resin. (b) Neat DCPD gel after 60 min of staging at 30 °C. (c) Neat DCPD gel mixed with 15 vol% CFs. (d) 3D printing ink obtained after additional 20 min of staging at 30 °C.

3D printing of flexural samples

Printing path is generated manually and fed into a Fisnar F5200N robot. Flexural samples are fabricated using a 0.6 mm stainless steel nozzle at a print speed of 1.2–2.6 mm/s and air pressure of 40–400 kPa depending on the concentration of carbon fibers (CF) (Table B1). 3D printed samples are designed to have 10% overlap between layers to manufacture void-free parts. This printing strategy was adopted to prevent void formation, i.e. under filling of interfilament spaces, caused by printing process.

Table B1. Printing speeds and printing pressures used for manufacturing flexural samples with various CF concentrations.

CF concentration (vol%)	Printing speed (mm/s)	Printing pressure (kPa)
0	1.2	40
5	1.7	100
10	2.4	230
15	2.6	400

Polishing procedure for optical imaging

Samples are mounted using a cold mounting epoxy resin (EpoxySet) in a plastic cup with a 2.54 cm diameter. The resin and hardener are thoroughly mixed with a mixing ratio of 10:3 and poured over the samples in the mounting cup. The cup is placed inside a vacuum chamber for 3–5 min, and the resin is allowed to be cured at room temperature for 2 h. After curing, the samples are ground and polished using the following method for optical imaging. First, samples are ground on a silicon carbide (SiC) 600 grit paper followed by a 1200 grit paper to remove the large scratches. After that, the samples are polished using various water-based polycrystalline diamond suspensions on separate low-napped polishing pads, starting at 9 mm followed by 6 mm, 3mm and 1 mm suspensions with time duration of 3 min for each step. In each step, samples are cleaned with DI water and isopropyl alcohol and dried with compressed air. All consumables are supplied from Allied High-Tech Products, Inc.

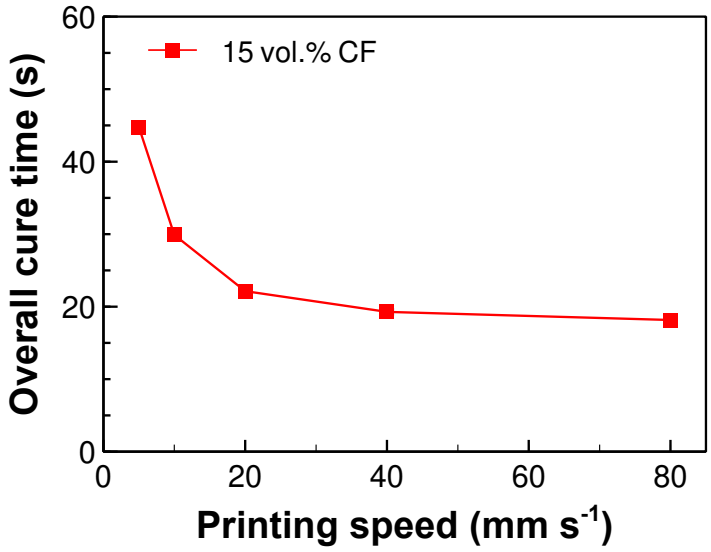

Figure B2. Overall cure time of a 200-mm long composite (15 vol% CF) filament printed at various speeds.

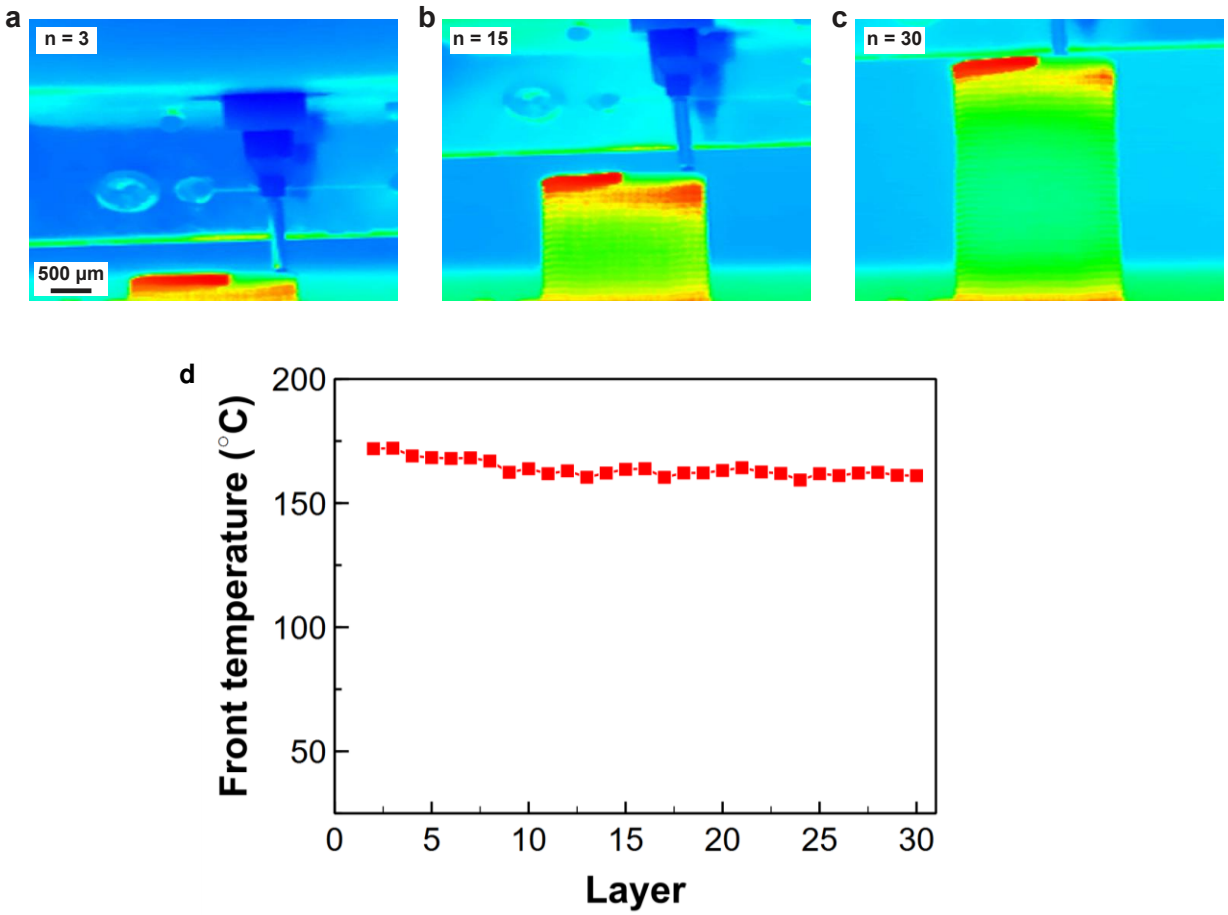

Figure B3. Asynchronous (layer-by-layer) printing of a composite hexagonal structure at a printing speed of 3 mm/s. (a-c) Thermal infrared images show a lag between the printing nozzle and reaction front, caused by the initial activation time of the FP reaction. Images are taken from printing of the 3rd layer (a), 15th layer (b), and 30th layer (c). (d) Front temperature at each layer of the composite structure, indicating a uniform front behavior across various layers.

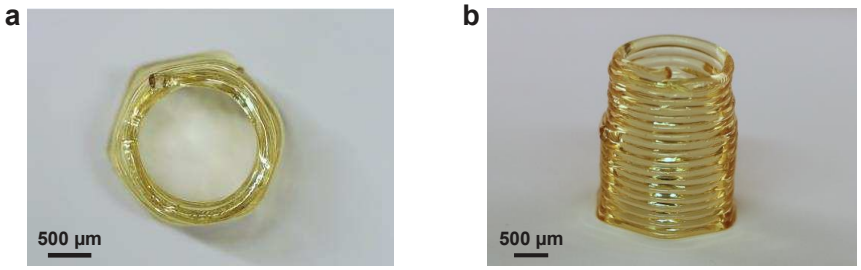

Figure B4. (a-b) Images of a neat pDCPD hexagonal structure printed by the asynchronous (layer-by-layer) printing strategy.

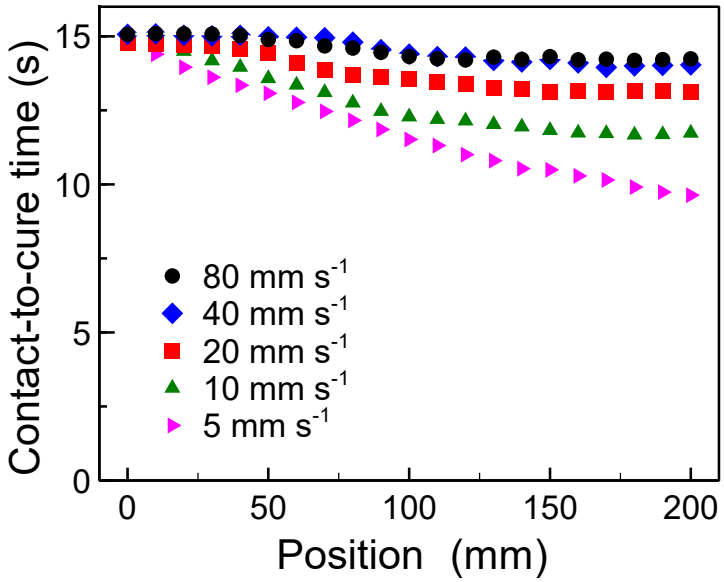

Figure B5. Time interval from the moment any part of the composite filament comes in contact with the hot substrate until that part fully cures. The contact-to-cure time is measured for 21 points along the length of a 200-mm filament printed at different speeds.

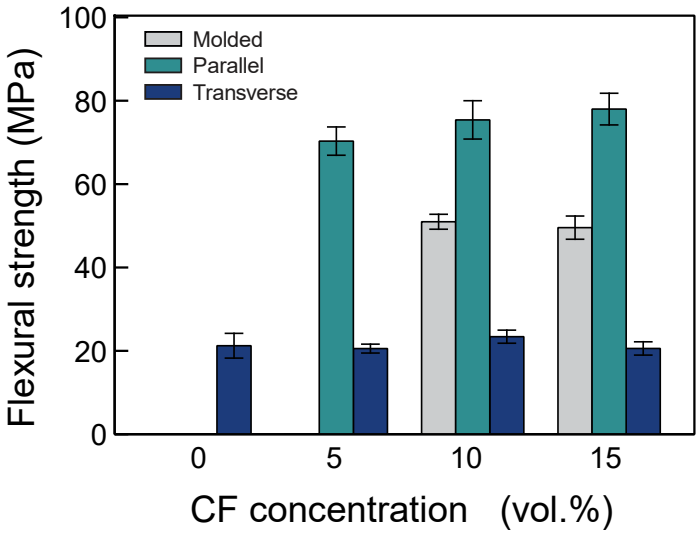

Figure B6. Flexural strength of printed and molded samples.

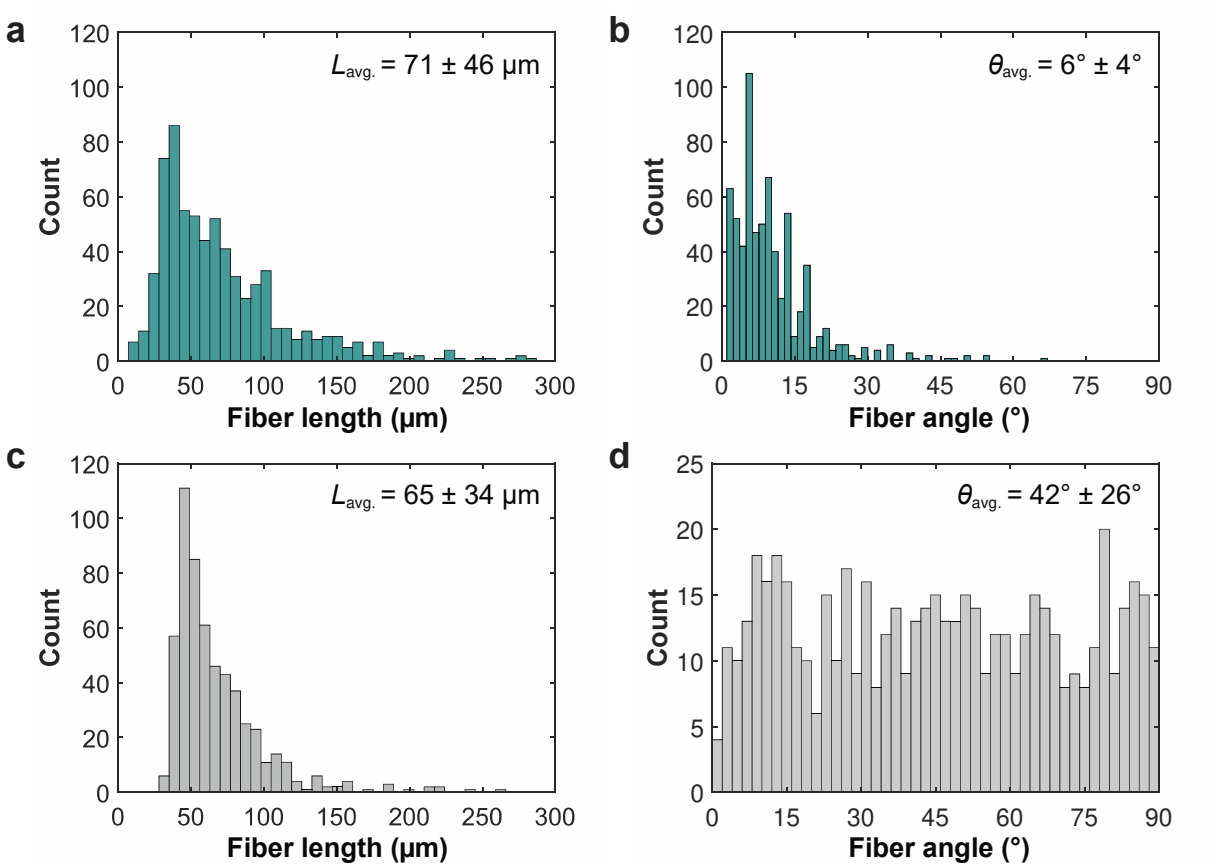

Figure B7. Histogram plots of fiber length and angle distribution in the printed (a, b) and molded (c, d) composite bar (15 vol% CF) bar specimens.

Table B2. Results of DSC measurements on printed and molded samples.

Sample	Degree of cure (%)	Glass transition temperature, T_g (°C)
Molded - 0 vol% CF	99.8	118.6
Printed - 0 vol% CF	98.1	114.1
Printed - 5 vol% CF	99.3	119.0
Printed - 10 vol% CF	99.6	122.6
Printed - 15 vol% CF	99.8	124.3

Matlab code used to generate x-y-z coordinates of the helix printed via FP

```
t = 0:pi/500:pi;
X(1,:) = sin(t).*cos(10*t);
X(2,:) = sin(t).*cos(12*t);
X(3,:) = sin(t).*cos(20*t);
```

G-codes used to print 3D structures

Table B3. G-code used to print helix.

line speed	2.59		
line start	147.02	168.00	83.97
line passing	147.17	167.96	83.97
line passing	147.29	167.86	83.97
line passing	147.38	167.72	83.96
line passing	147.42	167.54	83.96
line passing	147.40	167.34	83.95
line passing	147.31	167.13	83.94
line passing	147.15	166.94	83.93
line passing	146.93	166.78	83.92
line passing	146.65	166.67	83.91
line passing	146.32	166.64	83.89
line passing	145.97	166.68	83.88
line passing	145.62	166.81	83.86
line passing	145.28	167.04	83.84
line passing	144.98	167.35	83.82
line passing	144.75	167.75	83.80
line passing	144.60	168.22	83.77
line passing	144.55	168.73	83.75
line passing	144.61	169.28	83.72
line passing	144.80	169.82	83.70
line passing	145.11	170.33	83.67
line passing	145.54	170.79	83.64
line passing	146.09	171.17	83.60
line passing	146.72	171.43	83.57
line passing	147.43	171.56	83.53
line passing	148.17	171.55	83.50
line passing	148.93	171.37	83.46
line passing	149.65	171.03	83.42
line passing	150.31	170.53	83.38
line passing	150.88	169.88	83.34
line passing	151.32	169.11	83.29
line passing	151.59	168.24	83.25
line passing	151.69	167.30	83.20
line passing	151.59	166.33	83.15
line passing	151.29	165.38	83.10
line passing	150.78	164.48	83.05
line passing	150.09	163.69	83.00
line passing	149.23	163.03	82.95

line passing	148.23	162.55	82.89
line passing	147.13	162.28	82.83
line passing	145.96	162.23	82.78
line passing	144.79	162.42	82.72
line passing	143.65	162.86	82.66
line passing	142.60	163.53	82.59
line passing	141.68	164.42	82.53
line passing	140.95	165.49	82.47
line passing	140.44	166.72	82.40
line passing	140.19	168.05	82.33
line passing	140.20	169.43	82.26
line passing	140.50	170.80	82.19
line passing	141.08	172.11	82.12
line passing	141.92	173.30	82.05
line passing	143.01	174.32	81.98
line passing	144.29	175.11	81.90
line passing	145.74	175.63	81.82
line passing	147.29	175.86	81.75
line passing	148.87	175.77	81.67
line passing	150.43	175.35	81.59
line passing	151.90	174.63	81.50
line passing	153.21	173.61	81.42
line passing	154.31	172.32	81.34
line passing	155.14	170.83	81.25
line passing	155.66	169.17	81.16
line passing	155.84	167.42	81.08
line passing	155.66	165.64	80.99
line passing	155.13	163.92	80.90
line passing	154.25	162.31	80.81
line passing	153.05	160.89	80.71
line passing	151.57	159.73	80.62
line passing	149.88	158.88	80.52
line passing	148.02	158.37	80.43
line passing	146.07	158.25	80.33
line passing	144.12	158.52	80.23
line passing	142.24	159.18	80.13
line passing	140.51	160.22	80.03
line passing	139.01	161.59	79.93
line passing	137.80	163.26	79.83
line passing	136.94	165.15	79.72
line passing	136.46	167.20	79.62
line passing	136.41	169.32	79.51
line passing	136.78	171.43	79.40

line passing	137.58	173.44	79.30
line passing	138.77	175.27	79.19
line passing	140.32	176.85	79.08
line passing	142.17	178.09	78.96
line passing	144.24	178.94	78.85
line passing	146.47	179.37	78.74
line passing	148.75	179.35	78.62
line passing	151.00	178.86	78.51
line passing	153.13	177.93	78.39
line passing	155.05	176.58	78.28
line passing	156.67	174.87	78.16
line passing	157.92	172.85	78.04
line passing	158.75	170.60	77.92
line passing	159.13	168.21	77.80
line passing	159.01	165.79	77.68
line passing	158.41	163.41	77.55
line passing	157.35	161.19	77.43
line passing	155.85	159.21	77.31
line passing	153.97	157.56	77.18
line passing	151.79	156.31	77.05
line passing	149.38	155.51	76.93
line passing	146.85	155.21	76.80
line passing	144.30	155.42	76.67
line passing	141.82	156.13	76.54
line passing	139.52	157.34	76.41
line passing	137.50	158.98	76.28
line passing	135.84	161.01	76.15
line passing	134.60	163.34	76.02
line passing	133.86	165.89	75.89
line passing	133.63	168.54	75.75
line passing	133.94	171.21	75.62
line passing	134.78	173.76	75.48
line passing	136.12	176.12	75.35
line passing	137.90	178.16	75.21
line passing	140.07	179.82	75.08
line passing	142.54	181.02	74.94
line passing	145.21	181.70	74.80
line passing	147.97	181.84	74.66
line passing	150.72	181.43	74.52
line passing	153.33	180.47	74.38
line passing	155.72	179.01	74.24
line passing	157.77	177.09	74.10
line passing	159.41	174.79	73.96

line passing	160.56	172.21	73.82
line passing	161.17	169.43	73.68
line passing	161.22	166.59	73.53
line passing	160.70	163.78	73.39
line passing	159.62	161.12	73.25
line passing	158.04	158.72	73.10
line passing	156.00	156.68	72.96
line passing	153.59	155.08	72.81
line passing	150.90	154.00	72.67
line passing	148.04	153.46	72.52
line passing	145.13	153.51	72.38
line passing	142.28	154.14	72.23
line passing	139.60	155.33	72.09
line passing	137.21	157.03	71.94
line passing	135.21	159.17	71.79
line passing	133.66	161.68	71.64
line passing	132.65	164.45	71.50
line passing	132.20	167.37	71.35
line passing	132.35	170.33	71.20
line passing	133.08	173.20	71.05
line passing	134.38	175.87	70.90
line passing	136.18	178.23	70.75
line passing	138.42	180.19	70.60
line passing	141.01	181.67	70.46
line passing	143.84	182.60	70.31
line passing	146.80	182.95	70.16
line passing	149.78	182.70	70.01
line passing	152.65	181.87	69.86
line passing	155.29	180.48	69.71
line passing	157.61	178.58	69.56
line passing	159.51	176.27	69.41
line passing	160.90	173.62	69.26
line passing	161.75	170.75	69.11
line passing	162.00	167.76	68.96
line passing	161.65	164.79	68.81
line passing	160.72	161.94	68.66
line passing	159.24	159.34	68.51
line passing	157.27	157.08	68.36
line passing	154.89	155.27	68.21
line passing	152.20	153.96	68.06
line passing	149.31	153.22	67.91
line passing	146.33	153.06	67.76
line passing	143.37	153.51	67.61

line passing	140.57	154.53	67.46
line passing	138.04	156.09	67.31
line passing	135.86	158.12	67.16
line passing	134.14	160.54	67.01
line passing	132.93	163.25	66.87
line passing	132.29	166.14	66.72
line passing	132.23	169.10	66.57
line passing	132.77	172.00	66.42
line passing	133.87	174.74	66.27
line passing	135.50	177.20	66.13
line passing	137.57	179.28	65.98
line passing	140.01	180.90	65.83
line passing	142.72	182.00	65.68
line passing	145.59	182.53	65.54
line passing	148.51	182.49	65.39
line passing	151.34	181.87	65.25
line passing	153.99	180.69	65.10
line passing	156.35	179.02	64.96
line passing	158.32	176.92	64.81
line passing	159.83	174.47	64.67
line passing	160.82	171.78	64.53
line passing	161.25	168.96	64.38
line passing	161.11	166.12	64.24
line passing	160.41	163.37	64.10
line passing	159.18	160.82	63.96
line passing	157.47	158.58	63.82
line passing	155.36	156.73	63.67
line passing	152.93	155.34	63.53
line passing	150.28	154.47	63.40
line passing	147.53	154.14	63.26
line passing	144.77	154.37	63.12
line passing	142.13	155.14	62.98
line passing	139.70	156.41	62.84
line passing	137.59	158.14	62.71
line passing	135.87	160.24	62.57
line passing	134.61	162.63	62.43
line passing	133.86	165.21	62.30
line passing	133.63	167.88	62.17
line passing	133.94	170.53	62.03
line passing	134.77	173.04	61.90
line passing	136.07	175.33	61.77
line passing	137.80	177.31	61.64
line passing	139.87	178.89	61.51

line passing	142.21	180.01	61.38
line passing	144.70	180.65	61.25
line passing	147.26	180.78	61.12
line passing	149.78	180.40	60.99
line passing	152.15	179.52	60.87
line passing	154.29	178.20	60.74
line passing	156.11	176.50	60.61
line passing	157.55	174.47	60.49
line passing	158.54	172.22	60.37
line passing	159.06	169.83	60.24
line passing	159.10	167.40	60.12
line passing	158.65	165.03	60.00
line passing	157.75	162.81	59.88
line passing	156.43	160.84	59.76
line passing	154.76	159.18	59.65
line passing	152.80	157.89	59.53
line passing	150.65	157.03	59.41
line passing	148.39	156.62	59.30
line passing	146.11	156.67	59.18
line passing	143.90	157.17	59.07
line passing	141.85	158.09	58.96
line passing	140.05	159.38	58.85
line passing	138.56	161.00	58.74
line passing	137.42	162.87	58.63
line passing	136.70	164.90	58.52
line passing	136.39	167.02	58.41
line passing	136.51	169.14	58.31
line passing	137.05	171.17	58.20
line passing	137.97	173.03	58.10
line passing	139.23	174.65	57.99
line passing	140.78	175.97	57.89
line passing	142.53	176.95	57.79
line passing	144.43	177.55	57.69
line passing	146.39	177.76	57.59
line passing	148.32	177.57	57.50
line passing	150.16	177.01	57.40
line passing	151.83	176.10	57.31
line passing	153.26	174.90	57.21
line passing	154.41	173.45	57.12
line passing	155.24	171.81	57.03
line passing	155.71	170.07	56.94
line passing	155.83	168.30	56.85
line passing	155.60	166.56	56.76

line passing	155.02	164.92	56.68
line passing	154.15	163.46	56.59
line passing	153.01	162.21	56.51
line passing	151.67	161.24	56.42
line passing	150.19	160.56	56.34
line passing	148.62	160.20	56.26
line passing	147.03	160.16	56.18
line passing	145.50	160.43	56.10
line passing	144.08	161.00	56.03
line passing	142.82	161.83	55.95
line passing	141.77	162.88	55.88
line passing	140.97	164.09	55.81
line passing	140.43	165.41	55.74
line passing	140.18	166.79	55.67
line passing	140.21	168.17	55.60
line passing	140.51	169.48	55.53
line passing	141.06	170.69	55.46
line passing	141.82	171.74	55.40
line passing	142.76	172.59	55.34
line passing	143.82	173.23	55.27
line passing	144.97	173.62	55.21
line passing	146.15	173.78	55.15
line passing	147.31	173.69	55.10
line passing	148.40	173.39	55.04
line passing	149.38	172.87	54.99
line passing	150.21	172.19	54.93
line passing	150.88	171.38	54.88
line passing	151.35	170.47	54.83
line passing	151.62	169.51	54.78
line passing	151.69	168.55	54.73
line passing	151.56	167.62	54.69
line passing	151.26	166.76	54.64
line passing	150.80	166.01	54.60
line passing	150.21	165.38	54.55
line passing	149.54	164.91	54.51
line passing	148.81	164.59	54.47
line passing	148.05	164.44	54.44
line passing	147.31	164.45	54.40
line passing	146.62	164.60	54.37
line passing	145.99	164.88	54.33
line passing	145.47	165.27	54.30
line passing	145.05	165.74	54.27
line passing	144.76	166.27	54.24

line passing	144.59	166.81	54.21
line passing	144.55	167.35	54.19
line passing	144.61	167.86	54.16
line passing	144.78	168.32	54.14
line passing	145.03	168.70	54.12
line passing	145.33	169.00	54.10
line passing	145.68	169.21	54.08
line passing	146.03	169.33	54.06
line passing	146.38	169.36	54.04
line passing	146.69	169.31	54.03
line passing	146.96	169.20	54.02
line passing	147.18	169.03	54.01
line passing	147.33	168.84	54.00
line passing	147.41	168.63	53.99
line passing	147.42	168.43	53.98
line passing	147.37	168.25	53.98
line passing	147.28	168.12	53.97
line passing	147.15	168.03	53.97
line end	147.00	168.00	53.97

Table B4. G-code used to print lattice structure.

line speed	28			
call Subroutine	112.7	41.86667	106.988	13
call Subroutine	112.7	41.86667	106.316	13
call Subroutine	112.7	41.86667	105.644	13
call Subroutine	112.7	41.86667	104.972	13
call Subroutine	112.7	41.86667	104.3	13
call Subroutine	112.7	41.86667	103.628	13
call Subroutine	112.7	41.86667	102.956	13
call Subroutine	112.7	41.86667	102.284	13
call Subroutine	112.7	41.86667	101.612	13
call Subroutine	112.7	41.86667	100.94	13
end program				
line start	112.7	41.86667	106.988	
line passing	60.63333	41.86667	106.988	
line passing	60.63333	15.48667	106.988	
line passing	112.7	15.48667	106.988	
line passing	112.7	41.86667	106.988	
line passing	112.5	41.66667	106.988	
line passing	110.8333	38.78	106.988	
line passing	107.5	38.78	106.988	
line passing	105.8333	41.66667	106.988	
line passing	102.5	41.66667	106.988	
line passing	100.8333	38.78	106.988	
line passing	97.5	38.78	106.988	
line passing	95.83333	41.66667	106.988	
line passing	92.5	41.66667	106.988	
line passing	90.83333	38.78	106.988	
line passing	87.5	38.78	106.988	
line passing	85.83333	41.66667	106.988	
line passing	82.5	41.66667	106.988	
line passing	80.83333	38.78	106.988	
line passing	77.5	38.78	106.988	
line passing	75.83333	41.66667	106.988	
line passing	72.5	41.66667	106.988	
line passing	70.83333	38.78	106.988	
line passing	67.5	38.78	106.988	
line passing	65.83333	41.66667	106.988	
line passing	62.5	41.66667	106.988	
line passing	60.83333	38.78	106.988	

line passing	62.5	35.89333	106.988	
line passing	65.83333	35.89333	106.988	
line passing	67.5	38.78	106.988	
line passing	70.83333	38.78	106.988	
line passing	72.5	35.89333	106.988	
line passing	75.83333	35.89333	106.988	
line passing	77.5	38.78	106.988	
line passing	80.83333	38.78	106.988	
line passing	82.5	35.89333	106.988	
line passing	85.83333	35.89333	106.988	
line passing	87.5	38.78	106.988	
line passing	90.83333	38.78	106.988	
line passing	92.5	35.89333	106.988	
line passing	95.83333	35.89333	106.988	
line passing	97.5	38.78	106.988	
line passing	100.8333	38.78	106.988	
line passing	102.5	35.89333	106.988	
line passing	105.8333	35.89333	106.988	
line passing	107.5	38.78	106.988	
line passing	110.8333	38.78	106.988	
line passing	112.5	35.89333	106.988	
line passing	110.8333	33.00667	106.988	
line passing	107.5	33.00667	106.988	
line passing	105.8333	35.89333	106.988	
line passing	102.5	35.89333	106.988	
line passing	100.8333	33.00667	106.988	
line passing	97.5	33.00667	106.988	
line passing	95.83333	35.89333	106.988	
line passing	92.5	35.89333	106.988	
line passing	90.83333	33.00667	106.988	
line passing	87.5	33.00667	106.988	
line passing	85.83333	35.89333	106.988	
line passing	82.5	35.89333	106.988	
line passing	80.83333	33.00667	106.988	
line passing	77.5	33.00667	106.988	
line passing	75.83333	35.89333	106.988	
line passing	72.5	35.89333	106.988	
line passing	70.83333	33.00667	106.988	
line passing	67.5	33.00667	106.988	
line passing	65.83333	35.89333	106.988	
line passing	62.5	35.89333	106.988	
line passing	60.83333	33.00667	106.988	
line passing	62.5	30.12	106.988	

line passing	65.83333	30.12	106.988	
line passing	67.5	33.00667	106.988	
line passing	70.83333	33.00667	106.988	
line passing	72.5	30.12	106.988	
line passing	75.83333	30.12	106.988	
line passing	77.5	33.00667	106.988	
line passing	80.83333	33.00667	106.988	
line passing	82.5	30.12	106.988	
line passing	85.83333	30.12	106.988	
line passing	87.5	33.00667	106.988	
line passing	90.83333	33.00667	106.988	
line passing	92.5	30.12	106.988	
line passing	95.83333	30.12	106.988	
line passing	97.5	33.00667	106.988	
line passing	100.8333	33.00667	106.988	
line passing	102.5	30.12	106.988	
line passing	105.8333	30.12	106.988	
line passing	107.5	33.00667	106.988	
line passing	110.8333	33.00667	106.988	
line passing	112.5	30.12	106.988	
line passing	110.8333	27.23333	106.988	
line passing	107.5	27.23333	106.988	
line passing	105.8333	30.12	106.988	
line passing	102.5	30.12	106.988	
line passing	100.8333	27.23333	106.988	
line passing	97.5	27.23333	106.988	
line passing	95.83333	30.12	106.988	
line passing	92.5	30.12	106.988	
line passing	90.83333	27.23333	106.988	
line passing	87.5	27.23333	106.988	
line passing	85.83333	30.12	106.988	
line passing	82.5	30.12	106.988	
line passing	80.83333	27.23333	106.988	
line passing	77.5	27.23333	106.988	
line passing	75.83333	30.12	106.988	
line passing	72.5	30.12	106.988	
line passing	70.83333	27.23333	106.988	
line passing	67.5	27.23333	106.988	
line passing	65.83333	30.12	106.988	
line passing	62.5	30.12	106.988	
line passing	60.83333	27.23333	106.988	
line passing	62.5	24.34667	106.988	
line passing	65.83333	24.34667	106.988	

line passing	67.5	27.23333	106.988	
line passing	70.83333	27.23333	106.988	
line passing	72.5	24.34667	106.988	
line passing	75.83333	24.34667	106.988	
line passing	77.5	27.23333	106.988	
line passing	80.83333	27.23333	106.988	
line passing	82.5	24.34667	106.988	
line passing	85.83333	24.34667	106.988	
line passing	87.5	27.23333	106.988	
line passing	90.83333	27.23333	106.988	
line passing	92.5	24.34667	106.988	
line passing	95.83333	24.34667	106.988	
line passing	97.5	27.23333	106.988	
line passing	100.8333	27.23333	106.988	
line passing	102.5	24.34667	106.988	
line passing	105.8333	24.34667	106.988	
line passing	107.5	27.23333	106.988	
line passing	110.8333	27.23333	106.988	
line passing	112.5	24.34667	106.988	
line passing	110.8333	21.46	106.988	
line passing	107.5	21.46	106.988	
line passing	105.8333	24.34667	106.988	
line passing	102.5	24.34667	106.988	
line passing	100.8333	21.46	106.988	
line passing	97.5	21.46	106.988	
line passing	95.83333	24.34667	106.988	
line passing	92.5	24.34667	106.988	
line passing	90.83333	21.46	106.988	
line passing	87.5	21.46	106.988	
line passing	85.83333	24.34667	106.988	
line passing	82.5	24.34667	106.988	
line passing	80.83333	21.46	106.988	
line passing	77.5	21.46	106.988	
line passing	75.83333	24.34667	106.988	
line passing	72.5	24.34667	106.988	
line passing	70.83333	21.46	106.988	
line passing	67.5	21.46	106.988	
line passing	65.83333	24.34667	106.988	
line passing	62.5	24.34667	106.988	
line passing	60.83333	21.46	106.988	
line passing	62.5	18.57333	106.988	
line passing	65.83333	18.57333	106.988	
line passing	67.5	21.46	106.988	

line passing	70.83333	21.46	106.988	
line passing	72.5	18.57333	106.988	
line passing	75.83333	18.57333	106.988	
line passing	77.5	21.46	106.988	
line passing	80.83333	21.46	106.988	
line passing	82.5	18.57333	106.988	
line passing	85.83333	18.57333	106.988	
line passing	87.5	21.46	106.988	
line passing	90.83333	21.46	106.988	
line passing	92.5	18.57333	106.988	
line passing	95.83333	18.57333	106.988	
line passing	97.5	21.46	106.988	
line passing	100.8333	21.46	106.988	
line passing	102.5	18.57333	106.988	
line passing	105.8333	18.57333	106.988	
line passing	107.5	21.46	106.988	
line passing	110.8333	21.46	106.988	
line passing	112.5	18.57333	106.988	
line passing	110.8333	15.68667	106.988	
line passing	107.5	15.68667	106.988	
line passing	105.8333	18.57333	106.988	
line passing	102.5	18.57333	106.988	
line passing	100.8333	15.68667	106.988	
line passing	97.5	15.68667	106.988	
line passing	95.83333	18.57333	106.988	
line passing	92.5	18.57333	106.988	
line passing	90.83333	15.68667	106.988	
line passing	87.5	15.68667	106.988	
line passing	85.83333	18.57333	106.988	
line passing	82.5	18.57333	106.988	
line passing	80.83333	15.68667	106.988	
line passing	77.5	15.68667	106.988	
line passing	75.83333	18.57333	106.988	
line passing	72.5	18.57333	106.988	
line passing	70.83333	15.68667	106.988	
line passing	67.5	15.68667	106.988	
line passing	65.83333	18.57333	106.988	
line passing	62.5	18.57333	106.988	
line end	60.83333	15.68667	106.988	
end program				

Table B5. G-code used to print hexagon structure.

line speed	3		
line start	49	126	119.79
line passing	44	126	119.79
line passing	39	134.6603	119.79
line passing	29	134.6603	119.79
line passing	24	126	119.79
line passing	29	117.3397	119.79
line passing	39	117.3397	119.79
line passing	44	126	119.79
line passing	39	134.6603	118.5156
line passing	29	134.6603	118.5156
line passing	24	126	118.5156
line passing	29	117.3397	118.5156
line passing	39	117.3397	118.5156
line passing	44	126	118.5156
line passing	39	134.6603	117.2468
line passing	29	134.6603	117.2468
line passing	24	126	117.2468
line passing	29	117.3397	117.2468
line passing	39	117.3397	117.2468
line passing	44	126	117.2468
line passing	39	134.6603	115.9836
line passing	29	134.6603	115.9836
line passing	24	126	115.9836
line passing	29	117.3397	115.9836
line passing	39	117.3397	115.9836
line passing	44	126	115.9836
line passing	39	134.6603	114.726
line passing	29	134.6603	114.726
line passing	24	126	114.726
line passing	29	117.3397	114.726
line passing	39	117.3397	114.726
line passing	44	126	114.726
line passing	39	134.6603	113.474
line passing	29	134.6603	113.474
line passing	24	126	113.474
line passing	29	117.3397	113.474
line passing	39	117.3397	113.474
line passing	44	126	113.474

line passing	39	134.6603	112.2276
line passing	29	134.6603	112.2276
line passing	24	126	112.2276
line passing	29	117.3397	112.2276
line passing	39	117.3397	112.2276
line passing	44	126	112.2276
line passing	39	134.6603	110.9868
line passing	29	134.6603	110.9868
line passing	24	126	110.9868
line passing	29	117.3397	110.9868
line passing	39	117.3397	110.9868
line passing	44	126	110.9868
line passing	39	134.6603	109.7516
line passing	29	134.6603	109.7516
line passing	24	126	109.7516
line passing	29	117.3397	109.7516
line passing	39	117.3397	109.7516
line passing	44	126	109.7516
line passing	39	134.6603	108.522
line passing	29	134.6603	108.522
line passing	24	126	108.522
line passing	29	117.3397	108.522
line passing	39	117.3397	108.522
line passing	44	126	108.522
line passing	39	134.6603	107.298
line passing	29	134.6603	107.298
line passing	24	126	107.298
line passing	29	117.3397	107.298
line passing	39	117.3397	107.298
line passing	44	126	107.298
line passing	39	134.6603	106.0796
line passing	29	134.6603	106.0796
line passing	24	126	106.0796
line passing	29	117.3397	106.0796
line passing	39	117.3397	106.0796
line passing	44	126	106.0796
line passing	39	134.6603	104.8668
line passing	29	134.6603	104.8668
line passing	24	126	104.8668
line passing	29	117.3397	104.8668
line passing	39	117.3397	104.8668
line passing	44	126	104.8668
line passing	39	134.6603	103.6596

line passing	29	134.6603	103.6596
line passing	24	126	103.6596
line passing	29	117.3397	103.6596
line passing	39	117.3397	103.6596
line passing	44	126	103.6596
line passing	39	134.6603	102.458
line passing	29	134.6603	102.458
line passing	24	126	102.458
line passing	29	117.3397	102.458
line passing	39	117.3397	102.458
line passing	44	126	102.458
line passing	39	134.6603	101.262
line passing	29	134.6603	101.262
line passing	24	126	101.262
line passing	29	117.3397	101.262
line passing	39	117.3397	101.262
line passing	44	126	101.262
line passing	39	134.6603	100.0716
line passing	29	134.6603	100.0716
line passing	24	126	100.0716
line passing	29	117.3397	100.0716
line passing	39	117.3397	100.0716
line passing	44	126	100.0716
line passing	39	134.6603	98.8868
line passing	29	134.6603	98.8868
line passing	24	126	98.8868
line passing	29	117.3397	98.8868
line passing	39	117.3397	98.8868
line passing	44	126	98.8868
line passing	39	134.6603	97.7076
line passing	29	134.6603	97.7076
line passing	24	126	97.7076
line passing	29	117.3397	97.7076
line passing	39	117.3397	97.7076
line passing	44	126	97.7076
line passing	39	134.6603	96.534
line passing	29	134.6603	96.534
line passing	24	126	96.534
line passing	29	117.3397	96.534
line passing	39	117.3397	96.534
line passing	44	126	96.534
line passing	39	134.6603	95.366
line passing	29	134.6603	95.366

line passing	24	126	95.366
line passing	29	117.3397	95.366
line passing	39	117.3397	95.366
line passing	44	126	95.366
line passing	39	134.6603	94.2036
line passing	29	134.6603	94.2036
line passing	24	126	94.2036
line passing	29	117.3397	94.2036
line passing	39	117.3397	94.2036
line passing	44	126	94.2036
line passing	39	134.6603	93.0468
line passing	29	134.6603	93.0468
line passing	24	126	93.0468
line passing	29	117.3397	93.0468
line passing	39	117.3397	93.0468
line passing	44	126	93.0468
line passing	39	134.6603	91.8956
line passing	29	134.6603	91.8956
line passing	24	126	91.8956
line passing	29	117.3397	91.8956
line passing	39	117.3397	91.8956
line passing	44	126	91.8956
line passing	39	134.6603	90.75
line passing	29	134.6603	90.75
line passing	24	126	90.75
line passing	29	117.3397	90.75
line passing	39	117.3397	90.75
line passing	44	126	90.75
line passing	39	134.6603	89.61
line passing	29	134.6603	89.61
line passing	24	126	89.61
line passing	29	117.3397	89.61
line passing	39	117.3397	89.61
line passing	44	126	89.61
line passing	39	134.6603	88.4756
line passing	29	134.6603	88.4756
line passing	24	126	88.4756
line passing	29	117.3397	88.4756
line passing	39	117.3397	88.4756
line passing	44	126	88.4756
line passing	39	134.6603	87.3468
line passing	29	134.6603	87.3468
line passing	24	126	87.3468

line passing	29	117.3397	87.3468
line passing	39	117.3397	87.3468
line passing	44	126	87.3468
line passing	39	134.6603	86.2236
line passing	29	134.6603	86.2236
line passing	24	126	86.2236
line passing	29	117.3397	86.2236
line passing	39	117.3397	86.2236
line passing	44	126	86.2236
line passing	39	134.6603	85.106
line passing	29	134.6603	85.106
line passing	24	126	85.106
line passing	29	117.3397	85.106
line passing	39	117.3397	85.106
line passing	44	126	85.106
line passing	39	134.6603	83.994
line passing	29	134.6603	83.994
line passing	24	126	83.994
line passing	29	117.3397	83.994
line passing	39	117.3397	83.994
line passing	44	126	83.994
line passing	39	134.6603	82.8876
line passing	29	134.6603	82.8876
line passing	24	126	82.8876
line passing	29	117.3397	82.8876
line passing	39	117.3397	82.8876
line passing	44	126	82.8876
line passing	39	134.6603	81.7868
line passing	29	134.6603	81.7868
line passing	24	126	81.7868
line passing	29	117.3397	81.7868
line passing	39	117.3397	81.7868
line passing	44	126	81.7868
line passing	39	134.6603	80.6916
line passing	29	134.6603	80.6916
line passing	24	126	80.6916
line passing	29	117.3397	80.6916
line passing	39	117.3397	80.6916
line passing	44	126	80.6916
line passing	39	134.6603	79.602
line passing	29	134.6603	79.602
line passing	24	126	79.602
line passing	29	117.3397	79.602

line passing	39	117.3397	79.602
line passing	44	126	79.602
line passing	39	134.6603	78.518
line passing	29	134.6603	78.518
line passing	24	126	78.518
line passing	29	117.3397	78.518
line passing	39	117.3397	78.518
line passing	44	126	78.518
line passing	39	134.6603	77.4396
line passing	29	134.6603	77.4396
line passing	24	126	77.4396
line passing	29	117.3397	77.4396
line passing	39	117.3397	77.4396
line passing	44	126	77.4396
line passing	39	134.6603	76.3668
line passing	29	134.6603	76.3668
line passing	24	126	76.3668
line passing	29	117.3397	76.3668
line passing	39	117.3397	76.3668
line passing	44	126	76.3668
dispense ON/OFF	0		
wait point	15		
line end	44	126	30

Table B6. G-code used to print flexural samples in parallel to specimens' length.

line speed	2.6			
call subroutine	40	50	92.16	7
call subroutine	40	50	91.404	7
call subroutine	40	50	90.648	7
call subroutine	40	50	89.892	7
end program				
line start	40	50	92.16	
line passing	105	50	92.16	
line passing	105	50.756	92.16	
line passing	40	50.756	92.16	
line passing	40	51.512	92.16	
line passing	105	51.512	92.16	
line passing	105	52.268	92.16	
line passing	40	52.268	92.16	
line passing	40	53.024	92.16	
line passing	105	53.024	92.16	
line passing	105	53.78	92.16	
line passing	40	53.78	92.16	
line passing	40	54.536	92.16	
line passing	105	54.536	92.16	
line passing	105	55.292	92.16	
line passing	40	55.292	92.16	
line passing	40	56.048	92.16	
line passing	105	56.048	92.16	
line passing	105	56.804	92.16	
line passing	40	56.804	92.16	
line passing	40	57.56	92.16	
line passing	105	57.56	92.16	
line passing	105	58.316	92.16	
line passing	40	58.316	92.16	
line passing	40	59.072	92.16	
line passing	105	59.072	92.16	
line passing	105	59.828	92.16	
line passing	40	59.828	92.16	
line passing	40	60.584	92.16	
line passing	105	60.584	92.16	
line passing	105	61.34	92.16	
line end	40	61.34	92.16	
end program				

Table B7. G-code used to print flexural samples in transverse to specimens' length.

line speed	2.6			
call subroutine	96.976	62	92.16	7
call subroutine	96.976	62	91.404	7
call subroutine	96.976	62	90.648	7
call subroutine	96.976	62	89.892	7
end program				
line start	96.976	62	92.16	
line passing	96.22	62	92.16	
line passing	96.22	50	92.16	
line passing	95.464	50	92.16	
line passing	95.464	62	92.16	
line passing	94.708	62	92.16	
line passing	94.708	50	92.16	
line passing	93.952	50	92.16	
line passing	93.952	62	92.16	
line passing	93.196	62	92.16	
line passing	93.196	50	92.16	
line passing	92.44	50	92.16	
line passing	92.44	62	92.16	
line passing	91.684	62	92.16	
line passing	91.684	50	92.16	
line passing	90.928	50	92.16	
line passing	90.928	62	92.16	
line passing	90.172	62	92.16	
line passing	90.172	50	92.16	
line passing	89.416	50	92.16	
line passing	89.416	62	92.16	
line passing	88.66	62	92.16	
line passing	88.66	50	92.16	
line passing	87.904	50	92.16	
line passing	87.904	62	92.16	
line passing	87.148	62	92.16	
line passing	87.148	50	92.16	
line passing	86.392	50	92.16	
line passing	86.392	62	92.16	
line passing	85.636	62	92.16	
line passing	85.636	50	92.16	
line passing	84.88	50	92.16	
line passing	84.88	62	92.16	

line passing	84.124	62	92.16	
line passing	84.124	50	92.16	
line passing	83.368	50	92.16	
line passing	83.368	62	92.16	
line passing	82.612	62	92.16	
line passing	82.612	50	92.16	
line passing	81.856	50	92.16	
line passing	81.856	62	92.16	
line passing	81.1	62	92.16	
line passing	81.1	50	92.16	
line passing	80.344	50	92.16	
line passing	80.344	62	92.16	
line passing	79.588	62	92.16	
line passing	79.588	50	92.16	
line passing	78.832	50	92.16	
line passing	78.832	62	92.16	
line passing	78.076	62	92.16	
line passing	78.076	50	92.16	
line passing	77.32	50	92.16	
line passing	77.32	62	92.16	
line passing	76.564	62	92.16	
line passing	76.564	50	92.16	
line passing	75.808	50	92.16	
line passing	75.808	62	92.16	
line passing	75.052	62	92.16	
line passing	75.052	50	92.16	
line passing	74.296	50	92.16	
line passing	74.296	62	92.16	
line passing	73.54	62	92.16	
line passing	73.54	50	92.16	
line passing	72.784	50	92.16	
line passing	72.784	62	92.16	
line passing	72.028	62	92.16	
line passing	72.028	50	92.16	
line passing	71.272	50	92.16	
line passing	71.272	62	92.16	
line passing	70.516	62	92.16	
line passing	70.516	50	92.16	
line passing	69.76	50	92.16	
line passing	69.76	62	92.16	
line passing	69.004	62	92.16	
line passing	69.004	50	92.16	
line passing	68.248	50	92.16	

line passing	68.248	62	92.16	
line passing	67.492	62	92.16	
line passing	67.492	50	92.16	
line passing	66.736	50	92.16	
line passing	66.736	62	92.16	
line passing	65.98	62	92.16	
line passing	65.98	50	92.16	
line passing	65.224	50	92.16	
line passing	65.224	62	92.16	
line passing	64.468	62	92.16	
line passing	64.468	50	92.16	
line passing	63.712	50	92.16	
line passing	63.712	62	92.16	
line passing	62.956	62	92.16	
line passing	62.956	50	92.16	
line passing	62.2	50	92.16	
line passing	62.2	62	92.16	
line passing	61.444	62	92.16	
line passing	61.444	50	92.16	
line passing	60.688	50	92.16	
line passing	60.688	62	92.16	
line passing	59.932	62	92.16	
line passing	59.932	50	92.16	
line passing	59.176	50	92.16	
line passing	59.176	62	92.16	
line passing	58.42	62	92.16	
line passing	58.42	50	92.16	
line passing	57.664	50	92.16	
line passing	57.664	62	92.16	
line passing	56.908	62	92.16	
line passing	56.908	50	92.16	
line passing	56.152	50	92.16	
line passing	56.152	62	92.16	
line passing	55.396	62	92.16	
line passing	55.396	50	92.16	
line passing	54.64	50	92.16	
line passing	54.64	62	92.16	
line passing	53.884	62	92.16	
line passing	53.884	50	92.16	
line passing	53.128	50	92.16	
line passing	53.128	62	92.16	
line passing	52.372	62	92.16	
line passing	52.372	50	92.16	

line passing	51.616	50	92.16	
line passing	51.616	62	92.16	
line passing	50.86	62	92.16	
line passing	50.86	50	92.16	
line passing	50.104	50	92.16	
line passing	50.104	62	92.16	
line passing	49.348	62	92.16	
line passing	49.348	50	92.16	
line passing	48.592	50	92.16	
line passing	48.592	62	92.16	
line passing	47.836	62	92.16	
line passing	47.836	50	92.16	
line passing	47.08	50	92.16	
line passing	47.08	62	92.16	
line passing	46.324	62	92.16	
line passing	46.324	50	92.16	
line passing	45.568	50	92.16	
line passing	45.568	62	92.16	
line passing	44.812	62	92.16	
line passing	44.812	50	92.16	
line passing	44.056	50	92.16	
line passing	44.056	62	92.16	
line passing	43.3	62	92.16	
line passing	43.3	50	92.16	
line passing	42.544	50	92.16	
line passing	42.544	62	92.16	
line passing	41.788	62	92.16	
line passing	41.788	50	92.16	
line passing	41.032	50	92.16	
line passing	41.032	62	92.16	
line passing	40.276	62	92.16	
line passing	40.276	50	92.16	
line passing	39.52	50	92.16	
line passing	39.52	62	92.16	
line passing	38.764	62	92.16	
line passing	38.764	50	92.16	
line end	38.008	50	92.16	
end program				

Appendix C

Preparation of DML/DCPD resin

An appropriate amount of DML comonomer with various concentrations ranging from 0 to 50 wt% is measured on the Sartorius Quintix balance and mixed with DCPD/ENB solution for 1 min using the planetary centrifugal mixer (AR-100, Thinky USA). For all experiments, 3.21 mg GC2 (100 ppm) is weighed on the Mettler-Toledo microbalance and transferred to a 1.5 mL Eppendorf tube using a disposable Polypropylene spatula. The tube is then filled with 500 μL of PCH using the Ergonomic High-Performance micropipette to dissolve GC2. After adding PCH solvent, 1 μL TBP is measured by the volumetric syringe (Hamilton, precision 0.01 ml) and injected into the catalyst solution. The catalyst/inhibitor solution is sonicated (Barsonic cleaner) for 10 min and thoroughly mixed with the DML/DCPD using the planetary centrifugal mixer for 1 min.

Preparation of DMA samples

DML/DCPD resin solutions prepared with various DML concentrations are cast on a glass substrate sprayed with a polytetrafluoroethylene (PTFE) release agent and spread using a doctor blade to achieve films with a desired thickness. The glass substrate with the wet cast film is then placed on a hot plate with an average temperature of 100 °C for 2 min to frontally cure the resin through thickness. After curing, the glass substrate is removed and allowed to cool down to ambient temperature. Using this procedure, films with an average thickness of 0.6 mm to 0.7 mm are obtained. The thickness of films is evaluated from three measurements using a Mitutoyo digital caliper. Upon removal of cured films from the substrate, DMA specimens are cut into rectangular bars with 15 mm × 5.4 mm dimensions using a razor blade.

3D printing of CNT-filled inks

Prepared ink with proper rheological profile is transferred to a 10 mL-syringe barrel mounted on a three-axis gantry robot (F5200N, Fisnar). A custom cooling system is used to chill the ink at -5 °C using a pair of thermoelectric Peltier coolers embedded within the printhead to prevent background polymerization of 3D printing ink. The printer is equipped with a high-precision dispenser (DC100, Fisnar) to deposit the ink on a glass substrate. The glass substrate is heated to 80 °C using a 300 mm × 300 mm aluminum heater (CR-10S mk2a, Shenzhen Huachuang 3D Technology) attached on the underside of the glass substrate by applying a constant current of 8.2 A to enable *in-situ* curing of the ink during the printing process. The ink is extruded from a stainless-steel nozzle with an inner diameter of 0.8 mm and an air pressure of 70 kPa. The lattice and tall layered structures are printed using printing speed of 10 mm/s and the following G-codes.

G-codes used for 3D printing via FP

Table C1. G-code used to print lattice structures.

line speed	10		
line start	162	162	92.55
line passing	192	162	92.55
line passing	192	160	92.55
line passing	162	160	92.55
line passing	162	158	92.55
line passing	192	158	92.55
line passing	192	156	92.55
line passing	162	156	92.55
line passing	162	154	92.55
line passing	192	154	92.55
line passing	192	152	92.55
line passing	162	152	92.55
line passing	162	150	92.55
line passing	192	150	92.55
line passing	192	148	92.55
line passing	162	148	92.55
line passing	162	146	92.55
line passing	192	146	92.55
line passing	192	144	92.55
line passing	162	144	92.55
line passing	162	142	92.55
line passing	192	142	92.55
line passing	192	140	92.55
line passing	162	140	92.55
line passing	162	138	92.55
line passing	192	138	92.55
line passing	192	136	92.55
line passing	162	136	92.55
line passing	162	134	92.55
line passing	192	134	92.55
line passing	192	132	92.55
line end	162	132	92.55
line start	192	162	91.878
line passing	190	162	91.878
line passing	190	132	91.878
line passing	188	132	91.878
line passing	188	162	91.878
line passing	186	162	91.878

line passing	186	132	91.878
line passing	184	132	91.878
line passing	184	162	91.878
line passing	182	162	91.878
line passing	182	132	91.878
line passing	180	132	91.878
line passing	180	162	91.878
line passing	178	162	91.878
line passing	178	132	91.878
line passing	176	132	91.878
line passing	176	162	91.878
line passing	174	162	91.878
line passing	174	132	91.878
line passing	172	132	91.878
line passing	172	162	91.878
line passing	170	162	91.878
line passing	170	132	91.878
line passing	168	132	91.878
line passing	168	162	91.878
line passing	166	162	91.878
line passing	166	132	91.878
line passing	164	132	91.878
line end	164	162	91.878
line start	162	162	91.206
line passing	192	162	91.206
line passing	192	160	91.206
line passing	162	160	91.206
line passing	162	158	91.206
line passing	192	158	91.206
line passing	192	156	91.206
line passing	162	156	91.206
line passing	162	154	91.206
line passing	192	154	91.206
line passing	192	152	91.206
line passing	162	152	91.206
line passing	162	150	91.206
line passing	192	150	91.206
line passing	192	148	91.206
line passing	162	148	91.206
line passing	162	146	91.206
line passing	192	146	91.206
line passing	192	144	91.206
line passing	162	144	91.206

line passing	162	142	91.206
line passing	192	142	91.206
line passing	192	140	91.206
line passing	162	140	91.206
line passing	162	138	91.206
line passing	192	138	91.206
line passing	192	136	91.206
line passing	162	136	91.206
line passing	162	134	91.206
line passing	192	134	91.206
line passing	192	132	91.206
line end	162	132	91.206
line start	192	162	90.534
line passing	190	162	90.534
line passing	190	132	90.534
line passing	188	132	90.534
line passing	188	162	90.534
line passing	186	162	90.534
line passing	186	132	90.534
line passing	184	132	90.534
line passing	184	162	90.534
line passing	182	162	90.534
line passing	182	132	90.534
line passing	180	132	90.534
line passing	180	162	90.534
line passing	178	162	90.534
line passing	178	132	90.534
line passing	176	132	90.534
line passing	176	162	90.534
line passing	174	162	90.534
line passing	174	132	90.534
line passing	172	132	90.534
line passing	172	162	90.534
line passing	170	162	90.534
line passing	170	132	90.534
line passing	168	132	90.534
line passing	168	162	90.534
line passing	166	162	90.534
line passing	166	132	90.534
line passing	164	132	90.534
line end	164	162	90.534
line start	162	162	89.862
line passing	192	162	89.862

line passing	192	160	89.862
line passing	162	160	89.862
line passing	162	158	89.862
line passing	192	158	89.862
line passing	192	156	89.862
line passing	162	156	89.862
line passing	162	154	89.862
line passing	192	154	89.862
line passing	192	152	89.862
line passing	162	152	89.862
line passing	162	150	89.862
line passing	192	150	89.862
line passing	192	148	89.862
line passing	162	148	89.862
line passing	162	146	89.862
line passing	192	146	89.862
line passing	192	144	89.862
line passing	162	144	89.862
line passing	162	142	89.862
line passing	192	142	89.862
line passing	192	140	89.862
line passing	162	140	89.862
line passing	162	138	89.862
line passing	192	138	89.862
line passing	192	136	89.862
line passing	162	136	89.862
line passing	162	134	89.862
line passing	192	134	89.862
line passing	192	132	89.862
line end	162	132	89.862
line start	192	162	89.19
line passing	190	162	89.19
line passing	190	132	89.19
line passing	188	132	89.19
line passing	188	162	89.19
line passing	186	162	89.19
line passing	186	132	89.19
line passing	184	132	89.19
line passing	184	162	89.19
line passing	182	162	89.19
line passing	182	132	89.19
line passing	180	132	89.19
line passing	180	162	89.19

line passing	178	162	89.19
line passing	178	132	89.19
line passing	176	132	89.19
line passing	176	162	89.19
line passing	174	162	89.19
line passing	174	132	89.19
line passing	172	132	89.19
line passing	172	162	89.19
line passing	170	162	89.19
line passing	170	132	89.19
line passing	168	132	89.19
line passing	168	162	89.19
line passing	166	162	89.19
line passing	166	132	89.19
line passing	164	132	89.19
line end	164	162	89.19
line start	162	162	88.518
line passing	192	162	88.518
line passing	192	160	88.518
line passing	162	160	88.518
line passing	162	158	88.518
line passing	192	158	88.518
line passing	192	156	88.518
line passing	162	156	88.518
line passing	162	154	88.518
line passing	192	154	88.518
line passing	192	152	88.518
line passing	162	152	88.518
line passing	162	150	88.518
line passing	192	150	88.518
line passing	192	148	88.518
line passing	162	148	88.518
line passing	162	146	88.518
line passing	192	146	88.518
line passing	192	144	88.518
line passing	162	144	88.518
line passing	162	142	88.518
line passing	192	142	88.518
line passing	192	140	88.518
line passing	162	140	88.518
line passing	162	138	88.518
line passing	192	138	88.518
line passing	192	136	88.518

line passing	162	136	88.518
line passing	162	134	88.518
line passing	192	134	88.518
line passing	192	132	88.518
line end	162	132	88.518
line start	192	162	87.846
line passing	190	162	87.846
line passing	190	132	87.846
line passing	188	132	87.846
line passing	188	162	87.846
line passing	186	162	87.846
line passing	186	132	87.846
line passing	184	132	87.846
line passing	184	162	87.846
line passing	182	162	87.846
line passing	182	132	87.846
line passing	180	132	87.846
line passing	180	162	87.846
line passing	178	162	87.846
line passing	178	132	87.846
line passing	176	132	87.846
line passing	176	162	87.846
line passing	174	162	87.846
line passing	174	132	87.846
line passing	172	132	87.846
line passing	172	162	87.846
line passing	170	162	87.846
line passing	170	132	87.846
line passing	168	132	87.846
line passing	168	162	87.846
line passing	166	162	87.846
line passing	166	132	87.846
line passing	164	132	87.846
line end	164	162	87.846
line start	162	162	87.174
line passing	192	162	87.174
line passing	192	160	87.174
line passing	162	160	87.174
line passing	162	158	87.174
line passing	192	158	87.174
line passing	192	156	87.174
line passing	162	156	87.174
line passing	162	154	87.174

line passing	192	154	87.174
line passing	192	152	87.174
line passing	162	152	87.174
line passing	162	150	87.174
line passing	192	150	87.174
line passing	192	148	87.174
line passing	162	148	87.174
line passing	162	146	87.174
line passing	192	146	87.174
line passing	192	144	87.174
line passing	162	144	87.174
line passing	162	142	87.174
line passing	192	142	87.174
line passing	192	140	87.174
line passing	162	140	87.174
line passing	162	138	87.174
line passing	192	138	87.174
line passing	192	136	87.174
line passing	162	136	87.174
line passing	162	134	87.174
line passing	192	134	87.174
line passing	192	132	87.174
line end	162	132	87.174
line start	192	162	86.502
line passing	190	162	86.502
line passing	190	132	86.502
line passing	188	132	86.502
line passing	188	162	86.502
line passing	186	162	86.502
line passing	186	132	86.502
line passing	184	132	86.502
line passing	184	162	86.502
line passing	182	162	86.502
line passing	182	132	86.502
line passing	180	132	86.502
line passing	180	162	86.502
line passing	178	162	86.502
line passing	178	132	86.502
line passing	176	132	86.502
line passing	176	162	86.502
line passing	174	162	86.502
line passing	174	132	86.502
line passing	172	132	86.502

line passing	172	162	86.502
line passing	170	162	86.502
line passing	170	132	86.502
line passing	168	132	86.502
line passing	168	162	86.502
line passing	166	162	86.502
line passing	166	132	86.502
line passing	164	132	86.502
line end	164	162	86.502

Table C2. G-code used to print tall layered structure.

line speed	10			
line dispense setup	0.4	0.4	0	0
line start	65.49	126.9	116.14	
line passing	86.49	126.9	116.14	
line passing	86.49	128.4	116.14	
line passing	65.49	128.4	116.14	
line passing	65.49	129.9	116.14	
line passing	86.49	129.9	116.14	
line passing	86.49	131.4	116.14	
line passing	65.49	131.4	116.14	
line passing	65.49	132.9	116.14	
line passing	86.49	132.9	116.14	
line passing	86.49	134.4	116.14	
line passing	65.49	134.4	116.14	
line passing	65.49	135.9	116.14	
line passing	86.49	135.9	116.14	
line passing	86.49	137.4	116.14	
line passing	65.49	137.4	116.14	
line passing	65.49	138.9	116.14	
line passing	86.49	138.9	116.14	
line passing	86.49	140.4	116.14	
line passing	65.49	140.4	116.14	
line passing	65.49	141.9	116.14	
line passing	86.49	141.9	116.14	
line passing	86.49	143.4	116.14	
line passing	65.49	143.4	116.14	
line passing	65.49	144.9	116.14	
line passing	86.49	144.9	116.14	
line passing	86.49	146.4	116.14	
line passing	65.49	146.4	116.14	
line passing	65.49	147.9	116.14	
line end	86.49	147.9	116.14	
line dispense setup	0.4	0.4	0	0
line start	66.99	128.4	115.39	
line passing	66.99	146.4	115.39	
line passing	68.49	146.4	115.39	
line passing	68.49	128.4	115.39	
line passing	69.99	128.4	115.39	
line passing	69.99	146.4	115.39	

line passing	71.49	146.4	115.39	
line passing	71.49	128.4	115.39	
line passing	72.99	128.4	115.39	
line passing	72.99	146.4	115.39	
line passing	74.49	146.4	115.39	
line passing	74.49	128.4	115.39	
line passing	75.99	128.4	115.39	
line passing	75.99	146.4	115.39	
line passing	77.49	146.4	115.39	
line passing	77.49	128.4	115.39	
line passing	78.99	128.4	115.39	
line passing	78.99	146.4	115.39	
line passing	80.49	146.4	115.39	
line passing	80.49	128.4	115.39	
line passing	81.99	128.4	115.39	
line passing	81.99	146.4	115.39	
line passing	83.49	146.4	115.39	
line passing	83.49	128.4	115.39	
line passing	84.99	128.4	115.39	
line end	84.99	146.4	115.39	
line dispense setup	0.4	0.4	0	0
line start	68.49	129.9	114.64	
line passing	83.49	129.9	114.64	
line passing	83.49	131.4	114.64	
line passing	68.49	131.4	114.64	
line passing	68.49	132.9	114.64	
line passing	83.49	132.9	114.64	
line passing	83.49	134.4	114.64	
line passing	68.49	134.4	114.64	
line passing	68.49	135.9	114.64	
line passing	83.49	135.9	114.64	
line passing	83.49	137.4	114.64	
line passing	68.49	137.4	114.64	
line passing	68.49	138.9	114.64	
line passing	83.49	138.9	114.64	
line passing	83.49	140.4	114.64	
line passing	68.49	140.4	114.64	
line passing	68.49	141.9	114.64	
line passing	83.49	141.9	114.64	
line passing	83.49	143.4	114.64	
line passing	68.49	143.4	114.64	
line passing	68.49	144.9	114.64	
line end	83.49	144.9	114.64	

line dispense setup	0.4	0.4	0	0
line start	69.99	131.4	113.89	
line passing	69.99	143.4	113.89	
line passing	71.49	143.4	113.89	
line passing	71.49	131.4	113.89	
line passing	72.99	131.4	113.89	
line passing	72.99	143.4	113.89	
line passing	74.49	143.4	113.89	
line passing	74.49	131.4	113.89	
line passing	75.99	131.4	113.89	
line passing	75.99	143.4	113.89	
line passing	77.49	143.4	113.89	
line passing	77.49	131.4	113.89	
line passing	78.99	131.4	113.89	
line passing	78.99	143.4	113.89	
line passing	80.49	143.4	113.89	
line passing	80.49	131.4	113.89	
line passing	81.99	131.4	113.89	
line end	81.99	143.4	113.89	
line dispense setup	0.4	0.4	0	0
line start	71.49	132.9	113.14	
line passing	80.49	132.9	113.14	
line passing	80.49	134.4	113.14	
line passing	71.49	134.4	113.14	
line passing	71.49	135.9	113.14	
line passing	80.49	135.9	113.14	
line passing	80.49	137.4	113.14	
line passing	71.49	137.4	113.14	
line passing	71.49	138.9	113.14	
line passing	80.49	138.9	113.14	
line passing	80.49	140.4	113.14	
line passing	71.49	140.4	113.14	
line passing	71.49	141.9	113.14	
line end	80.49	141.9	113.14	
line dispense setup	0.4	0.4	0	0
line start	72.99	134.4	112.39	
line passing	72.99	140.4	112.39	
line passing	74.49	140.4	112.39	
line passing	74.49	134.4	112.39	
line passing	75.99	134.4	112.39	
line passing	75.99	140.4	112.39	
line passing	77.49	140.4	112.39	
line passing	77.49	134.4	112.39	

line passing	78.99	134.4	112.39	
line end	78.99	140.4	112.39	
line dispense setup	0.4	0.4	0	0
line start	72.99	134.4	111.64	
line passing	78.99	134.4	111.64	
line passing	78.99	135.9	111.64	
line passing	72.99	135.9	111.64	
line passing	72.99	137.4	111.64	
line passing	78.99	137.4	111.64	
line passing	78.99	138.9	111.64	
line passing	72.99	138.9	111.64	
line passing	72.99	140.4	111.64	
line end	78.99	140.4	111.64	
line dispense setup	0.4	0.4	0	0
line start	72.99	134.4	110.89	
line passing	72.99	140.4	110.89	
line passing	74.49	140.4	110.89	
line passing	74.49	134.4	110.89	
line passing	75.99	134.4	110.89	
line passing	75.99	140.4	110.89	
line passing	77.49	140.4	110.89	
line passing	77.49	134.4	110.89	
line passing	78.99	134.4	110.89	
line end	78.99	140.4	110.89	
line dispense setup	0.4	0.4	0	0
line start	72.99	134.4	110.14	
line passing	78.99	134.4	110.14	
line passing	78.99	135.9	110.14	
line passing	72.99	135.9	110.14	
line passing	72.99	137.4	110.14	
line passing	78.99	137.4	110.14	
line passing	78.99	138.9	110.14	
line passing	72.99	138.9	110.14	
line passing	72.99	140.4	110.14	
line end	78.99	140.4	110.14	
line dispense setup	0.4	0.4	0	0
line start	72.99	134.4	109.39	
line passing	72.99	140.4	109.39	
line passing	74.49	140.4	109.39	
line passing	74.49	134.4	109.39	
line passing	75.99	134.4	109.39	
line passing	75.99	140.4	109.39	
line passing	77.49	140.4	109.39	

line passing	77.49	134.4	109.39	
line passing	78.99	134.4	109.39	
line end	78.99	140.4	109.39	
line dispense setup	0.4	0.4	0	0
line start	72.99	134.4	108.64	
line passing	78.99	134.4	108.64	
line passing	78.99	135.9	108.64	
line passing	72.99	135.9	108.64	
line passing	72.99	137.4	108.64	
line passing	78.99	137.4	108.64	
line passing	78.99	138.9	108.64	
line passing	72.99	138.9	108.64	
line passing	72.99	140.4	108.64	
line end	78.99	140.4	108.64	
line dispense setup	0.4	0.4	0	0
line start	72.99	134.4	107.89	
line passing	72.99	140.4	107.89	
line passing	74.49	140.4	107.89	
line passing	74.49	134.4	107.89	
line passing	75.99	134.4	107.89	
line passing	75.99	140.4	107.89	
line passing	77.49	140.4	107.89	
line passing	77.49	134.4	107.89	
line passing	78.99	134.4	107.89	
line end	78.99	140.4	107.89	
line dispense setup	0.4	0.4	0	0
line start	72.99	134.4	107.14	
line passing	78.99	134.4	107.14	
line passing	78.99	135.9	107.14	
line passing	72.99	135.9	107.14	
line passing	72.99	137.4	107.14	
line passing	78.99	137.4	107.14	
line passing	78.99	138.9	107.14	
line passing	72.99	138.9	107.14	
line passing	72.99	140.4	107.14	
line end	78.99	140.4	107.14	
line dispense setup	0.4	0.4	0	0
line start	72.99	134.4	106.39	
line passing	72.99	140.4	106.39	
line passing	74.49	140.4	106.39	
line passing	74.49	134.4	106.39	
line passing	75.99	134.4	106.39	
line passing	75.99	140.4	106.39	

line passing	77.49	140.4	106.39	
line passing	77.49	134.4	106.39	
line passing	78.99	134.4	106.39	
line end	78.99	140.4	106.39	
line dispense setup	0.4	0.4	0	0
line start	72.99	134.4	105.64	
line passing	78.99	134.4	105.64	
line passing	78.99	135.9	105.64	
line passing	72.99	135.9	105.64	
line passing	72.99	137.4	105.64	
line passing	78.99	137.4	105.64	
line passing	78.99	138.9	105.64	
line passing	72.99	138.9	105.64	
line passing	72.99	140.4	105.64	
line end	78.99	140.4	105.64	
line dispense setup	0.4	0.4	0	0
line start	72.99	134.4	104.89	
line passing	72.99	140.4	104.89	
line passing	74.49	140.4	104.89	
line passing	74.49	134.4	104.89	
line passing	75.99	134.4	104.89	
line passing	75.99	140.4	104.89	
line passing	77.49	140.4	104.89	
line passing	77.49	134.4	104.89	
line passing	78.99	134.4	104.89	
line end	78.99	140.4	104.89	
line dispense setup	0.4	0.4	0	0
line start	72.99	134.4	104.14	
line passing	78.99	134.4	104.14	
line passing	78.99	135.9	104.14	
line passing	72.99	135.9	104.14	
line passing	72.99	137.4	104.14	
line passing	78.99	137.4	104.14	
line passing	78.99	138.9	104.14	
line passing	72.99	138.9	104.14	
line passing	72.99	140.4	104.14	
line end	78.99	140.4	104.14	
line dispense setup	0.4	0.4	0	0
line start	72.99	134.4	103.39	
line passing	72.99	140.4	103.39	
line passing	74.49	140.4	103.39	
line passing	74.49	134.4	103.39	
line passing	75.99	134.4	103.39	

line passing	75.99	140.4	103.39	
line passing	77.49	140.4	103.39	
line passing	77.49	134.4	103.39	
line passing	78.99	134.4	103.39	
line end	78.99	140.4	103.39	
line dispense setup	0.4	0.4	0	0
line start	72.99	134.4	102.64	
line passing	78.99	134.4	102.64	
line passing	78.99	135.9	102.64	
line passing	72.99	135.9	102.64	
line passing	72.99	137.4	102.64	
line passing	78.99	137.4	102.64	
line passing	78.99	138.9	102.64	
line passing	72.99	138.9	102.64	
line passing	72.99	140.4	102.64	
line end	78.99	140.4	102.64	
line dispense setup	0.4	0.4	0	0
line start	72.99	134.4	101.89	
line passing	72.99	140.4	101.89	
line passing	74.49	140.4	101.89	
line passing	74.49	134.4	101.89	
line passing	75.99	134.4	101.89	
line passing	75.99	140.4	101.89	
line passing	77.49	140.4	101.89	
line passing	77.49	134.4	101.89	
line passing	78.99	134.4	101.89	
line end	78.99	140.4	101.89	

Appendix D

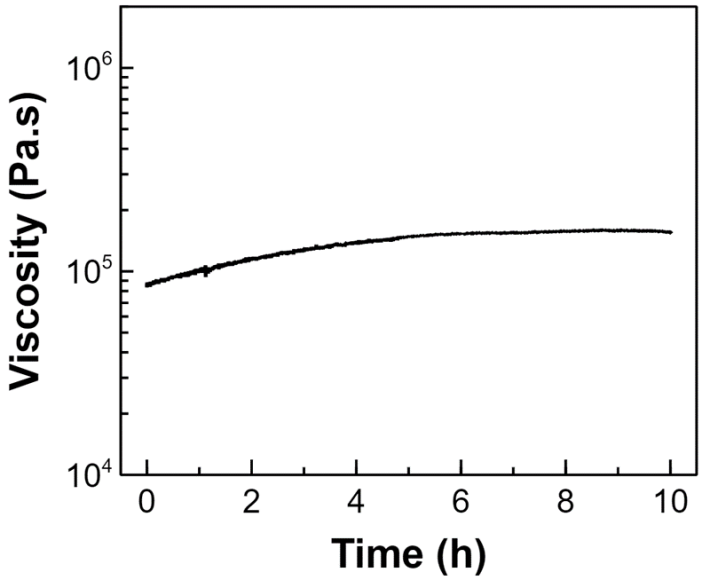

Figure D1. Viscosity of printing ink measured at -5 °C, indicating a constant viscosity profile over 10 h.

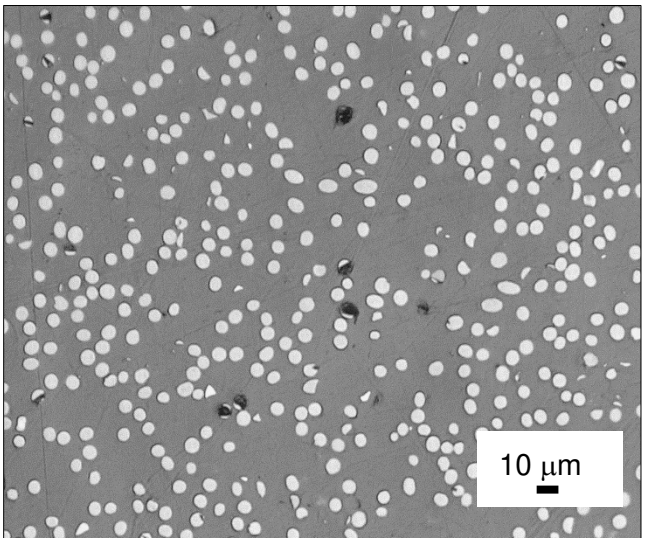

Figure D2. Magnified optical image captured from polished cross-section of a flexural bar specimen printed via laser in parallel to the bar length.

Matlab code used to generate x-y-z coordinates of the spring printed via laser

```
t = 0:pi/50:10*pi;
st = sin(t);
ct = cos(t);
```

G-codes used for 3D printing via laser

Table D1. G-code used to print bracket.

line speed	8.33			
line dispense setup	0.2	0.6	0	2
line start	160	130	95.55	
line passing	150	130	95.55	
line passing	135	130	88.05	
line passing	120	130	88.05	
line passing	105	130	95.55	
line end	95	130	95.55	
line start	160	128.9	95.55	
line passing	150	128.9	95.55	
line passing	135	128.9	88.05	
line passing	120	128.9	88.05	
line passing	105	128.9	95.55	
line end	95	128.9	95.55	
line start	160	127.8	95.55	
line passing	150	127.8	95.55	
line passing	135	127.8	88.05	
line passing	120	127.8	88.05	
line passing	105	127.8	95.55	
line end	95	127.8	95.55	
line start	160	126.7	95.55	
line passing	150	126.7	95.55	
line passing	135	126.7	88.05	
line passing	120	126.7	88.05	
line passing	105	126.7	95.55	
line end	95	126.7	95.55	
line start	160	130	94.45	
line passing	150	130	94.75	
line passing	135	130	87.25	
line passing	120	130	87.25	
line passing	105	130	94.75	
line end	95	130	94.75	
line start	160	128.9	94.45	
line passing	150	128.9	94.75	
line passing	135	128.9	87.25	
line passing	120	128.9	87.25	
line passing	105	128.9	94.75	
line end	95	128.9	94.75	
line start	160	127.8	94.45	

line passing	150	127.8	94.75	
line passing	135	127.8	87.25	
line passing	120	127.8	87.25	
line passing	105	127.8	94.75	
line end	95	127.8	94.75	
line start	160	126.7	94.45	
line passing	150	126.7	94.75	
line passing	135	126.7	87.25	
line passing	120	126.7	87.25	
line passing	105	126.7	94.75	
line end	95	126.7	94.75	

Table D2. G-code used to print spring.

line speed	0.3		
line start	51.13	104	131.874
wait point	8		
line passing	51.13	104	81.874
dispense ON/OFF	0		
wait point	0.5		
line end	51.13	104	0

Table D3. G-code used to print unsupported double cone structure.

line speed	0.4		
line start	115.96	131.88	125.12
wait point	4		
line passing	115.96	141.88	100.12
line end	115.96	131.88	75.12

Table D4. G-code used to print tall cylinder.

line speed	0.1		
line start	51.13	104	131.874
wait point	8		
line passing	51.13	104	81.874
dispense ON/OFF	0		
wait point	0.5		
line end	51.13	104	0

Table D5. G-code used to print flexural specimens in parallel direction.

.

line speed	8.33		
line start	100	100	93.11
line end	35	100	93.11
line start	100	101.44	93.11
line end	35	101.44	93.11
line start	100	102.88	93.11
line end	35	102.88	93.11
line start	100	104.32	93.11
line end	35	104.32	93.11
line start	100	105.76	93.11
line end	35	105.76	93.11
line start	100	107.2	93.11
line end	35	107.2	93.11
line start	100	108.64	93.11
line end	35	108.64	93.11
line start	100	110.08	93.11
line end	35	110.08	93.11
line start	100	111.52	93.11
line end	35	111.52	93.11
line start	100	100	91.67
line end	35	100	91.67
line start	100	101.44	91.67
line end	35	101.44	91.67
line start	100	102.88	91.67
line end	35	102.88	91.67
line start	100	104.32	91.67
line end	35	104.32	91.67
line start	100	105.76	91.67
line end	35	105.76	91.67
line start	100	107.2	91.67
line end	35	107.2	91.67
line start	100	108.64	91.67
line end	35	108.64	91.67
line start	100	110.08	91.67
line end	35	110.08	91.67
line start	100	111.52	91.67
line end	35	111.52	91.67

Table D6. G-code used to print flexural specimens in transverse direction.

line speed	8.33		
line start	100	100	93.11
line end	70	100	93.11
line start	100	101.44	93.11
line end	70	101.44	93.11
line start	100	102.88	93.11
line end	70	102.88	93.11
line start	100	104.32	93.11
line end	70	104.32	93.11
line start	100	105.76	93.11
line end	70	105.76	93.11
line start	100	107.2	93.11
line end	70	107.2	93.11
line start	100	108.64	93.11
line end	70	108.64	93.11
line start	100	110.08	93.11
line end	70	110.08	93.11
line start	100	111.52	93.11
line end	70	111.52	93.11
line start	100	112.96	93.11
line end	70	112.96	93.11
line start	100	114.4	93.11
line end	70	114.4	93.11
line start	100	115.84	93.11
line end	70	115.84	93.11
line start	100	117.28	93.11
line end	70	117.28	93.11
line start	100	118.72	93.11
line end	70	118.72	93.11
line start	100	120.16	93.11
line end	70	120.16	93.11
line start	100	121.6	93.11
line end	70	121.6	93.11
line start	100	123.04	93.11
line end	70	123.04	93.11
line start	100	124.48	93.11
line end	70	124.48	93.11
line start	100	125.92	93.11

line end	70	125.92	93.11
line start	100	127.36	93.11
line end	70	127.36	93.11
line start	100	128.8	93.11
line end	70	128.8	93.11
line start	100	130.24	93.11
line end	70	130.24	93.11
line start	100	131.68	93.11
line end	70	131.68	93.11
line start	100	133.12	93.11
line end	70	133.12	93.11
line start	100	134.56	93.11
line end	70	134.56	93.11
line start	100	136	93.11
line end	70	136	93.11
line start	100	137.44	93.11
line end	70	137.44	93.11
line start	100	138.88	93.11
line end	70	138.88	93.11
line start	100	140.32	93.11
line end	70	140.32	93.11
line start	100	141.76	93.11
line end	70	141.76	93.11
line start	100	143.2	93.11
line end	70	143.2	93.11
line start	100	144.64	93.11
line end	70	144.64	93.11
line start	100	146.08	93.11
line end	70	146.08	93.11
line start	100	147.52	93.11
line end	70	147.52	93.11
line start	100	148.96	93.11
line end	70	148.96	93.11
line start	100	150.4	93.11
line end	70	150.4	93.11
line start	100	151.84	93.11
line end	70	151.84	93.11
line start	100	153.28	93.11
line end	70	153.28	93.11
line start	100	154.72	93.11
line end	70	154.72	93.11
line start	100	156.16	93.11
line end	70	156.16	93.11

line start	100	157.6	93.11
line end	70	157.6	93.11
line start	100	159.04	93.11
line end	70	159.04	93.11
line start	100	160.48	93.11
line end	70	160.48	93.11
line start	100	161.92	93.11
line end	70	161.92	93.11
line start	100	163.36	93.11
line end	70	163.36	93.11
line start	100	164.8	93.11
line end	70	164.8	93.11
line start	100	100	91.67
line end	70	100	91.67
line start	100	101.44	91.67
line end	70	101.44	91.67
line start	100	102.88	91.67
line end	70	102.88	91.67
line start	100	104.32	91.67
line end	70	104.32	91.67
line start	100	105.76	91.67
line end	70	105.76	91.67
line start	100	107.2	91.67
line end	70	107.2	91.67
line start	100	108.64	91.67
line end	70	108.64	91.67
line start	100	110.08	91.67
line end	70	110.08	91.67
line start	100	111.52	91.67
line end	70	111.52	91.67
line start	100	112.96	91.67
line end	70	112.96	91.67
line start	100	114.4	91.67
line end	70	114.4	91.67
line start	100	115.84	91.67
line end	70	115.84	91.67
line start	100	117.28	91.67
line end	70	117.28	91.67
line start	100	118.72	91.67
line end	70	118.72	91.67
line start	100	120.16	91.67
line end	70	120.16	91.67
line start	100	121.6	91.67

line end	70	121.6	91.67
line start	100	123.04	91.67
line end	70	123.04	91.67
line start	100	124.48	91.67
line end	70	124.48	91.67
line start	100	125.92	91.67
line end	70	125.92	91.67
line start	100	127.36	91.67
line end	70	127.36	91.67
line start	100	128.8	91.67
line end	70	128.8	91.67
line start	100	130.24	91.67
line end	70	130.24	91.67
line start	100	131.68	91.67
line end	70	131.68	91.67
line start	100	133.12	91.67
line end	70	133.12	91.67
line start	100	134.56	91.67
line end	70	134.56	91.67
line start	100	136	91.67
line end	70	136	91.67
line start	100	137.44	91.67
line end	70	137.44	91.67
line start	100	138.88	91.67
line end	70	138.88	91.67
line start	100	140.32	91.67
line end	70	140.32	91.67
line start	100	141.76	91.67
line end	70	141.76	91.67
line start	100	143.2	91.67
line end	70	143.2	91.67
line start	100	144.64	91.67
line end	70	144.64	91.67
line start	100	146.08	91.67
line end	70	146.08	91.67
line start	100	147.52	91.67
line end	70	147.52	91.67
line start	100	148.96	91.67
line end	70	148.96	91.67
line start	100	150.4	91.67
line end	70	150.4	91.67
line start	100	151.84	91.67
line end	70	151.84	91.67

line start	100	153.28	91.67
line end	70	153.28	91.67
line start	100	154.72	91.67
line end	70	154.72	91.67
line start	100	156.16	91.67
line end	70	156.16	91.67
line start	100	157.6	91.67
line end	70	157.6	91.67
line start	100	159.04	91.67
line end	70	159.04	91.67
line start	100	160.48	91.67
line end	70	160.48	91.67
line start	100	161.92	91.67
line end	70	161.92	91.67
line start	100	163.36	91.67
line end	70	163.36	91.67
line start	100	164.8	91.67
line end	70	164.8	91.67